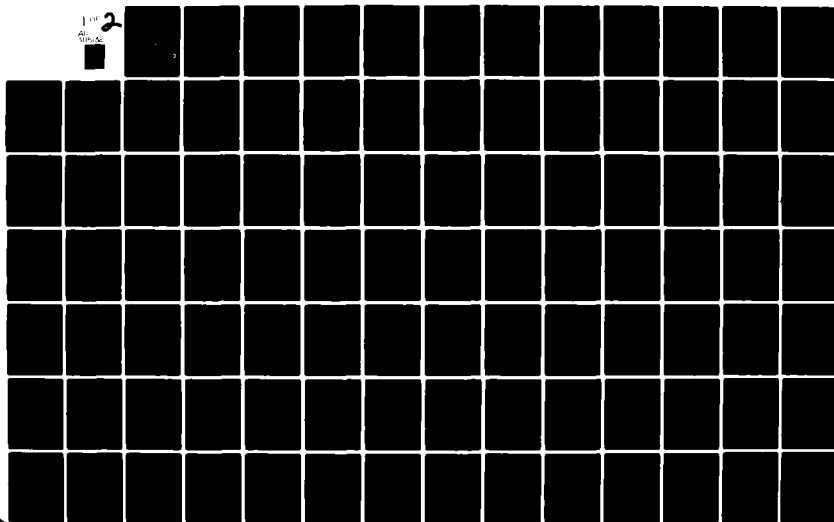


AD-A115 132

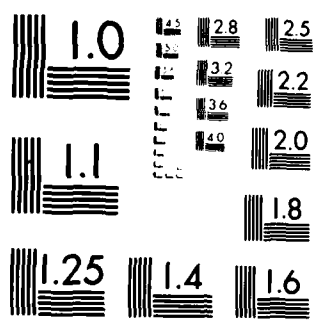
ATLANTIC RESEARCH CORP ALEXANDRIA VA F/G 11/4
NOTEBOOK ON ELECTROMAGNETIC PROPERTIES OF COMPOSITE MATERIALS B--ETC(U)
SEP 81 D R PFLUG, J A BIRKEN, R A WALLEMBERG N00019-80-C-0157
NAVAIR-AIR-518-9 NL

UNCLASSIFIED

1 of 2
2
[Small square icon]



OF 2
D
15132



MICROCOPY RESOLUTION TEST CHART
NATIONAL BUREAU OF STANDARDS 1963-A

NOTEBOOK ON
ELECTROMAGNETIC PROPERTIES
OF
COMPOSITE MATERIALS
BELOW 1 GHz

AD A115132



Copy available to DTIC does not
permit fully legible reproduction

DTIC
ELECTE
JUN 3 1982
S **D**
A

DTIC FILE COPY

NAVAL AIR SYSTEM COMMAND
U.S. DEPARTMENT OF THE NAVY

82 06 03 006

APPROVED FOR PUBLIC RELEASE
DISTRIBUTION UNLIMITED

SECURITY CLASSIFICATION OF THIS PAGE (When Data Entered)

REPORT DOCUMENTATION PAGE		READ INSTRUCTIONS BEFORE COMPLETING FORM
1. REPORT NUMBER NAVAIR AIR-518-9	2. GOVT ACCESSION NO. 110-A115132	3. RECIPIENT'S CATALOG NUMBER
4. TITLE (and Subtitle) Notebook on Electromagnetic Properties of Composite Materials below 1 GHz		5. TYPE OF REPORT & PERIOD COVERED Final Technical Report
7. AUTHOR(s) Pflug, D. R. Auckland, D.T. Birken, J.A. Wallenberg, R.A.		6. PERFORMING ORG. REPORT NUMBER N/A
8. PERFORMING ORGANIZATION NAME AND ADDRESS Atlantic Research Corporation 5390 Cherokee Ave. Alexandria, Virginia 22314		9. CONTRACT OR GRANT NUMBER(s) N00019-80-C-0157
10. CONTROLLING OFFICE NAME AND ADDRESS Naval Air Systems Command Washington, D. C. 20361		11. PROGRAM ELEMENT, PROJECT, TASK AREA & WORK UNIT NUMBERS 6270F 63 45400130 62414
12. MONITORING AGENCY NAME & ADDRESS (if different from Controlling Office) Same		13. REPORT DATE September 1981
		14. NUMBER OF PAGES 86
		15. SECURITY CLASS. (of this report) Unclassified
		16. DECLASSIFICATION/DOWNGRADING SCHEDULE N/A
17. DISTRIBUTION STATEMENT (of this Report) Approved for public release; distribution unlimited.		Accession For NTIS GPO Unlimited Distribution
18. DISTRIBUTION STATEMENT (of the abstract entered in Block 20, if different from Report) Same		
19. SUPPLEMENTARY NOTES Program Engineer: John A. Birken (AIR-5161D)		20. ABSTRACT (Continue on reverse side if necessary and identify by block number) This report is the seventh in a series of reports on the electromagnetic properties of composite materials. The report quantitatively delineates: the vast differences in electromagnetic behavior exhibited by the principle composite materials (Graphite/epoxy & Kelvar), how to predict these different properties based on the materials intrinsic electrical properties (conductivity, permeability and permittivity) and how the airframe shape influences electromagnetic coupling. The electromagnetic threats of lightning electromagnetic pulse (LEMP), nuclear Electromagnetic Pulse (NEMP).
21. KEY WORDS (Continue on reverse side if necessary and identify by block number) ADVANCE COMPOSITE AIRCRAFT ADVANCED COMPOSITE MATERIALS ELECTROMAGNETIC ENVIRONMENT LIGHTNING AND AIRCRAFT INTERACTION		22. KEY WORDS (Continue on reverse side if necessary and identify by block number) LASER EFFECTS ON COMPOSITES RIBBON CABLE NUCLEAR ELECTROMAGNETIC PULSE ELECTROMAGNETIC PROTECTION

DD FORM 1 JAN 73 1473

EDITION OF 1 NOV 65 IS OBSOLETE
S/N 0102-LF-014-6607

SECURITY CLASSIFICATION OF THIS PAGE (When Data Entered)

**NOTEBOOK ON ELECTROMAGNETIC PROPERTIES OF COMPOSITES
FOR FREQUENCIES BELOW 1 GHz**

Table of Contents

	<u>Page</u>
I. Composite Material Electromagnetic Intrinsic Properties	1-1
1.1 Intrinsic Material Properties	1-1
Permeability	1-1
Permittivity	1-2
Conductivity, Bulk and Surface	1-5
o Kevlar	1-5
o Boron/Epoxy	1-9
o Graphite/Epoxy	1-15
1.2 Improvements of Intrinsic Properties	1-26
o Doping	1-26
o Intercalation	1-30
1.3 Thermal Modification of EM Properties	1-38
1.4 Environmental Modification of EM Intrinsic Properties	1-41
o Moisture Effects	1-41
1.5 Non-Linear Effects	1-41
II. Composite Electromagnetic Shielding	2-1
2.0 Composite Material Shielding Effective Transfer Impedance and Joint Admittance	2-1
2.1 Shielding Effectiveness Theory	2-3
2.1.1 Uniform Magnetic Field	2-3
2.1.2 Uniform Electric Field	2-6
2.1.3 Transfer Impedance Relation to Shielding Effectiveness	2-8
2.2 Measures and Predicted Composite Material Shielding Effectiveness	2-9
2.3 Composite Joint Coupling	2-32
2.3.1 Theory	2-32
2.3.2 Shielding Effectiveness Plus Joint Admittance	2-37

Table of Contents
(Cont'd.)

	<u>Page</u>
2.4 Ranking and Low Weight Penalties Imposed by Thin Metallic Coatings	2-44
2.5 References	2-46
3.0 Electromagnetic Threats	3-1
3.1 Natural Threats	3-1
3.2 Friend/Foe Threat	3-26
3.3 References	3-38
4.0 Application of Composite Parameter to Existing Aircraft	4-1

1.0 INTRINSIC MATERIAL PROPERTIES

The electromagnetic behavior of composite materials is ultimately determined by their intrinsic material properties. The key properties considered in this section are the composite material permeability, permittivity, and conductivity as a function of frequency and field strength. A brief analysis of composite material resistivity is presented separately. Property modification is discussed and includes property improvement through doping and intercalation, and property changes due to thermal and environmental effects. Non-linear properties of composites are also briefly considered.

1.1 Material EM Parameters: Theory and Measurement

The measured relative values of permeability and permittivity and the measured values of conductivity as functions of frequency and field strength, for boron/epoxy, Kelvar/epoxy and graphite/epoxy composites are tabulated in this section. Some data is presented on the resistivity of composites. Separate data is given on the conductivity of boron/epoxy and graphite/epoxy for individual fibers, the epoxy and bulk composite material.

1.1.1 Permeability

The basic macroscopic parameter used to characterize the magnetic state of a material is the permeability. This parameter (designated by μ) is defined in terms of the magnetic induction (\vec{B}) and the magnetic field intensity (\vec{H}) by the equation

$$\vec{B} = \mu \vec{H} \quad (1-1)$$

In view of the fact that the composites boron/epoxy, graphite/epoxy and Kevlar/epoxy are presently fabricated using non-magnetic materials, it may be anticipated that their magnetic permeability will be essentially that of free space.

Permeability measurements for the composites boron/epoxy, graphite/epoxy and Kevlar/epoxy have been performed^(3,4) using the standard testing procedures specified by the American Society for Testing and Materials (ASTM). The permeabilities of representative samples of each composite were determined at D.C. and 60 Hz using the sample weighing technique and at 100 Hz using the more sensitive vibrating sample magnetometer. All results indicated that these materials were weakly diamagnetic with a measured magnetic susceptibility $X_m \times 10^{-7}$. The permeability is given in terms of the magnetic susceptibility by the equation

$$\mu = \mu_0 (1 + X_m) \quad (1-2)$$

where μ_0 is the permeability of free space. The results are tabulated in Table 1.1 in terms of the relative permeability μ/μ_0 . These results indicate that boron/epoxy, graphite/epoxy and Kevlar/epoxy all have the permeability of free space to the accuracy measured and the frequencies checked. Due to the apparent lack of sensitivity of the measured permeabilities to frequency, no higher frequency measurements have been undertaken. Further details on the measurement process may be found in the ASTM section on measurement, test and evaluation or in the references.^(3,4,6)

1.1.2 Permittivity

The electrical parameter analogous to the magnetic permeability is the electric permittivity (designated by ϵ) and is defined in terms of the applied electric field (E) and electric displacement (D) by the equation

$$D = \epsilon E \quad (1-3)$$

Because composite materials are heterogenous substances by virtue of their process of manufacture, the permittivity of these materials can be expected to be anisotropic and to be frequency dependent. A further complicating factor in the measurement of the permittivity is the existence of conducting charge in the composite material. As a consequence, the conduction current

	BORON/EPOXY	KEVLAR/EPOXY	GRAPHITE/EPOXY
RELATIVE PERMEABILITY			
μ/μ_0			
at D.C., 60 Hz	1.0	1.0	1.0
and 100 Hz			

Table 1.1. Composite Material Relative Permeability. (3,4)

(as measured by the conductivity σ) and the displacement current (as measured by the permittivity ϵ) are mixed together as shown in the equation

$$\nabla \times \vec{H} = (\sigma + j\omega\epsilon) \vec{E} \quad (1-4)$$

where ω is the angular frequency. The measureability of the permittivity ϵ then depends on the magnitude of the material conductivity.

The standard ASTM method used to measure permittivity involves the measurement of the capacitance of a composite filled capacitor. Details of the measurement process are given in ASTM section on measurement, test and evaluation and in the references. (3,4,6)

The relative permittivity ϵ/ϵ_0 (also called the dielectric constant where ϵ_0 is the permittivity of free space) of Kevlar/epoxy, graphite/epoxy and boron/epoxy have been measured from D.C. to 50 MHz. (3,4) The results are tabulated in Table 1.2. These results show that Kevlar/epoxy is a very good insulator with the permittivity essentially a constant independent of direction and frequency. The range of values reported for the Kevlar/epoxy permittivity are attributed to variations in epoxy chemistry.

The permittivity of graphite/epoxy was found to be essentially unmeasurable at any test frequency due to the high value ($10^2 - 10^4$ mhos/m) of the conductivity in any direction in the composite. (3,4) It has been estimated that the permittivity of graphite/epoxy will not be measurable until frequencies are of the order of 10^{12} Hz. (4)

The permittivity of boron/epoxy falls between the two extreme cases of Kevlar/epoxy and graphite/epoxy. This permittivity was found to be measurable only when the existing fields were normal to the direction of the composite fibers. In this case the permittivity was constant and frequency independent from D.C. to 50 MHz. The permittivity in the direction parallel to the composite fibers proved to be unmeasurable due to high fiber conductivity. (4)

Finally the permittivity of the epoxy resins which hold the fibers was measured from D.C. to 50 MHz with the result listed in Table 1.2 for 1 MHz. The permittivity of the epoxy resin was found to be independent of direction and frequency in the range considered.^(3,4)

1.1.3 Conductivity

In this section, the conductivity of Kevlar/epoxy, boron/epoxy and graphite/epoxy composite materials is discussed in detail. Measured conductivities are given for Kevlar/epoxy at two frequencies. Conductivities for boron/epoxy and graphite/epoxy are reported for the bulk composite in several ply orientations as well as for the constituent fibers and epoxy.

1.1.3.1 Kevlar/Epoxy

The conductivity of several samples Kevlar/epoxy have been investigated⁽³⁾ to a limited extent as a function of frequency and electric field strength.⁽³⁾ The experimental method used was the standard two-point probe method specified by the American Society for Testing and Material (ASTM). Details on this method and related methods can be found in ASTM section on Measurement, Test and Evaluation and in the references.⁽⁴⁾ These investigations show that Kevlar/epoxy conductivity has a slight dependence on frequency and field strength. The conductivity decreases slightly with increasing frequency and increases slightly with increasing field strength. The results are also independent of direction. The conductivity results for frequency are tabulated in Table 1.3 and the results for field strength are graphed in Figure 1.1. Because of the apparent insensitivity of the conductivity to low frequency, high frequency conductivities have not been investigated to date.

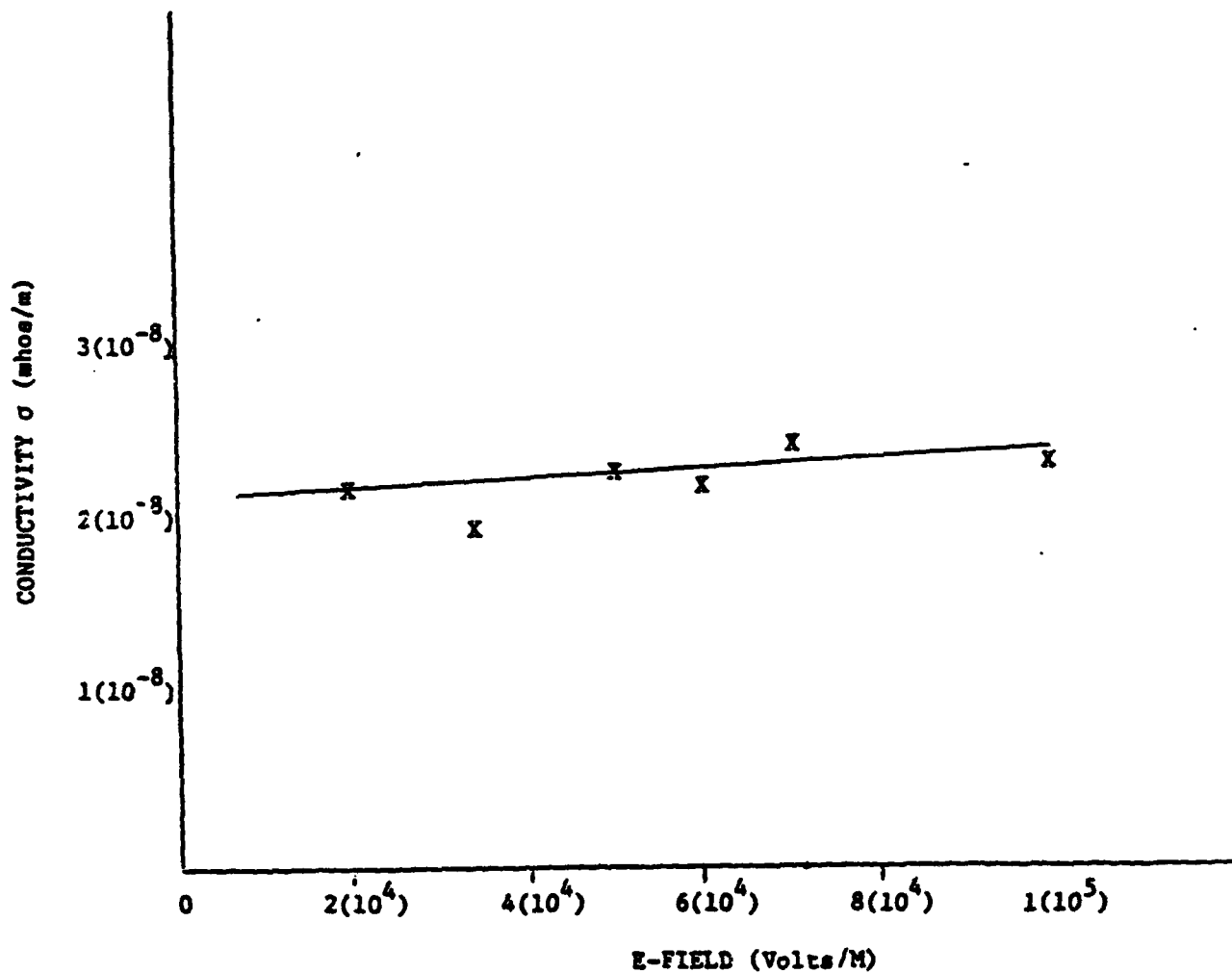


Figure 1.1. Conductivity σ (mhos/m) of Kevlar/Epoxy as a Function of E-Field.(3)

RELATIVE PERMITTIVITY	KELVAR/ EPOXY	GRAPHITE/ EPOXY	BORON/ EPOXY		EPOXY RESIN
			PARALLEL TO COMPOSITE FIBERS	NORMAL TO COMPOSITE FIBERS	
ϵ/ϵ_0	3.6-5.85	Unmeasureable	Unmeasureable	5.6	3.4

Table 1.2. Relative Permittivity (Dielectric Constant) of Kevlar/Epoxy, Boron/Epoxy, Epoxy Resin, and Graphite/Epoxy in the Frequency Range D.C. - 50 MHz. (3,4)

	D.C.	100 kHz
σ	2.2×10^{-8}	5×10^{-9}

Table 1.3. The Conductivity σ (mhos/m) of Kevlar/Epoxy as a Function of Frequency.⁽³⁾

1.1.3.2 Boron/Epoxy

Conductivity studies on boron/epoxy have dealt with the conductivity of the individual boron fibers, of the epoxy resin matrix holding the fibers, and of the total boron/epoxy composite. These results are presented and discussed in the three separate sections that follow.

1.1.3.2.1 Boron Epoxy Resins

Samples of the uncured epoxy resins were obtained from AVCO, a maker of boron/epoxy composite, and heated as is done during the manufacture of the composite. The conductivity was then measured at a frequency of 1 MHz.⁽⁴⁾ The result is listed in Table 1.4. This results was found to be frequency and direction independent in the range D.C. - 50 MHz.

1.1.3.2.2 Boron Fibers⁽²⁾

Boron fibers used in boron/epoxy composite materials are typically 10^{-2} cm in diameter. Although considerably larger than graphite fibers, boron fibers prove hard to characterize electrically because of the difficulty in fabricating reliable, low resistance ohmic contacts to the fibers. The reasons for these difficulties lie in the process used to make the fibers. Boron is deposited on hot tungsten wire (of diameter 1.8×10^{-3} cm) in an atmosphere of hydrogen (H_2) and boron chloride (BCl_3). The boron reacts with the tungsten to form an inner core of boron-tungsten compounds (such as WB_4 , W_2B_5 with possibly some free tungsten) surrounded by an outer sheath of pure boron. The details of the process are proprietary.

Great care is necessary in fabricating the electrical contacts. Mounting the fiber using conducting points or ink give very non-linear, even memory-displaying V-I characteristics. One successful approach is to plate nickel contacts onto the sheath and the core separately. Linear V-I characteristics result and it is possible to characterize the sheath and core by conductivities together with an effective fiber conductivity.

	BORON FIBERS ⁽²⁾			EPOXY ⁽⁴⁾ RESIN
	CORE	SHEATH	FIBER	
CONDUCTIVITY (mhos/m)	3×10^5	0.25	2.3×10^3	6×10^{-8}

Table 1.4. Conductivities of Boron/Epoxy Fibers and Resin in Frequency Range D.C. - 50 MHz.^(2,4)

These conductivities are given in Table 1.4. Boron fibers conductivities are seen to be very anisotropic with most of the current confined to the inner core of the fiber.

1.1.3.2.3 Boron/Epoxy Composite

There have been several investigations on the conductivity of boron/epoxy with varying results. One set of effective conductivities were obtained by Skouby⁽¹⁾ in an investigation of the shielding effectiveness of advanced composites. His shielding data becomes consistent with shielding theory provided the effective conductivity of boron/epoxy is taken as $\sigma \approx 10$ mhos/m at low frequencies (50 kHz-70 MHz) and $\sigma \approx 100$ mhos/m at high frequencies (100 MHz-18 GHz). These boron/epoxy test specimens range from 1-ply to 8-ply and involve several ply orientation as listed in Table 1.5. Preliminary investigation reported by Allen et.al.⁽⁴⁾ on samples of AVCO Rigidite 5505 Boron/epoxy over a frequency range from D.C. to 50 MHz. (given in Table 1.6) tend to confirm these results. More recent work involving great care in forming ohmic contacts using thin nickel-plated films onto abraded edges of boron/epoxy has resulted in revised figures for the longitudinal conductivities of multi-ply unidirectional samples.⁽³⁾ These results are given in Table 1.7. They show conductivities much higher than previously reported with an average of about 1000 mhos/m. Included for comparison in Table 1.7 is a unidirectional conductivity value (σ_{wh}) obtained by Walker and Heintz⁽⁵⁾ using a standing wave pattern on a slotted stripline at a frequency of 2 GHz. This conductivity value is significantly higher than values obtained by other methods and does not depend on ohmic contacts made to the composite. The basic conclusion reached by Gajda⁽³⁾ was that the longitudinal conductivity of boron/epoxy is about 1000 mhos/m while the transverse conductivity is about 2×10^{-8} mhos/m. The large anisotropy in conductivity is explained by the lack of fiber-to-fiber contact (confirmed by optical micrographs) in boron/epoxy. Little dependence on frequency was observed for low frequency conductivities; however the high conductivity value obtained by Walker, Heintz at 2 GHz raises the possibility of significantly higher conductivities at frequencies higher than 50 MHz.

PLIES	PLY ORIENTATION	σ (mhos/m)	
		50 kHz-70 MHz	100 MHz - 18 GHz
1	0°	≈ 10	≈ 100
2	$0^\circ, 90^\circ$		
4	$0^\circ, \pm 45^\circ, 90^\circ$		
8	$0^\circ, \pm 45^\circ, 90^\circ$		

Table 1.5. Effective Conductivity of Boron/epoxy as a function of number of plies and ply orientation. These results are calculated by Schouby using electromagnetic shielding results.(1)

Table 1.6. Preliminary Conductivities for Multi-ply Boron/epoxy Composites from Allen.⁽⁴⁾ (DC to 50 MHz)

PLIES	PLY ORIENTATION	CONDUCTIVITY (mhos/m)
7	0°, 0°, 0°, 90°	$\sigma_0 = 25^{(a)}$ $\sigma_{90} = 3.8^{(b)}$
1-8	Unidirectional	$\sigma_L = 20^{(c)}$ $\sigma_T = 2 \times 10^{-8} \text{ (d)}$

- a. Corresponds to currents parallel to 0° fibers.
- b. Corresponds to currents parallel to 90° fibers.
- c. Corresponds to current longitudinal to fibers.
- d. Corresponds to currents transverse to fibers.

Table 1.7. Final Boron/epoxy Conductivities of Multi-ply Unidirectional Samples Together With An Average Conductivity From Gajda. (3)

PLIES	TRANSVERSE CONDUCTIVITY σ_L (mhos/m)	
2	3300	
5	1400	$\sigma_{AV} \approx 1000^{(a)}$
17	1400	$\sigma_{WH} = 7 \times 10^4^{(b)}$
20	1100	

- a. This is the average conductivity found for unidirectional multi-ply samples.
- b. Value of conductivity for unidirectional samples at 2 GHz using standing wave techniques from Walker, Heintz. (5)

1.1.3.3 Graphite/Epoxy

Conductivity measurements have been performed on the epoxy resins and graphite fibers used in making graphite/epoxy as well as on the composite material itself. These results are presented in (1.1.3.3.1 - 1.1.3.3.3).

1.1.3.3.1 Graphite/Epoxy Fibers

The electrical characteristics of individual graphite fibers have been studied for one fiber type - Thornel T300 which is found in Narmco 5208 pre-preg tapes.⁽²⁴⁾ Some variation in conductivities is to be expected in fibers produced by different companies.

The fiber tows were unwound and cleaned with solvent and mounted on glass slides. Ohmic contact was made with conductive ink. All fiber displayed linear V-I characteristics up to fields of 4000 volts/m. Nonlinear characteristics were also observed and these results are given in Section 1.5 on nonlinear properties of composites. Conductivities of a 60 fiber sample are listed in Table 1.8. These results indicate that graphite fibers may be classed as reasonably good conductors with an average conductivity of 2×10^4 mhos/m. Fibers with conductivities of 2×10^5 mhos/m have also been reported.⁽⁹⁾ Because of their high conductivity, the permittivity of the graphite fibers could not be measured in the frequency range D.C. - 50 MHz. All measurements were done at D.C. but it was verified that the conductivities of graphite fibers are independent of frequency in the range D.C. - 50 MHz.

1.1.3.3.2 Epoxy Resins

The resins used in graphite/epoxy had similar electrical permittivity and conductivity as was given for boron/epoxy resins. The permittivity is listed in Table 1.2 and the conductivity in Table 1.4.

	CONDUCTIVITY OF GRAPHITE FIBERS (mhos/m)
MINIMUM FOUND	1.4×10^4
MAXIMUM FOUND	3×10^4
AVERAGE	2×10^4

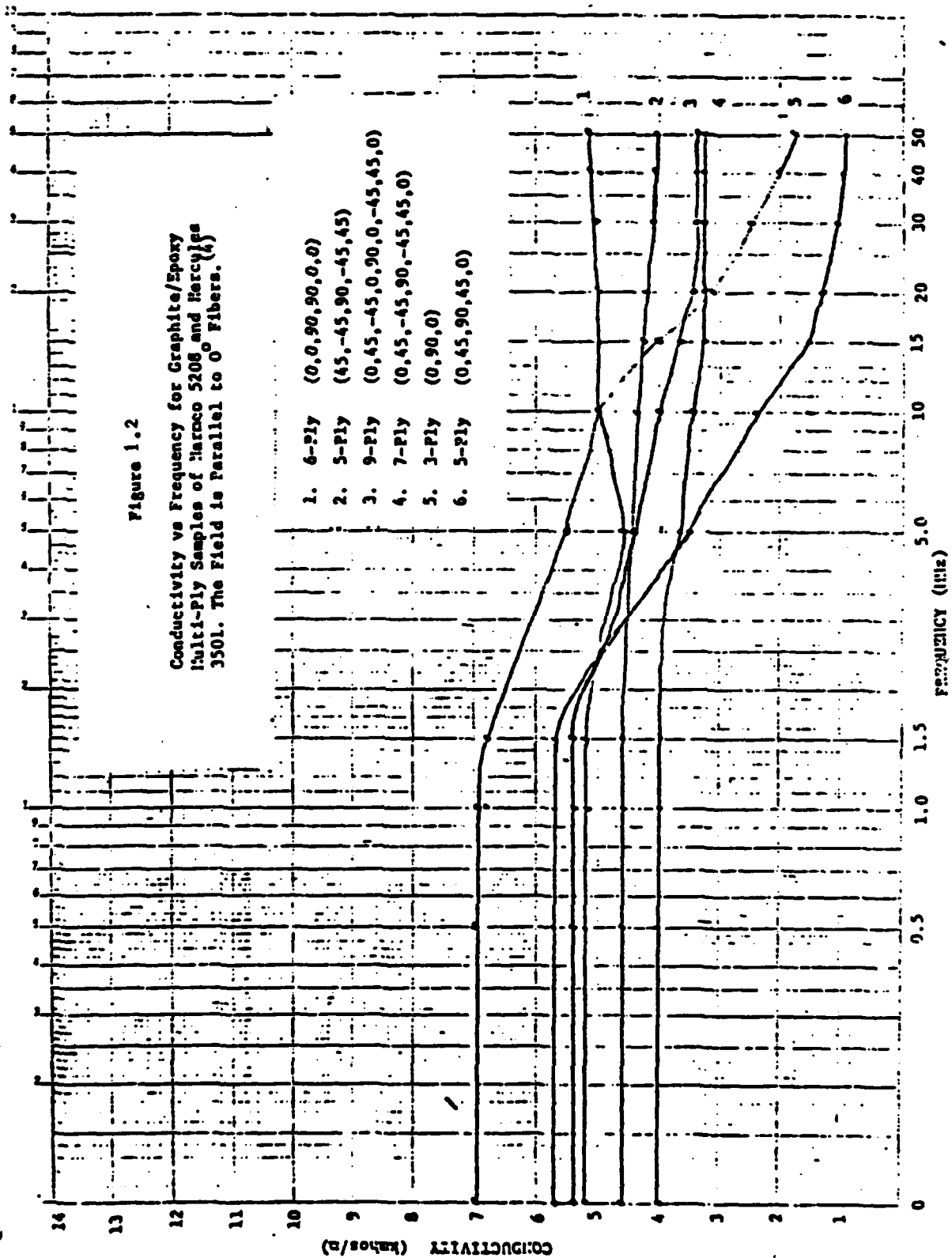
Table 1.8. Maximum, Minimum and Average Conductivities Found in a 60 Fiber Sample of Thornel T300 Fiber-type Taken From Narmco 5209 Pre-ply Types of Graphite/epoxy.(2,4)

1.1.3.3.3 Graphite/Epoxy Composites

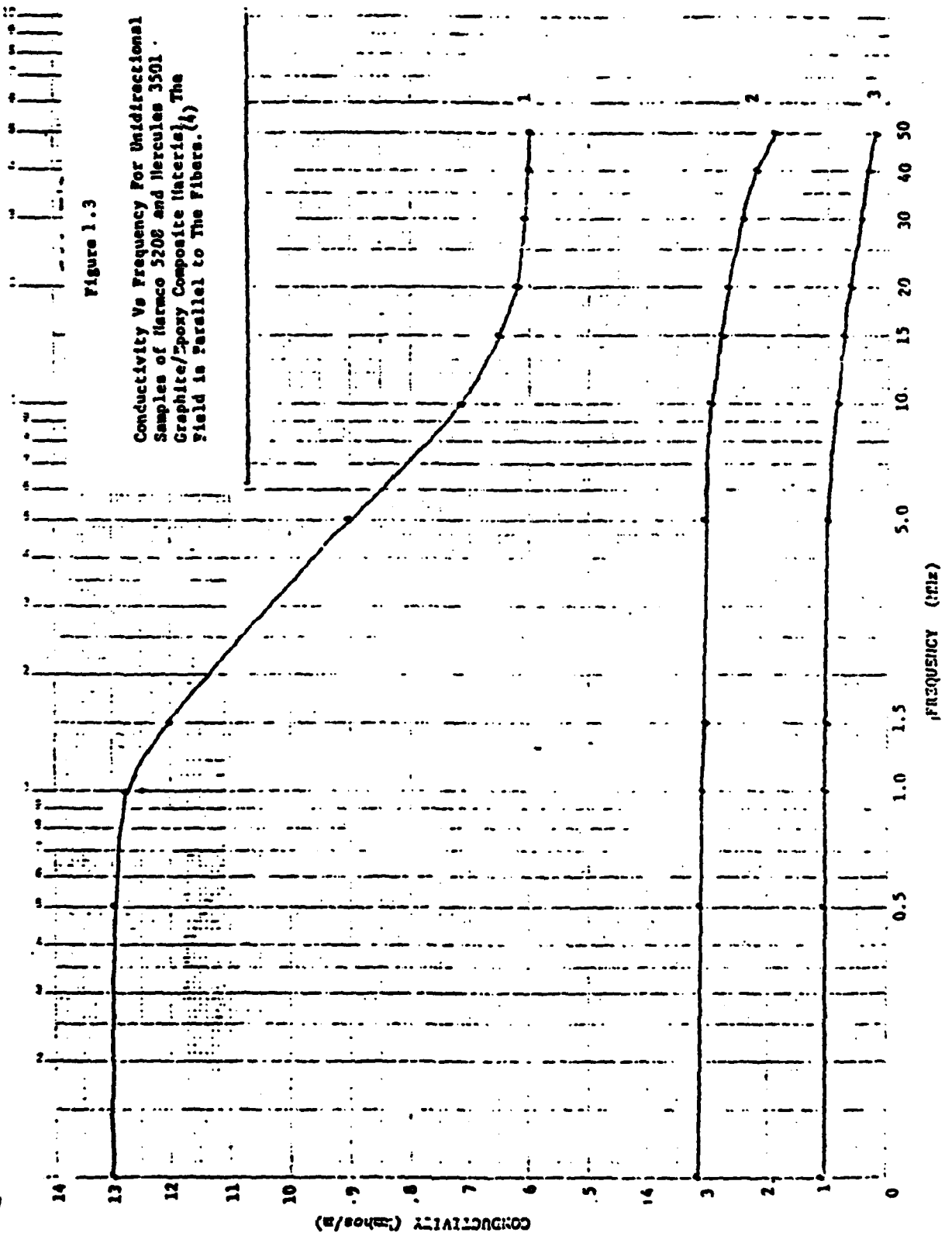
There have been several investigations into the conductivity of graphite/epoxy as a function of frequency. One set of measurements was done by Gajda⁽⁴⁾ in the frequency range D.C. - 50 MHz. The details of the measurement process are described in ASTM section on Measurement, Test and Evaluation and in the references.^(4,6) The results are illustrated in Figures 1.2 - 1.4. Figure 1.2 is a plot of conductivity vs frequency for multiply laminates for the case of the existing field parallel to the 0° fibers. Figure 1.3 is a plot of conductivity vs frequency for unidirectional graphite/epoxy sample with the existing field parallel to the fibers. Figure 1.4 is a plot of conductivity vs frequency for multiply samples with the field normal to the 0° fibers. The conductivity for all samples is essentially constant below 5 MHz after which it may increase or decrease slightly. A combination of skin effect and inductive and capacitive coupling between fibers have been used to explain and model this effect.

Higher frequency conductivity data has been reported by Walker and Heintz⁽⁵⁾ for unidirectional samples of graphite/epoxy with the field parallel to the fibers. The measurement apparatus used was a slotted strip line with the conductivity being extracted from the standing wave data. Details are given in ASTM section on Measurement, Test and Evaluation and in the references.⁽⁵⁾ The results are plotted in Figure 1.5. Included for comparison are conductivities of aluminum, boron/epoxy and transverse conductivity of the graphite/epoxy at selected frequencies. All conductivities were computed by the same stripline method. These results are particularly important because these measurements are essentially free of the electrical contact ambiguities present in other measurements.

A further investigation of the conductivity of graphite/epoxy was undertaken by Boeing Corp.⁽⁷⁾ Boeing measured the free space transmissivities of 2-ply (0,90) and 4-ply (0,145,90) samples



100% GEMILON-ASTIMIDE 70 3501C
 SAMPLES OF THE ABOVE COMPOSITES
 WERE TESTED BY THE FOLLOWING METHOD



1000 BRILLIANTIDER 36 7 1971
JAN 10 1972
GRAPHIC BY 10000

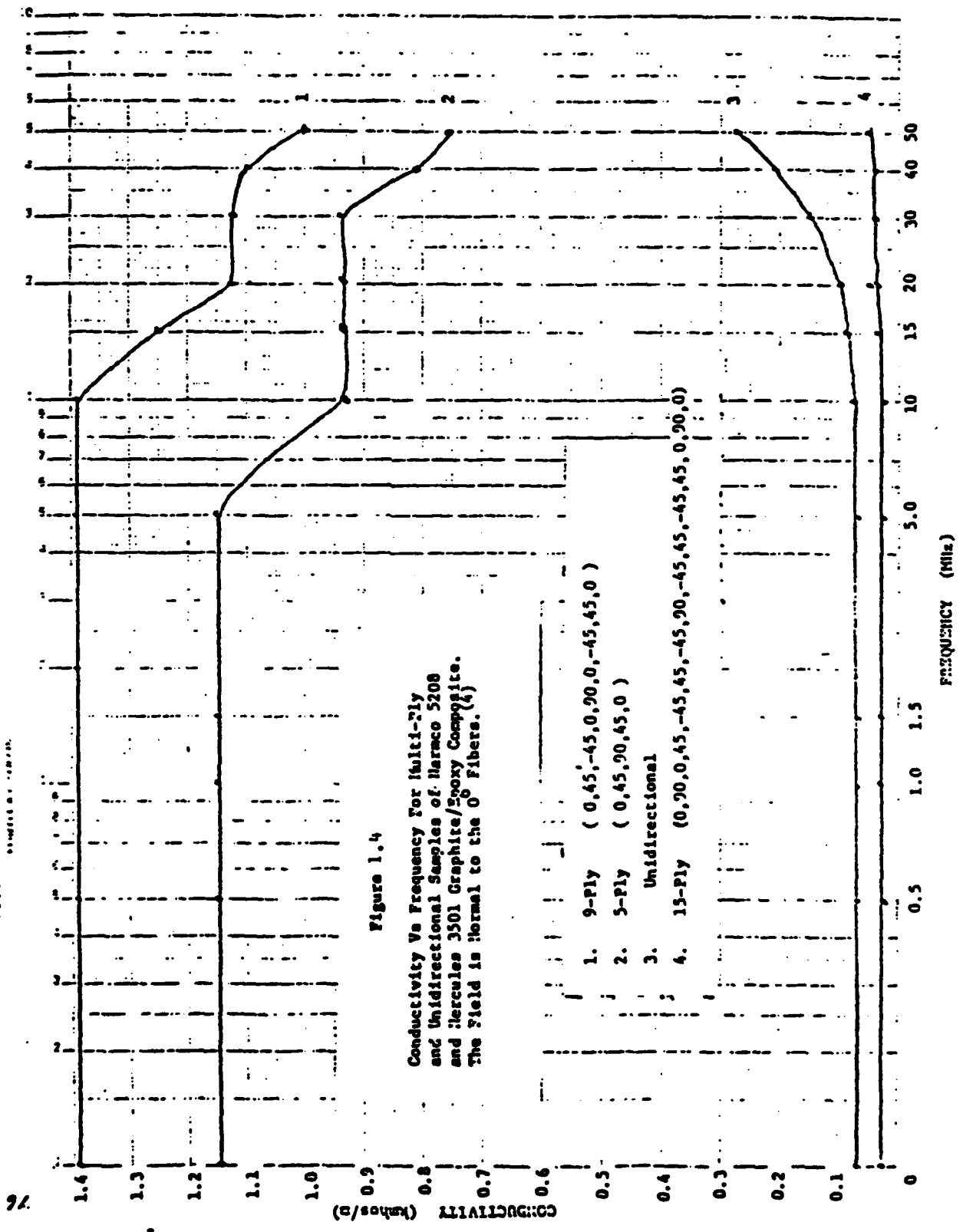


Figure 1.4

Conductivity Vs Frequency For Multi-Ply
and Unidirectional Samples of Harmac 5208
and Hercules 3501 Graphite/Epoxy Composites.
The Field is Normal to the 0° Fibers. (4)

- 1. 9-Ply (0.45, -45, 0, 90, 0, -45, 45, 0)
- 2. 5-Ply (0.45, 90, 45, 0)
- 3. Unidirectional
- 4. 13-Ply (0.90, 0, 45, -45, 45, -45, 90, -45, 45, 0, 90, 0)

16-5 SEMI-LOGARITHMIC 48 5913
 A RECT. & TRI. WAVE. GENERATOR
 SAMPLE SOURCE

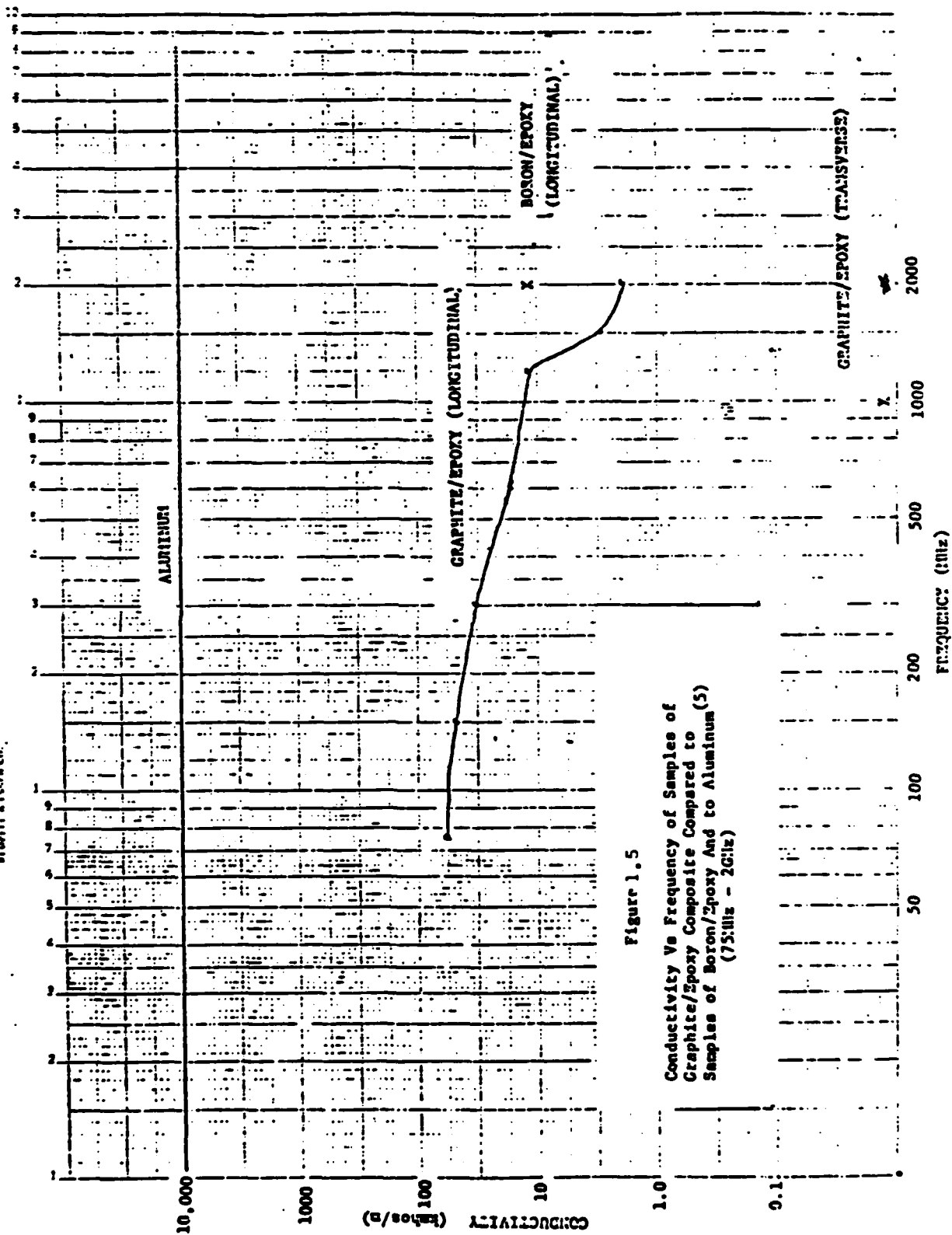


Figure 1.5

Conductivity Vs Frequency of Samples of
 Graphite/Epoxy Composite Compared to
 Samples of Boron/Epoxy And to Aluminum (5)
 (75MHz - 2GHz)

made from Hercules AS 3501-6B material over the frequency range 1.0 - 18 GHz. Measurements were taken using an Anechoic Chamber test system described in detail elsewhere.⁽⁷⁾ The transmission data was smoothed using least squares method and the conductivity extracted from the data using standard theory. The results are shown in Figure 1.6. for bulk conductivity (fields penetrating the material) and Figure 1.7 for surface conductivity (fields propagating parallel to the surface). Surface conductivity data was taken using waveguide methods.

All existing conductivity data indicates that graphite/epoxy is a good conductor even in the direction transverse to the fibers. The conductivity is nearly constant for low frequencies and generally decreases as the frequency increases. The relatively large value of the conductivity perpendicular to the fiber direction is a direct result of the high fiber-to-fiber contact (observable by optical micrograph) in graphite/epoxy composite. This contact is a consequence of the manufacturing process in which large numbers of individual fibers are wound together to make a tow which is then implanted in the composite.

1.1.4 Resistivity

A few limited measurements of the resistance of graphite/epoxy laminates have been reported by Boeing.⁽⁷⁾ All measurements were made at a frequency of 1 kHz.

The edge-to-edge resistivity of 16-ply and 32-ply laminates were measured with the results listed in Table 1.9. The epoxy surface coating was removed from the edges and copper contacts deposited by plating.

The volume resistivity of 4-ply, 16-ply and 32-ply laminates were also measured using a pressure contact method. The resistance was measured as a function of pressure until linear slope was obtained. Such a slope was presumed to indicate a good electrical contact. The resistance at zero pressure was then determined by extrapolation. The resulting resistivities are given in Table 1.10.

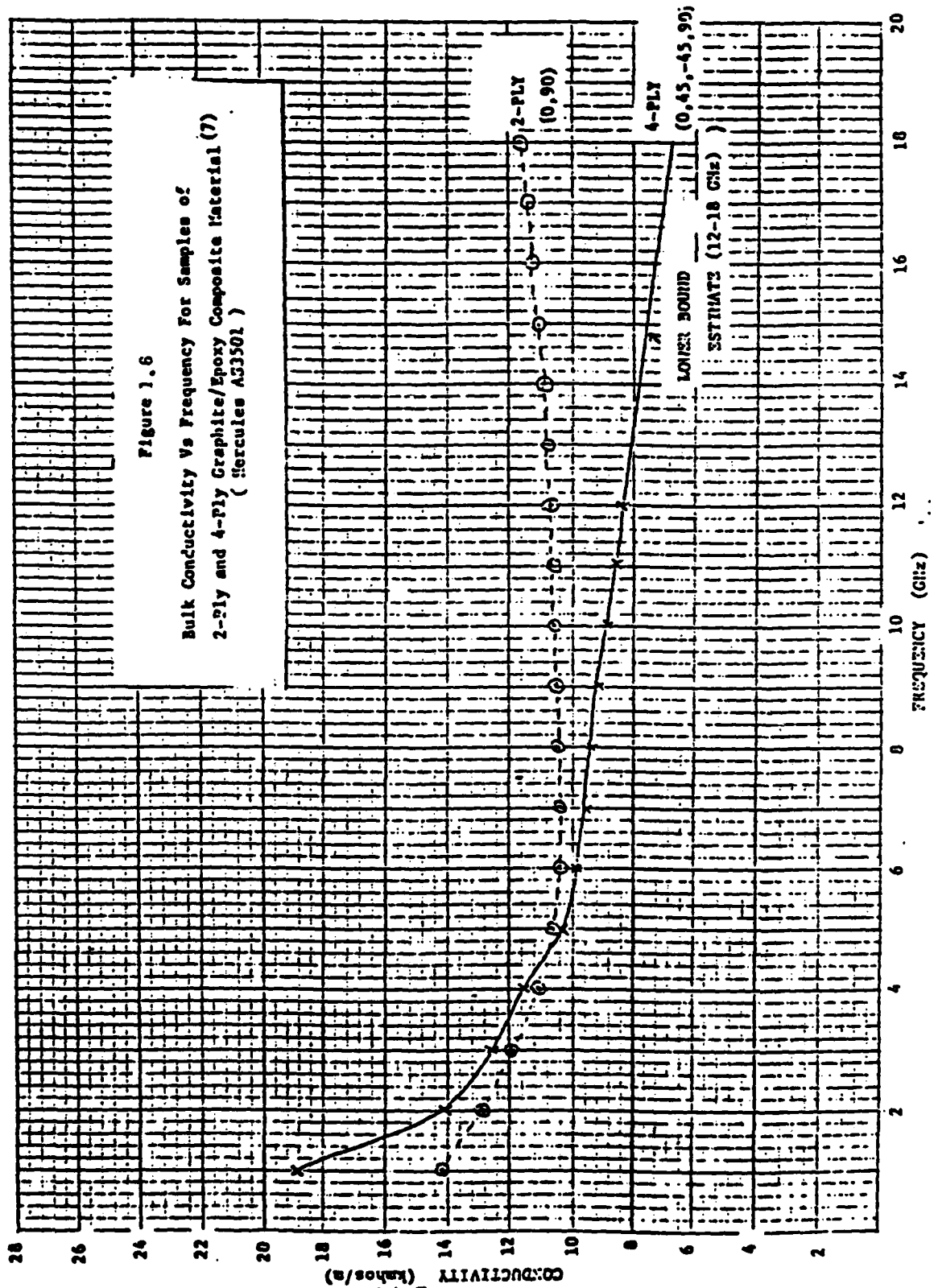
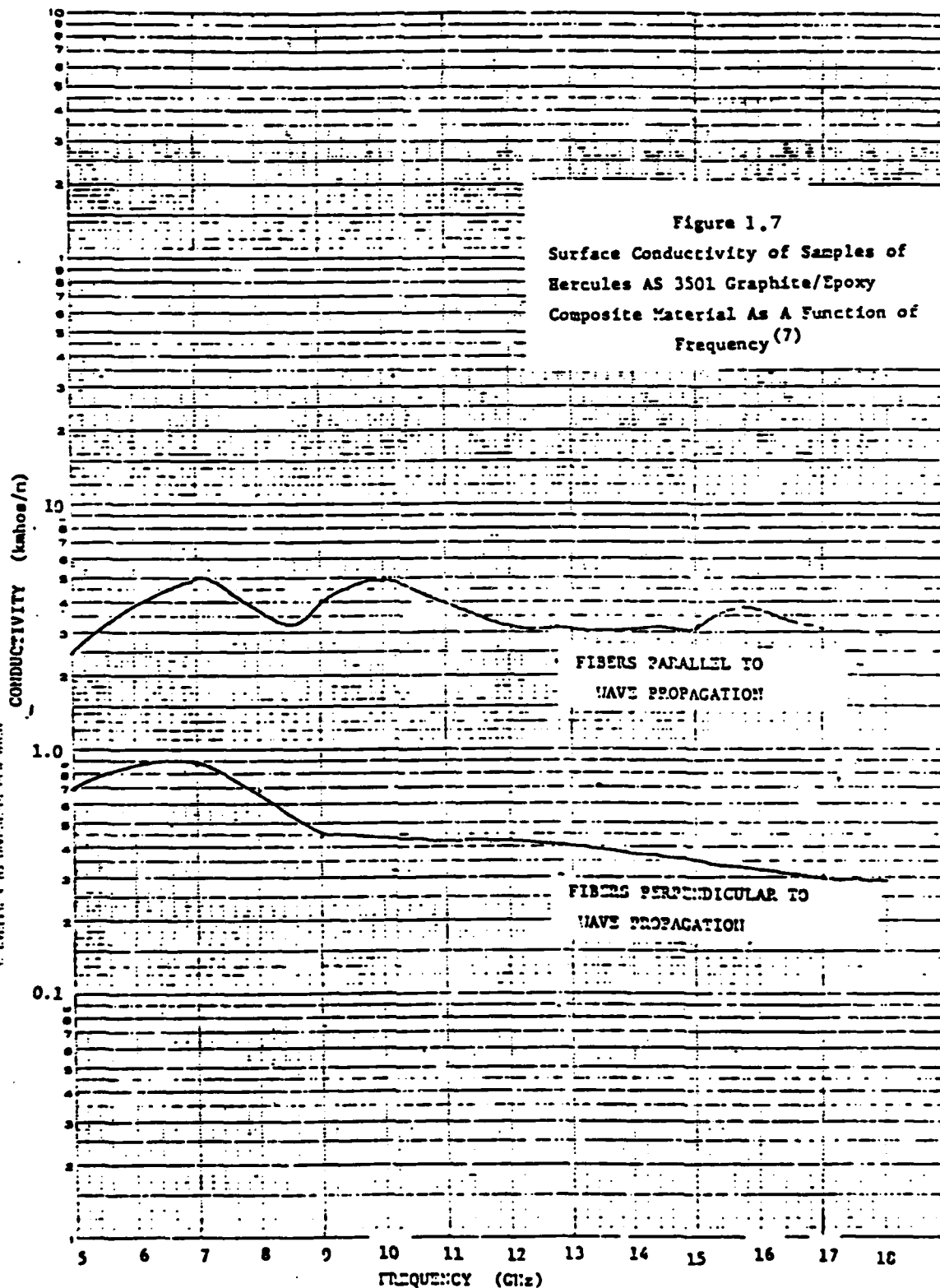


FIGURE 1.7

REU. 2-60 15100 MEASUREMENT SYSTEM
 BY THE INSTRUMENTATION
 DIVISION OF THE AIR FORCE



PLY THICKNESS	EDGE-TO-EDGE RESISTIVITY ρ (ohms/m)
16	64.3×10^{-6}
32	65.7×10^{-6}

Table 1.9. Edge-to-Edge Resistivity of Graphite/epoxy as a Function of Ply Thickness at 1 kHz.(7)

PLY THICKNESS	VOLUME RESISTIVITY ρ (ohm/m)
4	82×10^{-3}
16	51.2×10^{-3}
32	45.9×10^{-3}

Table 1.10. Volume Resistivity of Graphite/epoxy as a Function of Ply Thickness at 1 kHz.(7)

It proved impossible to uniquely define a surface resistivity at 1 kHz for the laminates used. At this frequency the skin depth or penetration of the radiation is far larger than the laminate thickness. All "surface" resistances are then actually volume resistances and show the expected increase in resistance with laminate thickness.

1.2 Improvement of Intrinsic Parameters

This section describes the methods currently in use to improve the EM performance of composite materials by changing the intrinsic properties of the composite. All methods fall under the general headings of doping of the composite fibers and intercalation of the composite layers. Most efforts to date have concentrated on increasing the composite conductivity in order to better approximate the properties of a metal. The basic constraint that must be observed in any method of change the intrinsic EM properties of a composite is that the mechanical properties should not be degraded in the process. This immediately rules out increasing fiber-to-fiber contact in a composite to increase the conductivity because microbuckling in the composite will greatly increase and the mechanical strength will correspondingly decrease.⁽⁴⁾ Coating the fibers with metallic sheaths to increase conductivity and/or permeability is ruled out for similar reasons and for adding an unacceptable weight penalty. Other methods are required and are discussed in the following sections.

1.2.1 Doping

In semiconductor physics, doping is the process of adding carefully controlled amounts of impurities to certain semiconductor crystals in order to increase electron and hole densities and/or mobilities. The conductivity will then be increased, possibly by many orders of magnitude. In the cases of graphite (crystallized carbon) and boron, their positions in the periodic chart of the elements makes them fairly good candidates for semiconductors. Some supporting evidence is available to support this statement.^(2,3)

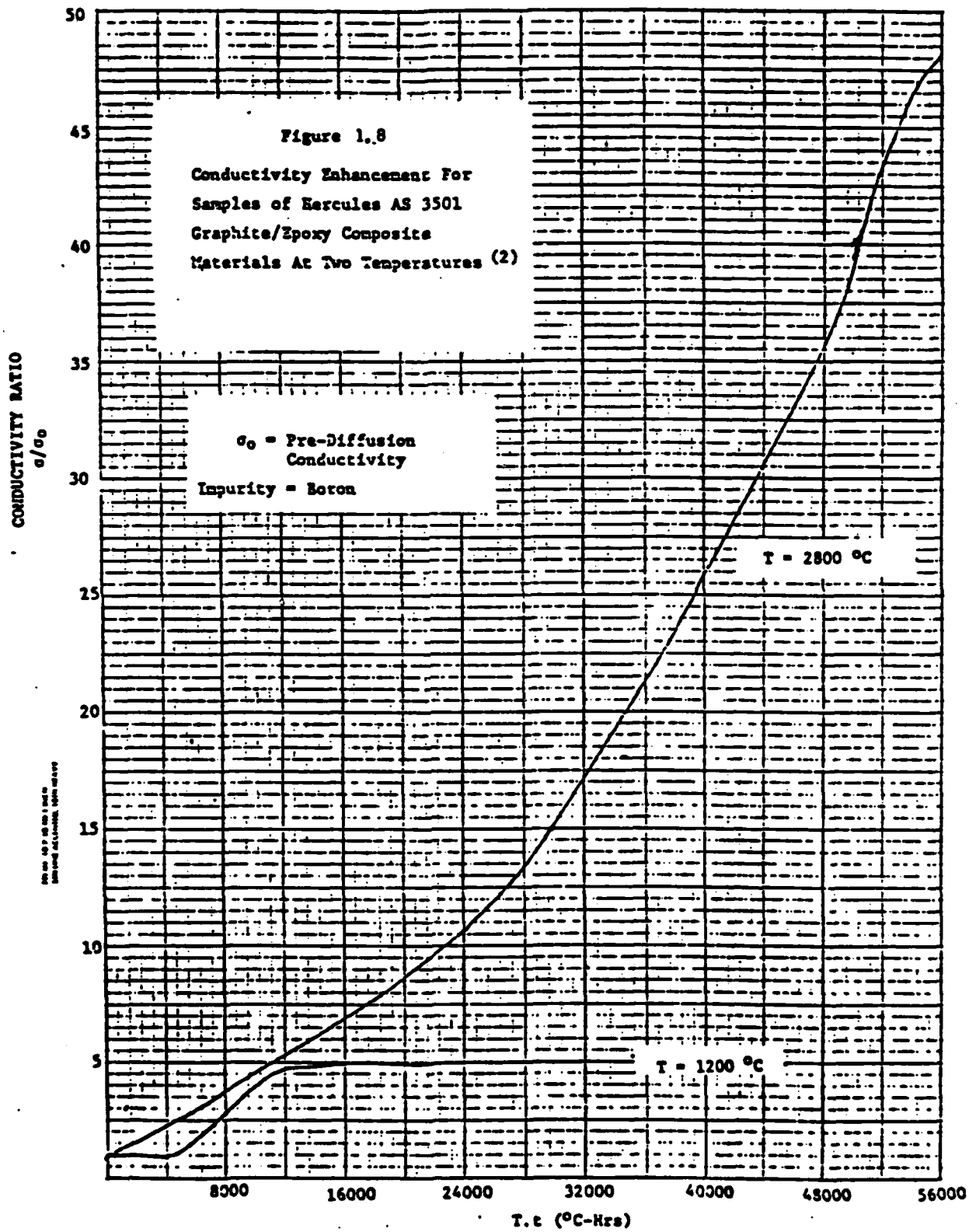
However, most semiconductor activity depends on a high degree of crystalline order. While most details of the manufacturing process of composite fibers are not available, most fibers are not ordered crystals and consequently conductivity improvements by doping techniques can be expected to be less than for crystalline semiconductors. More attention could be given to the fiber manufacturing process in order to optimize the efficiency of the doping process.

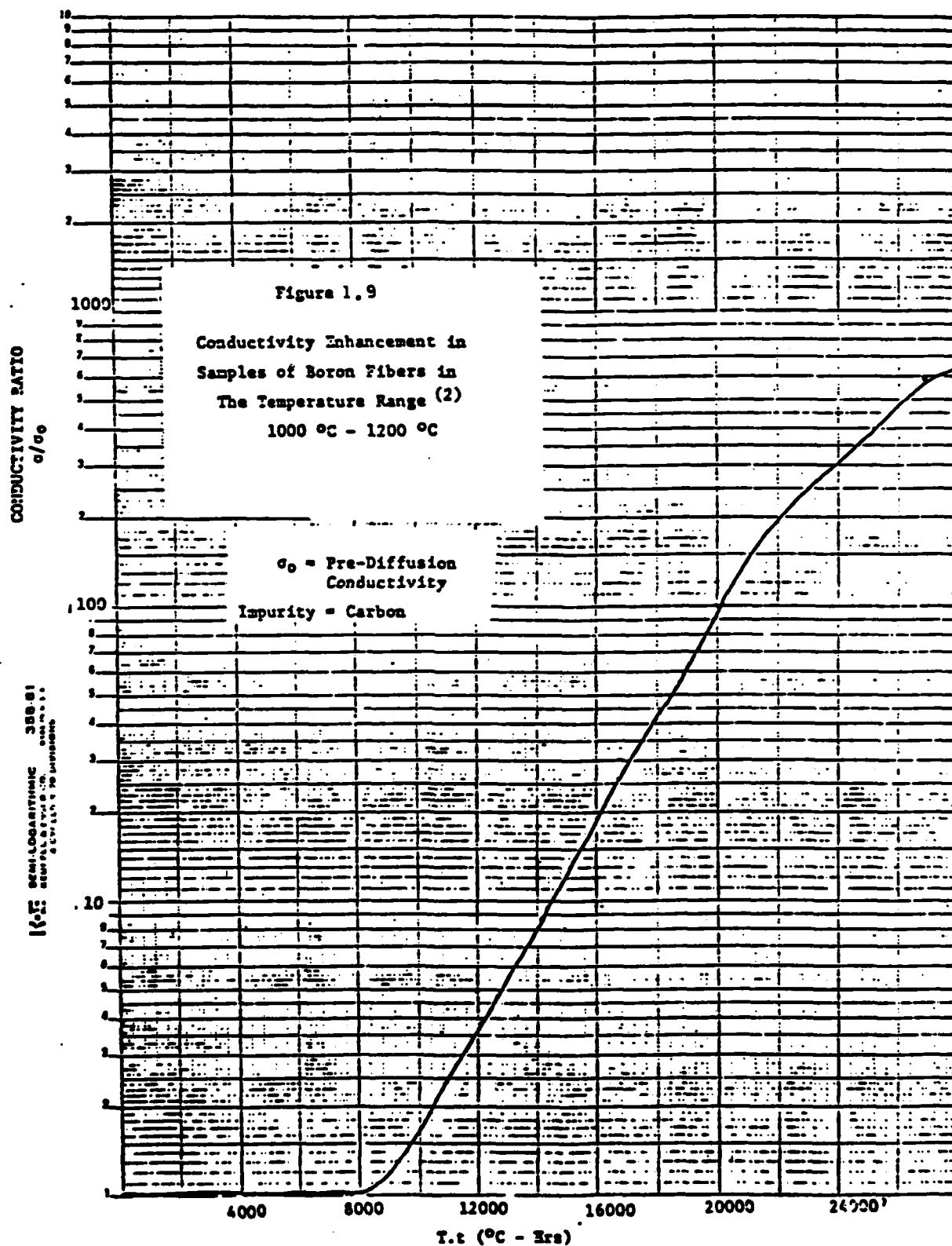
A thermal diffusion process was investigated by Gajda⁽²⁾ to access in a preliminary manner the effects of doping on graphite and boron fibers. The details of the diffusion process are described in ASTM section on Measurements, Testing and Evaluation and in the references.⁽²⁾

One set of experiments involved using borosilicate compounds and boron nitride (BN) as the impurity for graphite fibers. The semiconductor process is the doping of graphite with boron. The experiments were carried out at temperatures up to 1200°C and for as long as 20 hours. A second set of experiments using improved equipment were performed at a temperature of 2800°C. The results are shown in Figure 1.8.

For the lower temperature case, conductivities were not increased more than a factor of five even after 20 hours of baking in the diffusion oven. At the higher temperature conductivity increased by a factor of 50 with some fiber conductivities reading 10^6 mhos/m.

Only a few experiments were done with boron doped with carbon due to the difficulties with proper ohmic contacts. The first experiments were run at 1000°- 1200°C for up to 20 hours. The results are given in Figure 1.9 and show significant increases in conductivity.





1.2.2 Intercalation⁽⁸⁻¹⁰⁾

One procedure that holds great promise for increasing the conductivity of graphite/epoxy composite is the intercalation of graphite fibers with various metallic or non-metallic molecular species. The intercalation process is very much dependent for its success upon the physical and chemical properties of graphite.

Pure graphite is a crystallized form of carbon whose crystal structure is shown in Figure 1.10. All the carbon atoms are hexagonally packed into individual planar layers. The intra-plane chemical bonds holding the carbon atoms in a given plane are sp^2 hybridized σ -type bonds and are quite strong. These bonds give the planar layer a high degree of stability and order. The various carbon planes are then stacked on top of each other in an ABAB... sequence as shown in Figure 1.10. The inter-plane chemical bonds holding the carbon planes together are π -type bonds and are weak compared to the intra-plane σ -bonds. Because the inter-plane bonds are weak, it is possible to insert various chemical species between the carbon layers to form what are called intercalation compounds. The composition of these compounds is described by stage, the definition of which is portrayed in Figure 1.11.

The molecular species used in the intercalation process are characterized as electron donors or acceptors. Donors are typically metals usually from Group I in the periodic table (the alkali metals). Common choices are potassium, cesium, rubidium and lithium. In addition, many additional compounds that also act as donors can be formed from these metals together with hydrogen and aromatic molecules such as benzene and toluene. Acceptors are usually nonmetallic compounds such as bromine, sulphuric acid, nitric acid and halide and oxide compounds. The intercalation of the graphite fibers is easily accomplished by simple exposure of the fibers to the liquid or vapor of the intercalant.

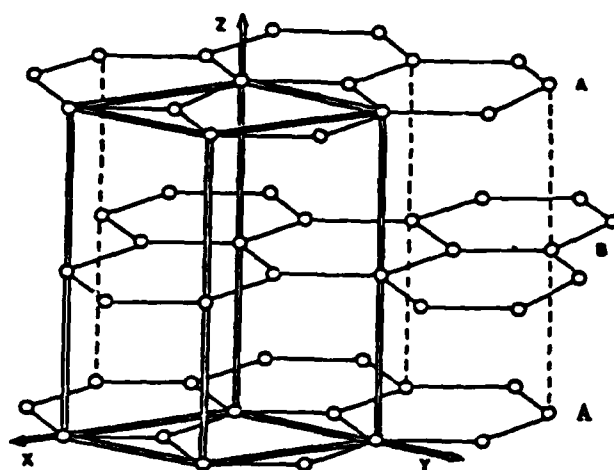


Figure 1.10 Graphite Crystal Structure⁽⁸⁾

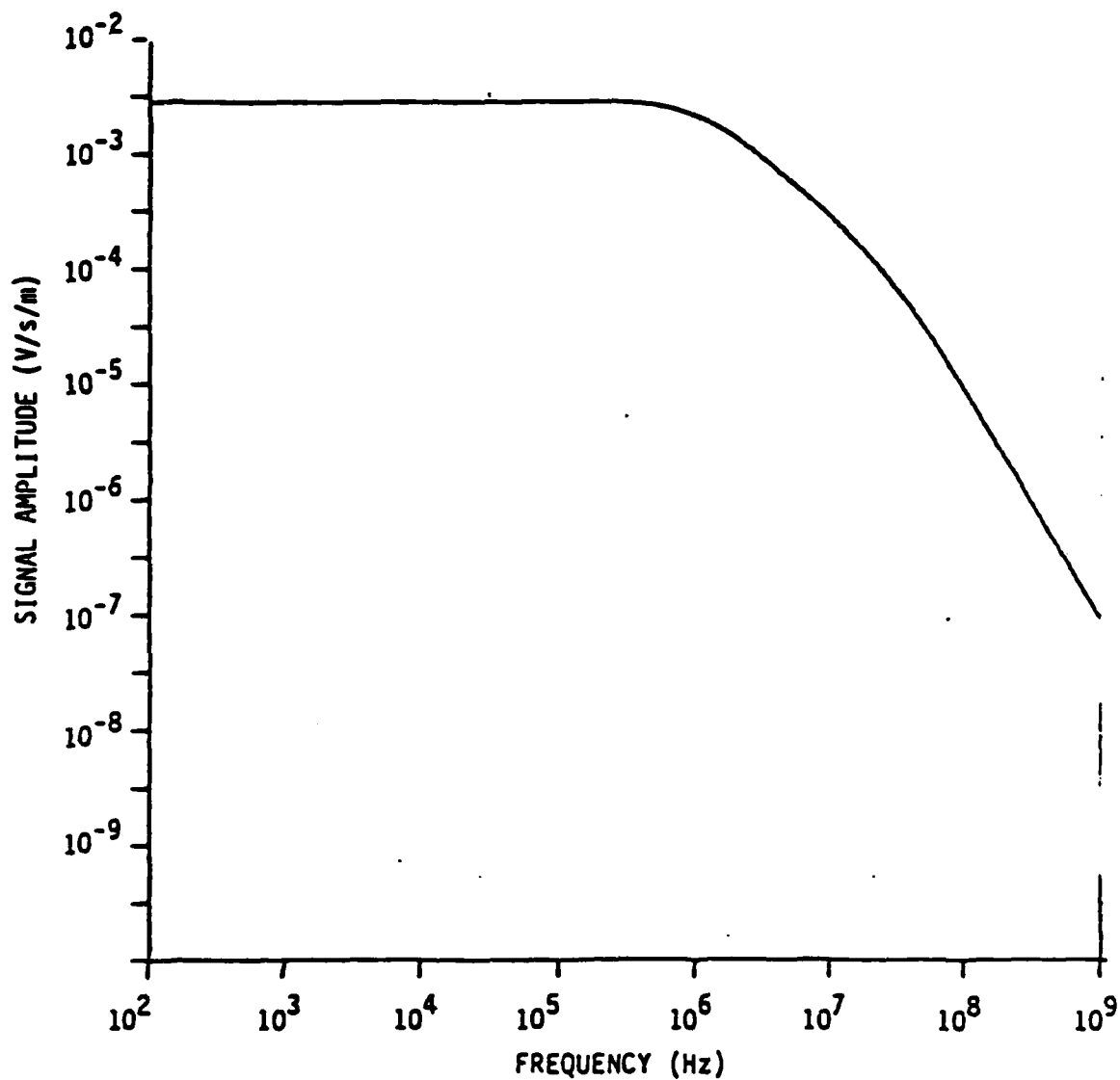


Figure 3.18 EMP in Frequency Domain⁽⁵⁾

A list of conductivities for selected acceptor and doner intercalated graphite compounds is given in Table 1.11 together with the conductivities of pure graphite and various metal conductors. Compared to graphite, doner intercalated graphite increased the inter-plane conductivity by a factor of six to eight while for acceptor intercalated graphite, the increase was a factor of fifteen or more. Intra-plane conductivities are increased for doner compounds and decreased for acceptor compounds. Conductivities of acceptor intercalated graphite are comparable and even superior to conductivities of copper, aluminum and silver.

Less dramatic results are obtained when commercially available graphite fiber is intercalated because the conductivity of such fibers is one to two orders of magnitude below the intra-plane conductivity of pure graphite (see Table 1.8). The fiber may be viewed as a highly defective graphite crystal having lower electron mobility and hence lower conductivity. Conductivities of typical 3-ply graphite/epoxy laminates with and without intercalated fibers are shown in Figure 1.12 as a function of fiber content. For a given fiber filling factor, the intercalated composite is about a factor of twenty to forty times nigner than the regular composite. These results suggest that more attention should be given to the manufacturing process of graphite fibers to have as high a conducting fiber as possible.

An important trade-off to be considered is the effect of intercalation on the graphite/epoxy mechanical properties. Reports of no decrease and significant decrease in tensile strength and elastic modules have been made in the literature⁽⁹⁾ depending on the intercalation process used. It is also possible to enhance certain mechanical properties. Table 1.12 shows the results of intercalating Thornel 75 graphite/fibers with red, fuming nitric acid (HNO_3). There was a 17% average decrease in tensile strength and a 69% average increase in elastic modulus. The tensile strength is sensitive to micro defects in the fibers which act

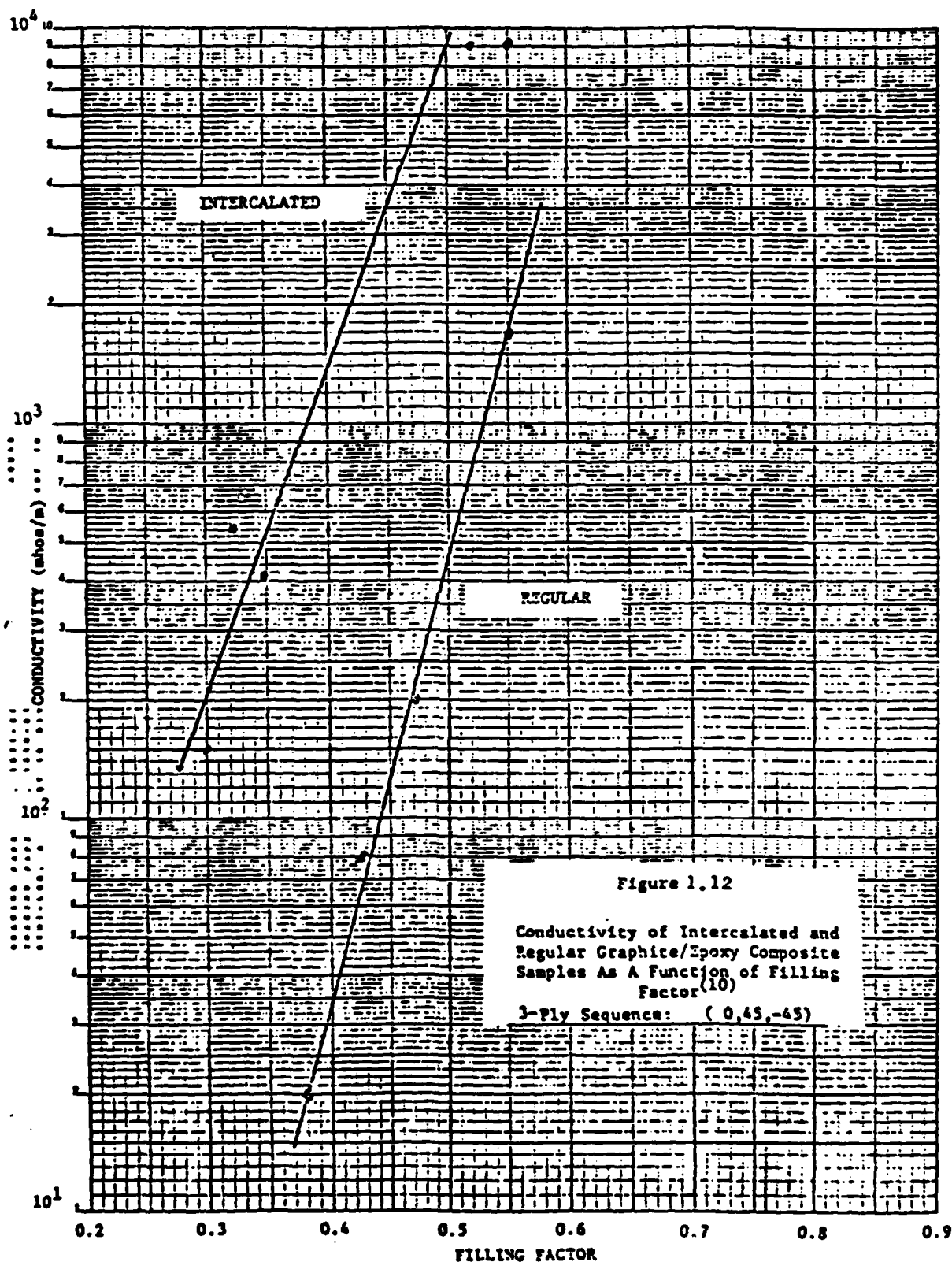


Figure 1.12

Conductivity of Intercalated and Regular Graphite/Epoxy Composite Samples As A Function of Filling Factor⁽¹⁰⁾

3-Ply Sequence: (0,45,-45)

Table 1.11 Conductivities of Selected Doner and Acceptor Intercalated Graphite Compounds Compared to Pure Graphite and Common Metals⁽⁸⁾

Compound and Stage	Inter-Plane Conductivity σ_a (mhos/m)	Intra-Plane Conductivity σ_c (mhos/m)
Doner Intercalated Compounds		
K-1	1.1×10^7	
2	1.7×10^7	
3	2.1×10^7	
Rb-1	1.0×10^7	Range of Values for Doner Compounds is 10^3 - 10^4
2	1.5×10^7	
Cs-1	1.0×10^7	
3	1.2×10^7	
Li-1	1.0×10^7	
Acceptor Intercalated Compounds		
NNO ₃ -1	1.7×10^7	200
2	3.3×10^7	-
3	2.9×10^7	-
4	2.4×10^7	-
AsF ₅ -1	5.0×10^7	23
2	6.3×10^7	24
3	5.8×10^7	26
SbF ₅ -1	3.5×10^7	-
2	4.0×10^7	-
3	1.0×10^7	-
6	5.8×10^7	-
FeCl ₃ -1	1.1×10^7	1000
2	2.5×10^7	-
Common Conductors		
Copper	5.9×10^7	-
Aluminum	3.8×10^7	-
Silver	6.3×10^7	-
Pure Graphite	2.6×10^6	10-1000

Table 1.12 Changes in Mechanical Properties of Thornel
75 Graphite Fibers after Intercalation with HNO_3 ⁽⁹⁾

Sample	Conductivity (mhos/m)		Tensile Strength (psi)		Modulus (psi)	
	Initial	Final	Initial	Final	Initial	Final
1.	1.3×10^5	1.4×10^6	4.5×10^5	2.5×10^5	82×10^6	99×10^6
2.	1.7×10^5	1.3×10^6	4.0×10^5	3.8×10^5	65×10^6	108×10^6
3.	1.5×10^5	1.1×10^6	2.6×10^5	2.3×10^5	42×10^6	92×10^6

as concentrators of stress. Fuming, red nitric acid etches out surface impurities leaving voids in the fiber which act as defects. The elastic modulus is sensitive to the crystal perfection. Intercalation serves to reorder the ABAB...graphite crystal pattern to AAA... on either side of the intercalated layer. The result is a greater crystal perfection and a higher modulus.

1.3 Thermal Modification of EM Intrinsic Properties

A preliminary investigation on the temperature dependence of conductivity has been done by Gajda.⁽²⁾ No work on the temperature dependence of the permittivity or permeability has been found.

1.3.1 Conductivity

Since graphite and boron display semiconductor behavior to some extent, it is useful to display a conductivity vs. temperature curve for a typical semiconductor. Such a curve is shown in Figure 1-13 and is composed of three regions: intrinsic, extrinsic and freeze out. In the intrinsic region, the thermally generated charge carriers are large in number compared to the carriers of the impurity. There is an exponential dependence on the reciprocal of the absolute temperature. The extrinsic region is characterized by the thermal charge carriers being few compared to the impurity charge carriers. The freeze-out region begins typically at 100°K and is not significant here.

Preliminary studies were made with boron fibers whose resistance was measured as a function of temperature. In terms of resistance R, the conductivity σ is given by

$$R = \frac{v}{\sigma} \quad (1-5)$$

where v depends on the fiber geometry and is essentially constant (neglecting thermal expansion effects). The results are shown in Figure 1.14 and show boron to be in the intrinsic range.

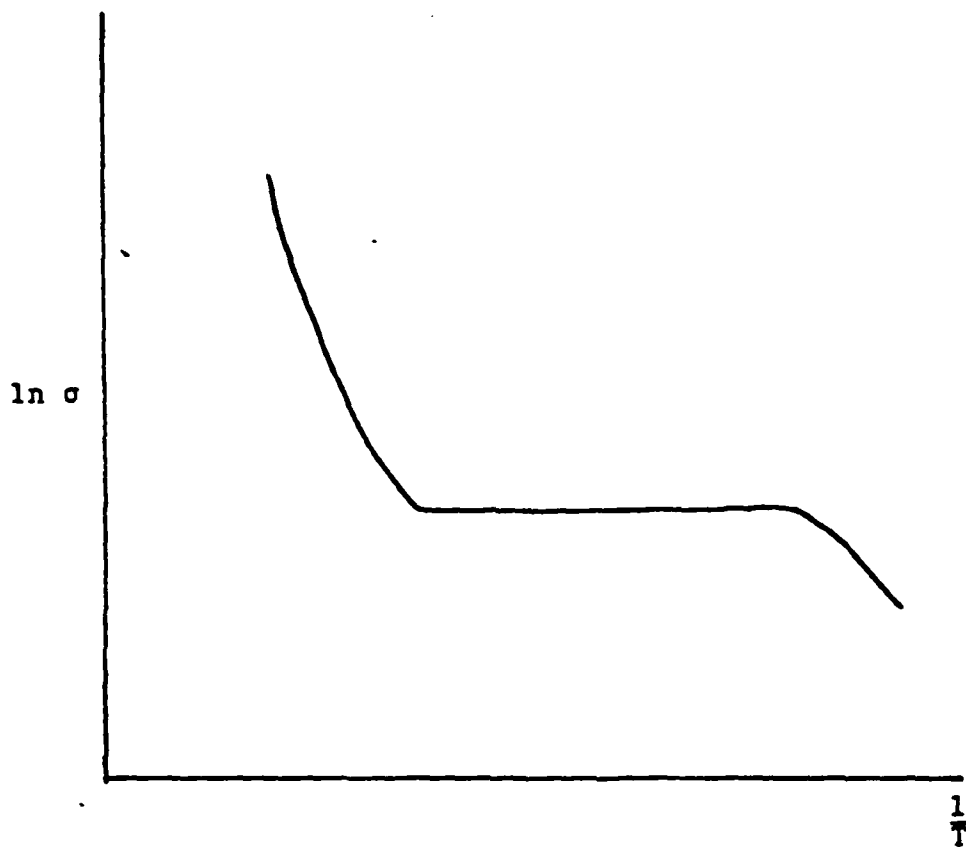
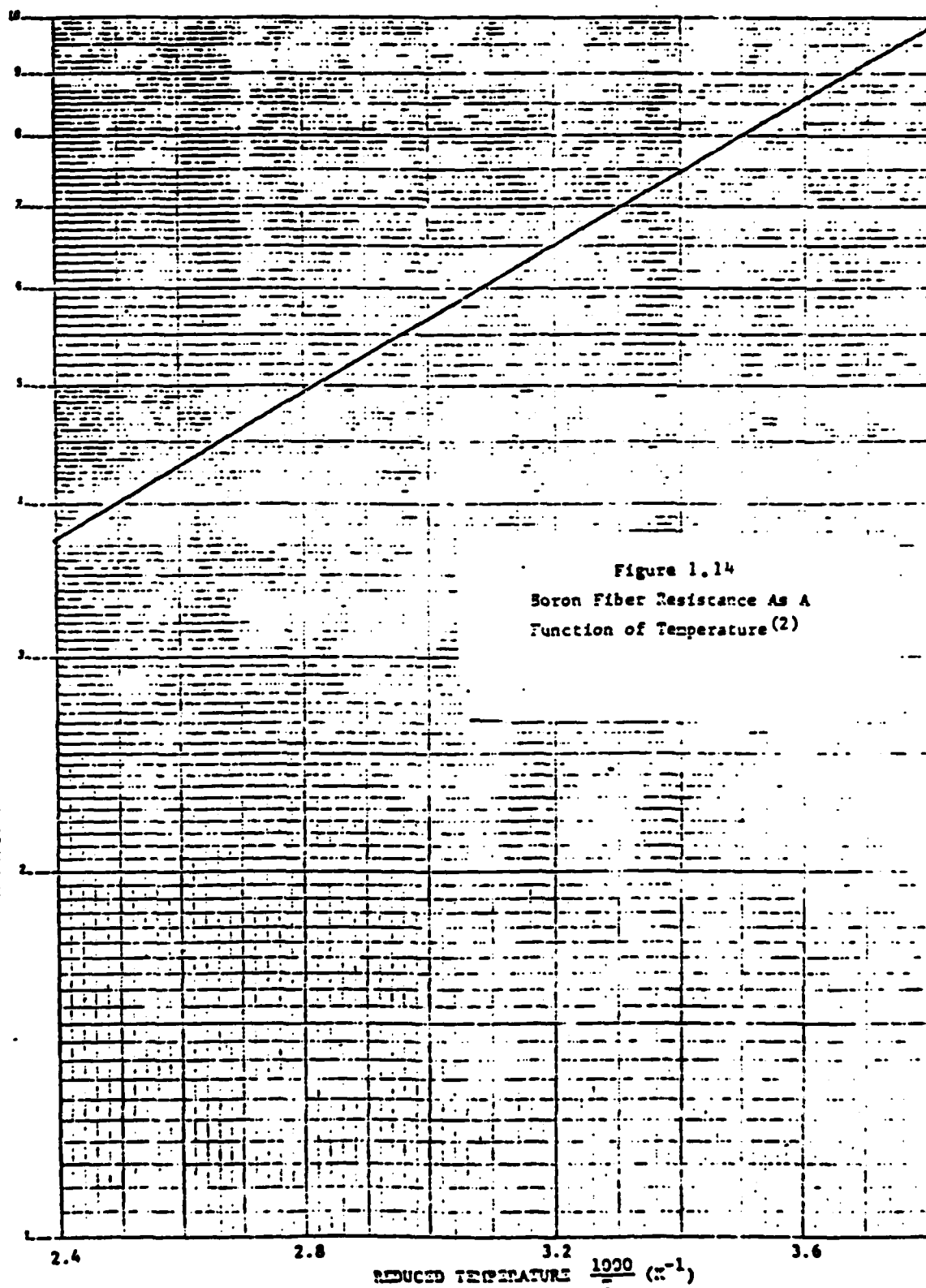


Figure 1-13. Typical Conductivity-Temperature Profile for a Semiconductor⁽²⁾

125 BIRMINGHAM. 46 4073
1941 = " 1941-1942. 1941-1942.
1941-1942 = 1941-1942.



1.4 Environmental Modification of EM Intrinsic Properties

A limited investigation⁽²⁾ on the effects of moisture on the EM properties of composite materials is given in this section.

1.4.1 Moisture

Because of the anticipated exposure of composites to high temperatures and high humidities (e.g., in tropical environments), it is important that the effects of moisture on composites be studied. Most moisture studies have been concerned with its effect on the mechanical properties. One study on the effects of moisture on conductivity of composites has been done by Gajda.⁽²⁾

Samples of Kevlar/epoxy, boron/epoxy and graphite/epoxy were immersed in distilled, deionized water for up to 40 days (to simulate a "worst case" humidity) and their conductivities measured. No changes in Kevlar/epoxy or boron/epoxy were found for any direction of the current. For unidirectional sample of graphite/epoxy (the only samples measured) changes in conductivity were found to occur only in the transverse direction. There was a fairly large decrease in conductivity found and the results are shown in Figure 1-15. One explanation for this behavior is the following. The major mechanical effect of the absorbed water is expansion of the epoxy and a reduction in fiber-to-fiber contact. The transverse conductivity thus decreases.

1.5 Non-Linear Effects

A limited investigation on high field conductivities of graphite/epoxy is given in this section.

1.5.1 High-Field Effects

Non-linear thresholds for unidirectional samples of Narmco 5213 single ply laminates have been determined at D.C. The voltage-current characteristics were determined in the longitudinal and transverse direction. All current was confined to the surface. The voltage-current characteristics are given in Figures 1.15 - 1.17 while the non-linear thresholds are listed in Table 1.18. In the longitudinal case, the current is linear up to the threshold at which time the current is greater than a linear response. In the transverse case the current is less than a linear response after the threshold is passed. The transverse non linearity is explained as local ohmic heating causing a decrease in fiber-to-fiber contact and a subsequent drop in conductance. No explanation is available for the longitudinal non-linearity.

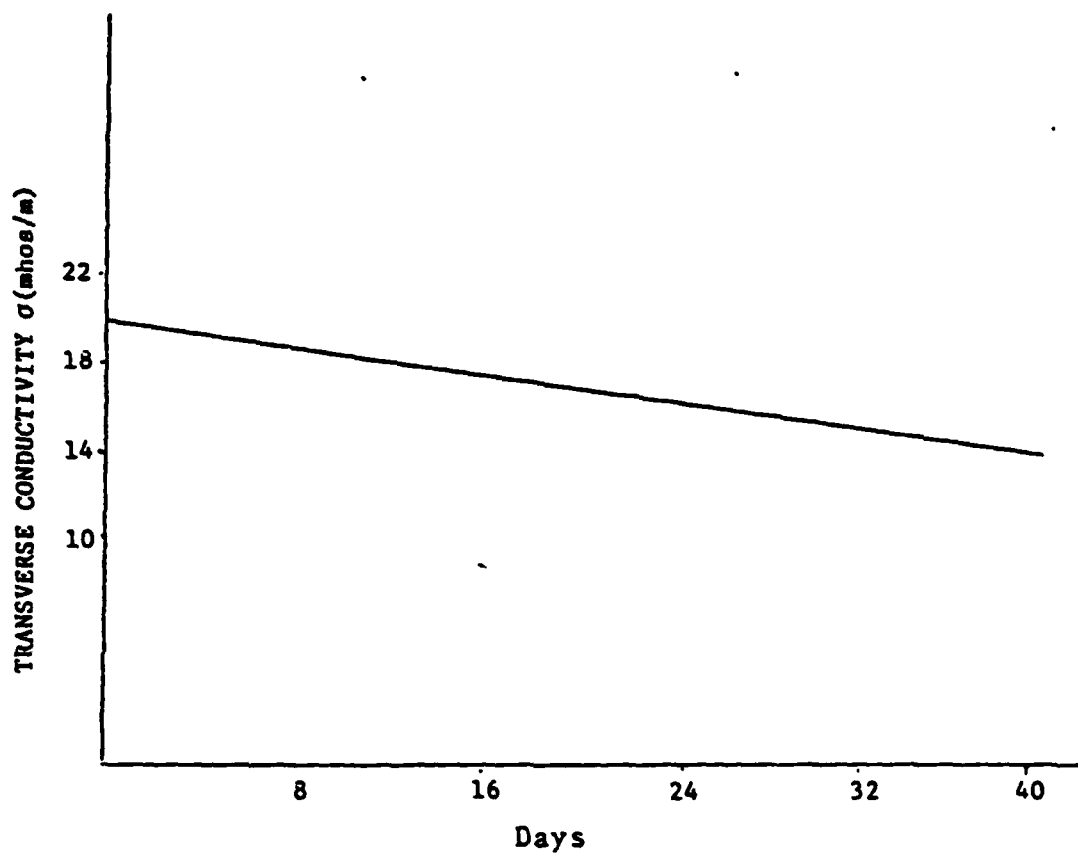


Figure 1.15. Transverse Conductivity of Graphite/epoxy (Unidirectional) as a Function of Immersion Time in Water at 23°C. (2)

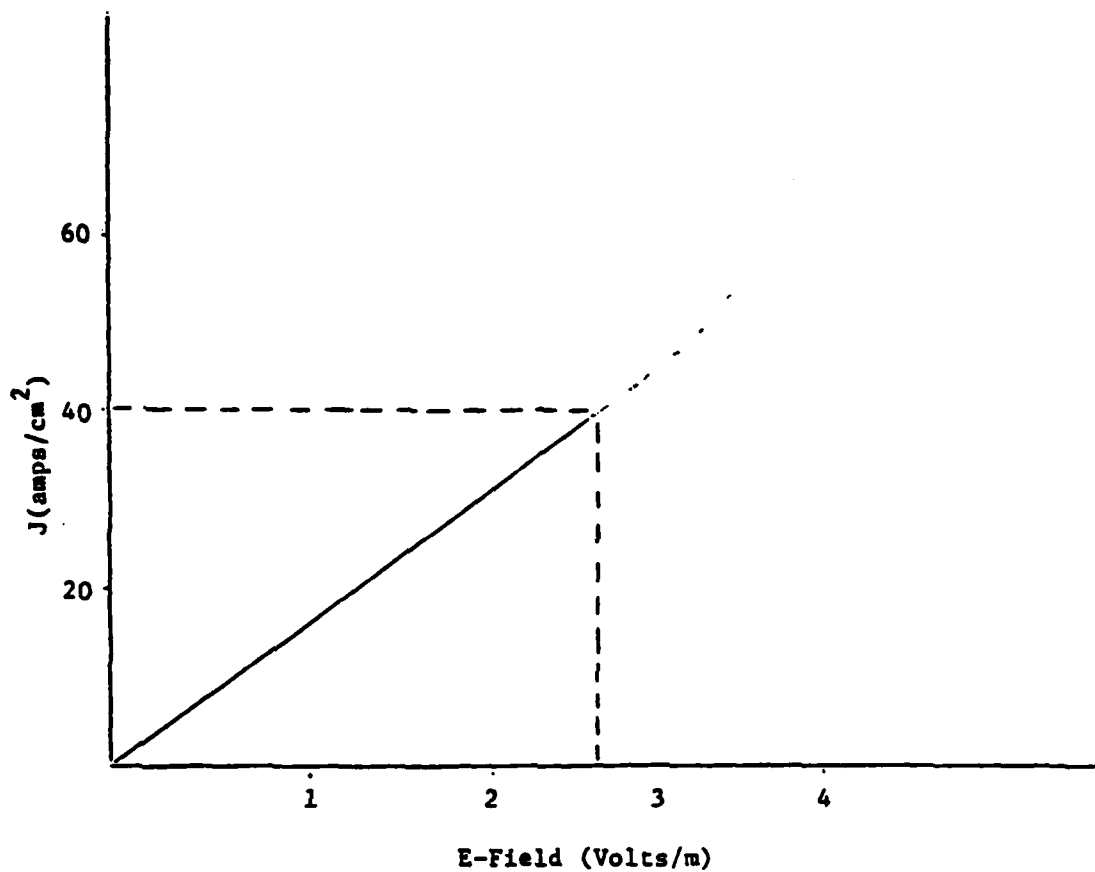


Figure 1.16. Current-field Characteristics for Unidirectional Uni-ply Graphite/epoxy in Longitudinal Direction.^(2.4)

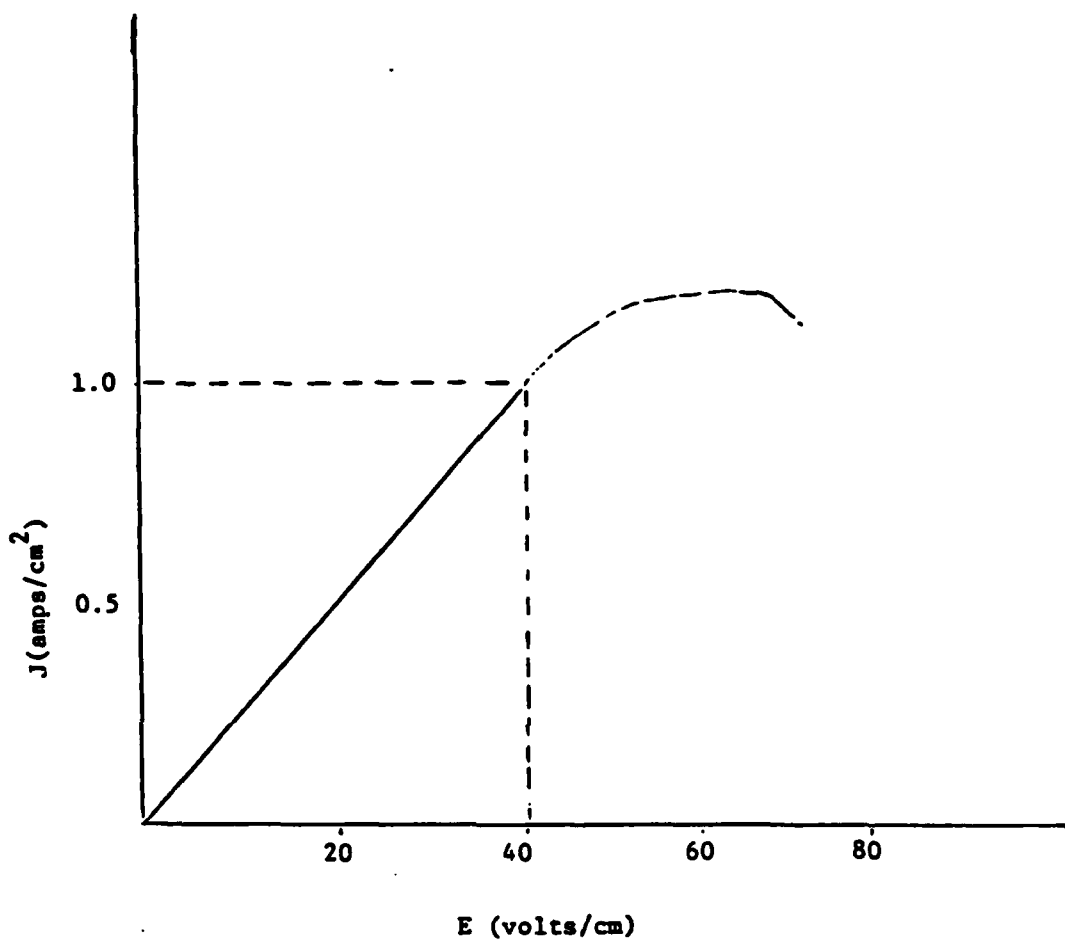


Figure 1.17. Current-field characteristics for unidirectional uni-ply graphite/epoxy in transverse direction^(2,4)

CURRENT DIRECTION	E-FIELD (VOLTS/m)	J (AMPS/m ²) CURRENT DENSITY
LONGITUDINAL	250	4×10^5
TRANSVERSE	4000	1×10^4

Table 1.18. Non-linear Thresholds for Unidirectional Uni-ply Graphite/epoxy. (2)

1.6 References

1. W. J. Gajda, A Fundamental Study of the Electromagnetic Properties of Advanced Composite Materials, RADC-TR-78-158, July 1978.
2. W. J. Gajda, Measurement of the Electrical Properties of Composite Materials in the Frequency Range of D.C. to 30 MHz.
3. J.L. Allen et.al, Electromagnetic Properties and Effects of Advanced Composite Materials: Measurement and Modeling, RADC-TR-78-156, June 1978.
4. W.F. Walker and Roger E. Heintz, Measurement of Electrical Conductivity in Carbon/Epoxy Composite Material Over the Frequency Range 5MHz to 2.0 GHz, RADC-TR-79-255, October 1979.
5. A Technology Plan for Electromagnetic Characteristics of Advanced Composites, RADC-TR-76-206, July 1976
6. R. Force, P. Green et. al., Investigation on Effects of Electromagnetic Energy on Advanced Composite Aircraft Structures and Their Associated Avionic/Electrical Equipment, Phase II, Vol. I Boeing Aircraft Corp. (D180-20186-4), September 1977.
7. Vogel, F.L., Intercalation Compounds of Graphite, Molecular Metals, Plenum Publishing Co., 1979.
8. Vogel, F.L., Carbon, 14, 175 (1976).
9. Vogel, F.L., Some Potential Applications for Intercalations Compounds of Graphite with High Electric Conductivity (to be published)

2.0 COMPOSITE MATERIAL SHIELDING EFFECTIVES TRANSFER IMPEDANCE AND JOINT ADMITTANCE

Figure 2.1 compiles published electrical and magnetic shielding effectiveness of composite materials. The high electrical shielding effectiveness at low frequencies is caused by the measurement fixture, consequently the data published is that of the fixture. The low frequency magnetic shielding allows sizeable coupling, consequently the magnetic shielding is not affected by the fixture and published data has general agreement. Airframe shape also influences shielding effectiveness rendering shielding effectiveness to be a confusing electromagnetic parameter. Transfer impedance Z_{st} overcomes these difficulties and should be used in lieu of shielding effectiveness.

In this chapter shielding effectiveness and transfer impedance are formulated to easily evaluated formulas. Shielding effectiveness $S_E S_H$ is related to transfer impedance Z_t and airframe shape. It is then shown how well this theory relates to empirical data. Finally a brief discussion is given on the effect of joint coupling on shielding.

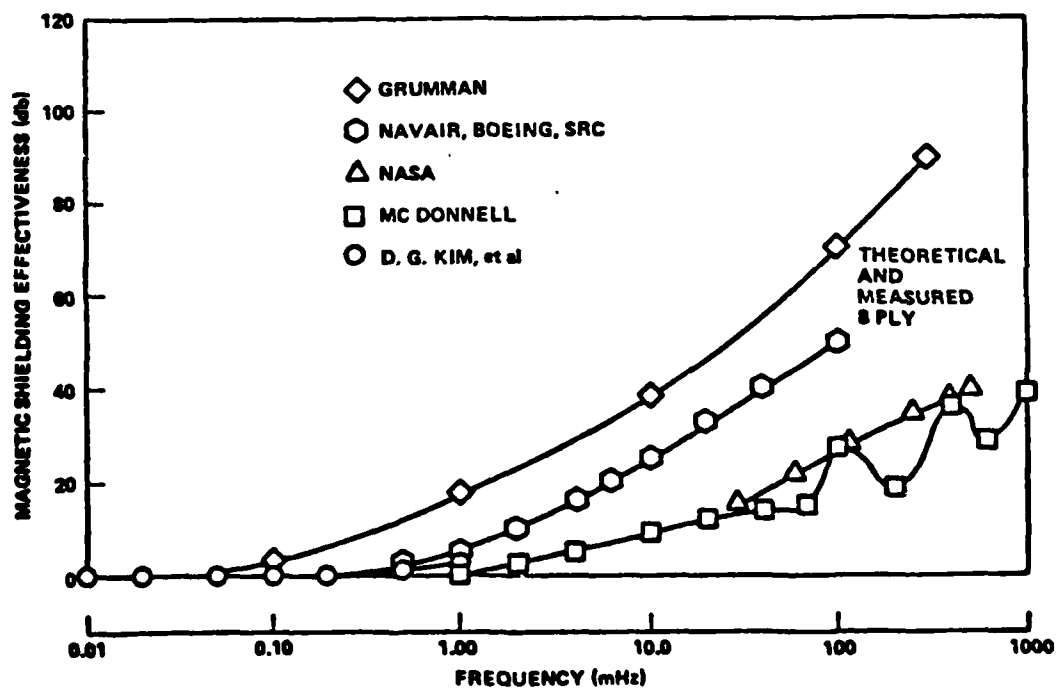
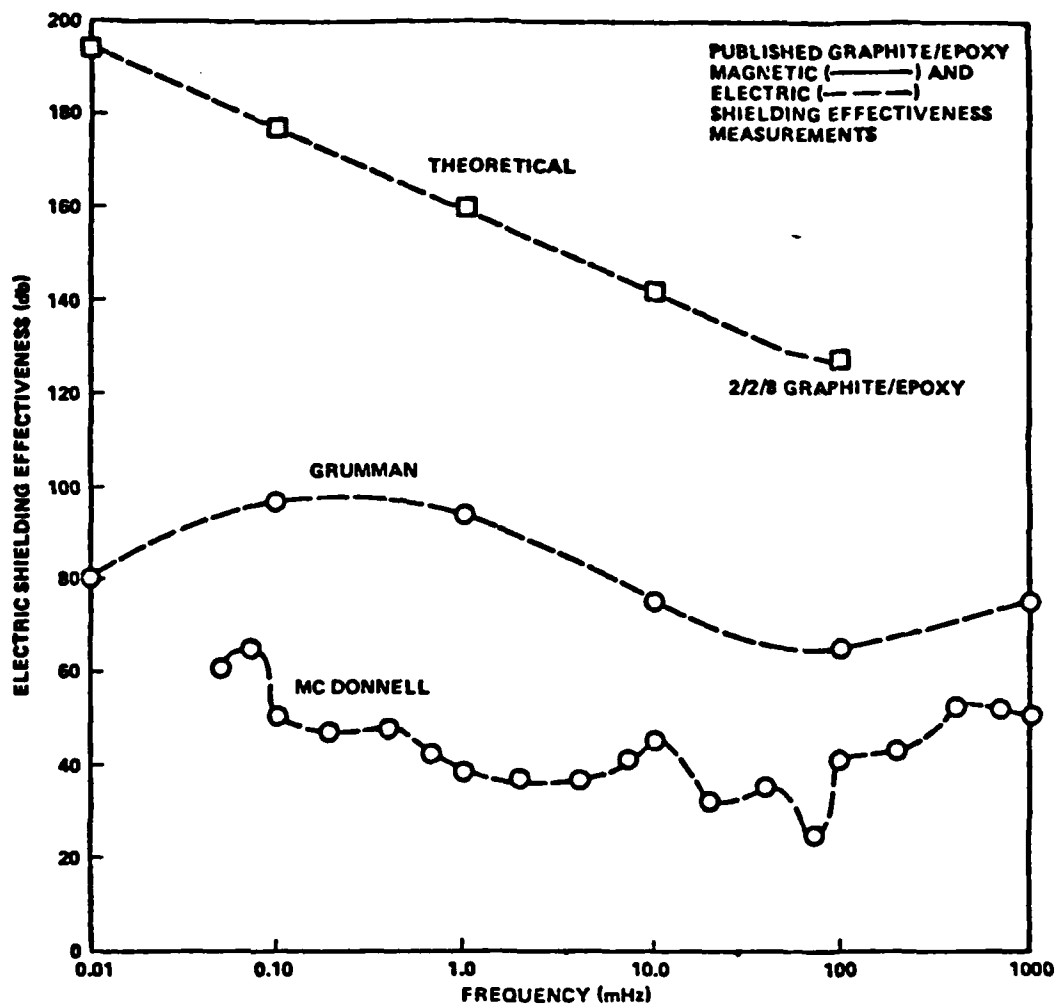


Figure 2.1 Published graphite/epoxy magnetic and electric shielding effectiveness

2.1 Shielding Effectiveness - Theoretical Considerations

Composite air frames, equipment boxes, etc., generally afford less EM shielding than their metal counterparts. The shielding effectiveness of composite enclosures is generally a function of enclosure shape and internal complexity (e.g., devices, tables, support structures) as well as the composite thickness, and constitutive parameters, and frequency and direction of excitation and source location and type. In this section a general discussion of shielding effectiveness for composite airframes is presented.

Shielding effectiveness, for plane wave penetration of an infinite flat, isotropic, homogeneous material with identical media on either side, has been defined by Schelkunoff as^(1,2)

$$S = -20 \log|T|$$

where T is the normal incidence transmission coefficient derived by Schelkunoff from analogy with transmission line theory as

2.1.1 Shielding Effectiveness For a Uniform Magnetic Field

The magnetic shielding effectiveness is commonly⁽³⁾ defined by the expression.

$$MSE = 20 \log_{10}|MSR^{-1}|$$

where the inverse magnetic shielding ratio, MSR^{-1} , is given by

$$MSR^{-1} = \frac{H_{INCIDENT}}{H_{INTERIOR}}$$

and $H_{INCIDENT}$ and $H_{INTERIOR}$ are the H-fields incident on the shield and interior to the shield respectively. A general problem with this definition is that it is very dependent on shield geometry and is not unique to the material and the incident radiation. For uniform magnetic fields and certain geometric shapes, the magnetic shielding effectiveness can be characterized uniquely.

2.1.1.1 Flat Plate Geometry

The exact expression for the magnetic shielding effectiveness is⁽³⁾

$$MSE = 20 \log_{10} \left| \cosh(\gamma d) + \frac{377}{\eta} \sinh(\gamma d) \right| \quad (2-1)$$

where

$$\gamma = [j\omega\mu\sigma]^{1/2}$$

$$\eta = [j\omega\mu/\sigma]^{1/2}$$

d = shield thickness

For low frequencies, the magnetic shielding effectiveness in (2-1) can be well-approximated by

$$MSE \approx 20 \log_{10} |1 + 377\sigma d|$$

where the frequency f satisfies

$$f < \frac{0.1}{2\pi\mu\sigma d^2}$$

The low frequency shielding effectiveness is determined by the shield thickness and conductivity, i.e., material parameters only.

For $f < \frac{0.1}{2\pi\mu\sigma d^2}$ the shielding effectiveness increases sharply with frequency as in (2-1).

2.1.1.2 Enclosure Geometries

For enclosure geometries such as parallel plates, cylindrical shells and spherical shells, the magnetic shielding effectiveness can be written as: (3)

$$MSE = 20 \log_{10} \left| \cosh(\gamma d) + \frac{V}{S} \gamma \sinh(\gamma d) \right| \quad (2-2)$$

where $\frac{V}{S}$ is the volume-to-surface ratio in MSK units of the enclosure.

$$\text{For low frequencies satisfying} \quad f < \frac{0.1}{2\pi\mu\sigma d^2}$$

the magnetic shielding effectiveness in (2-2) can be written as:

$$MSE \approx 20 \log_{10} \left| 1 + \frac{V}{S} \gamma^2 d \right| \quad (2-3)$$

For the enclosure geometries, the magnetic shielding effectiveness depends on the incident magnetic field frequency and the enclosure geometry (expressed as $\frac{V}{S}$) as well as the material parameters (σ and d) of the shield. At a frequency given by

$$f_b = \frac{1}{2\pi(V/S)\mu\sigma d}$$

the magnetic shielding effectiveness in (2-3) has a "break point" below which the shielding effectiveness is essentially zero above this frequency, the shielding effectiveness increases as

$$20 \log_{10} \left(\frac{f}{f_b} \right)$$

For high frequencies satisfying

$$f > \frac{0.1}{2\pi\mu\sigma d^2} \quad (2-4)$$

For frequencies less than (2-4), the magnetic shielding effectiveness is given by

$$MSE = 20 \log_{10} \left| \cosh(\gamma d) + \frac{1}{3} \left(\frac{j\omega\mu R}{\eta} + \frac{2\eta}{j\omega\mu R} \right) \sinh(\gamma d) \right| \quad (2-5)$$

2.1.2 Shielding Effectiveness For a Uniform Electric Field

In analogy with magnetic shielding effectiveness, electric shielding effectiveness can be defined as

$$ESE = 20 \log_{10} | ESR^{-1} | \quad (2-6)$$

where the inverse electric shielding ratio is

$$ESR^{-1} = \frac{E_{INCIDENT}}{E_{INTERIOR}}$$

The same problems infect this definition of electric shielding as for magnetic shielding. Following Schelkunoff, (2-6) can be written as

$$ESE = A + R + B$$

where A is absorption loss, R is reflection loss and B accounts for loss due to multiple reflections in thin shields.

For a planar interface, the absorption loss is given by

$$A = 8.686 \frac{d}{\delta} \quad (2-7)$$

where d is the shield thickness and δ is the skin depth. Since

$$\delta = \sqrt{\frac{2}{\omega\mu\sigma}} \quad (2-7) \text{ becomes}$$

$$A = 8.686 d \sqrt{\frac{\omega\mu\sigma}{2}} \quad (2-8)$$

Reflective losses occur primarily as a characteristic impedance difference between different media. The reflection loss can then be written as

$$B = 20 \log_{10} \frac{4|Z_1|}{|n|} \quad (2-9)$$

where Z_1 is the wave impedance of the media multiple reflection loss (B) is small for incident electric fields due to the large impedance mismatch present.

The inverse electric shielding ratio for enclosures (cylinder, parallel plates and spheres) is

$$ESR^{-1} = \frac{\gamma \sinh(\gamma d)}{(4\pi/\lambda)^2 V/S} \quad (2-10)$$

For frequencies sufficiently low that the skin depth is greater than $\sqrt{20d}$ (d is shield thickness) and

$$\omega < \frac{0.1}{4\sigma d^2}$$

$$ESE = 20 \log_{10} \left[\frac{\sigma d}{8\pi\epsilon(V/S)} \right] - 20 \log_{10} f \quad (2-11)$$

and is primarily reflective loss at frequencies where the skin depth is close to $\sqrt{20d}$ absorption losses become large and grow exponentially. The result is a minimum in the electric shielding effectiveness at a frequency where the skin depth is approximately one-third the shield thickness.

2.1.3

Transfer Impedance as Relation to a Measure of Shielding Effectiveness

The main difficulty with the usual methods of measuring the EM shielding effectiveness of materials, is that the shielding effectiveness so measured depends upon the material geometry as well as the material physical properties. The measured values of shielding effectiveness are then valid only for the geometry of the measurement and cannot be extended to more complex geometries.⁽³⁾

One concept, valid for shields that are thin compared to their radii or curvature and for which the wavelength of the incident EM field within the shield is much smaller than that external to the shield, is that of transfer impedance.⁽³⁾ The surface transfer impedance of a homogeneous conducting shield (also applicable to mixed-orientation graphite/epoxy composites) is given by the ratio of the interior tangential electric field to the exterior current induced by the external field.

$$Z_{st} = \frac{E_t}{J} = \eta \cosh(rd) \quad (2-12)$$

where

$$\eta = [j\omega\mu/\sigma]^{1/2}$$

$$r = [j\omega\mu\sigma]^{1/2}$$

d = shield thickness

The low frequency limit for the surface transfer impedance is

$$Z_{st} = \frac{1}{\sigma d} \quad (w \text{ small}) \quad (2-13)$$

which depends only on material thickness and conductivity.

The surface transfer impedance can be related to the magnetic shielding effectiveness for the case of a uniform magnetic field by the relation⁽³⁾

$$MSE = 20 \log_{10} \left| \frac{Z}{Z_{st}} \right| \quad (2-14)$$

where

$$Z = \left(\frac{\mu}{\epsilon}\right)^{1/2} \text{ for flat plate}$$

$$Z = \left(\frac{V}{S}\right) j\omega\mu \quad \text{for a cylindrical, spherical or parallel plate enclosure with volume-to-surface ratio } \frac{V}{S}$$

For a homogeneous conducting enclosure (parallel plates, cylinder or sphere) the surface transfer impedance is related to the electric shielding effectiveness by ⁽³⁾

$$ESE = 20 \log_{10} \left| \frac{Z}{Z_{st}} \right| \quad (2-15)$$

where

$$Z = \frac{j}{8\pi\epsilon f \left(\frac{V}{S}\right)}$$

Both (2-14) and (2-15) are valid over a frequency interval dependent on shield geometry, conductivity and thickness.

The dependence of surface transfer impedance function of frequency is shown in Figure 2.1. Measured surface transfer impedance of 24-ply T-300 Graphite/Epoxy is shown in Figure 2.2.

2.2 Measured and Predicted Composite Shielding Effectiveness

In this section, the shielding effectiveness of graphite and boron composite materials is presented in graphical form as a function of frequency. A comparison is made to the titanium where data is available. Several different composite laminates are considered in several geometrical shapes to show the dependence of shielding effectiveness on the enclosure geometry.

The shielding effectiveness data will be presented in two parts, low frequency data (frequency less than 1 GHz) and a few general comments on trends in higher frequency data.

MATERIAL THICKNESS CORRESPONDS TO 8 PLY COMPOSITE
MATERIAL AT 0.00525 IN/PLY

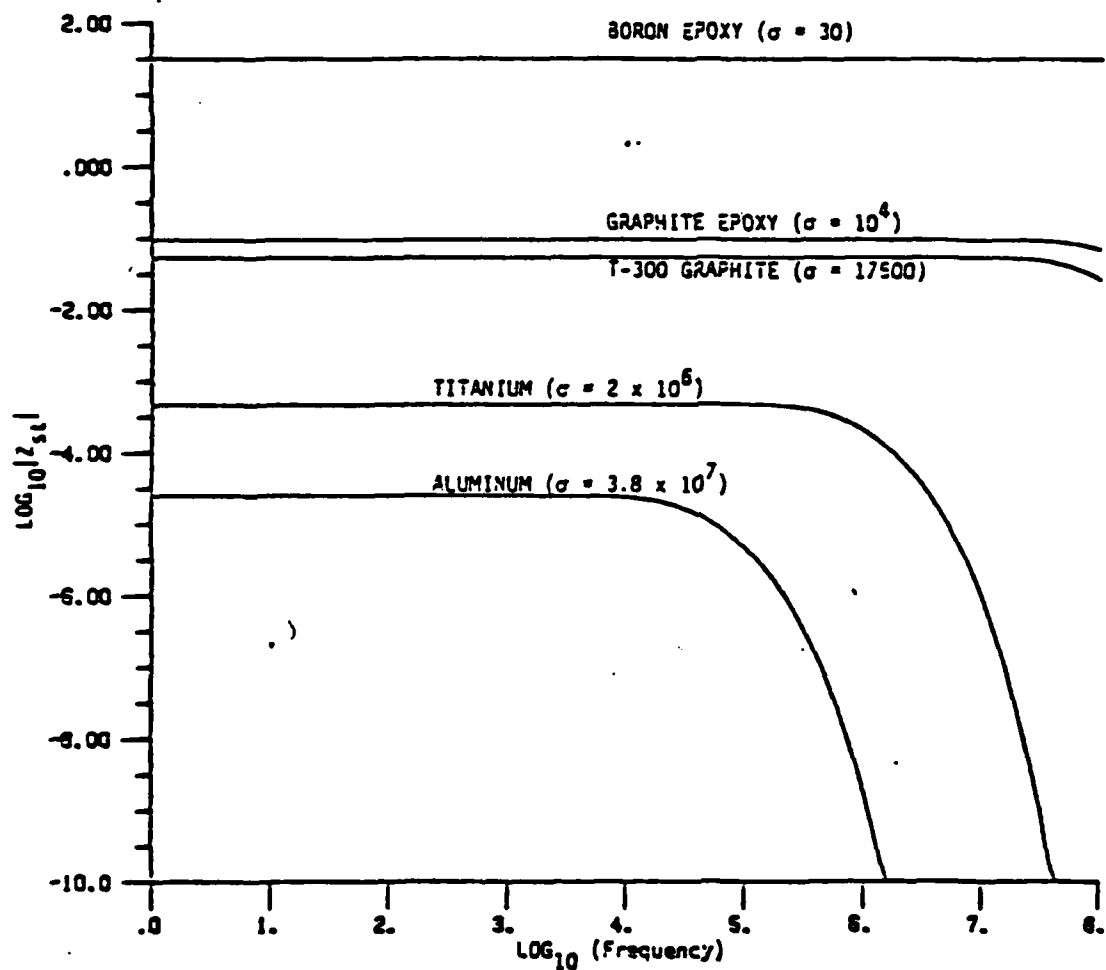


Figure 2.2 Surface Transfer Impedance as a Function of Frequency (3)

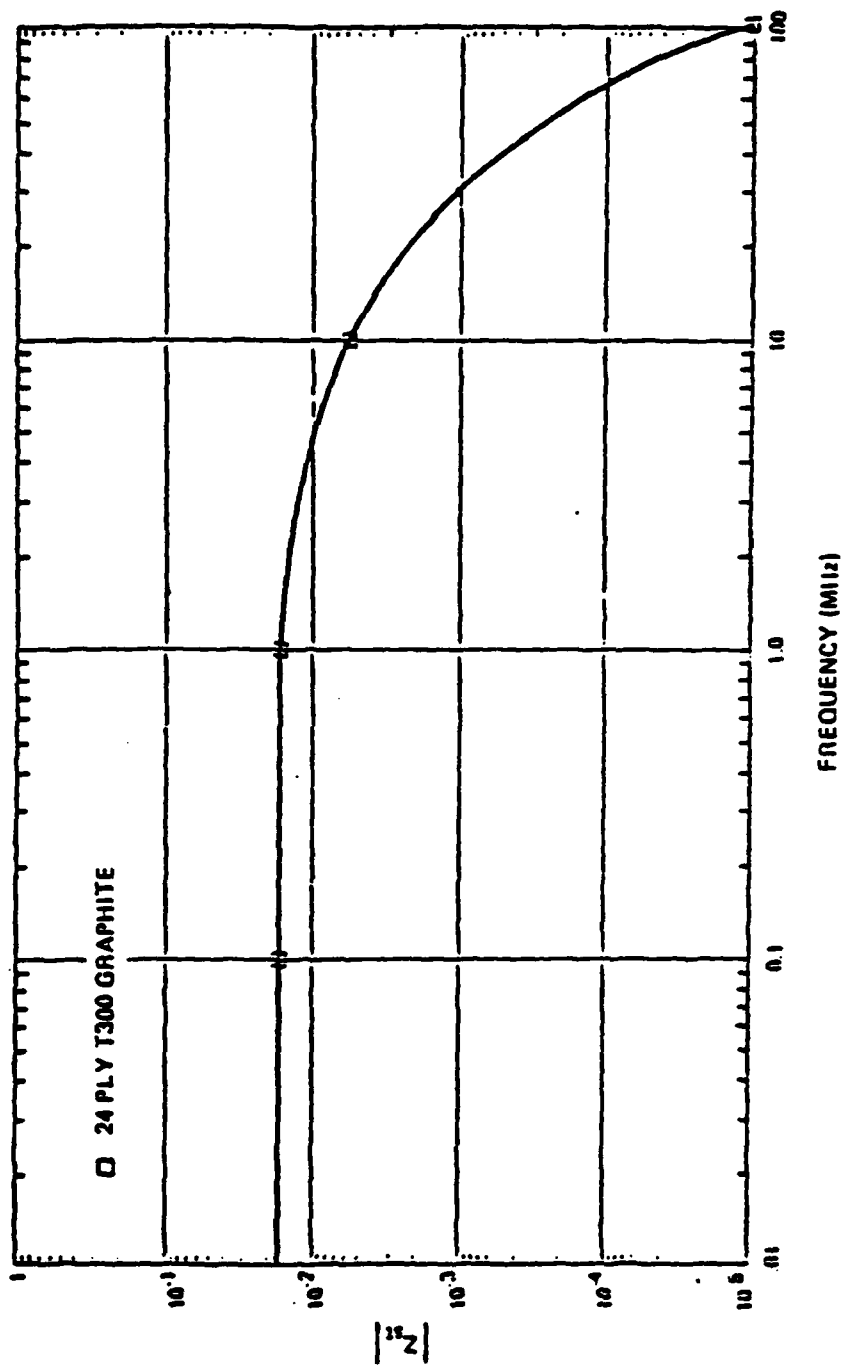


Figure 2.3 Measured Surface Transfer Impedance of 24 Ply T-300 Graphite/Epoxy (3,4)

2.2.1 Low Frequency Shielding

The low frequency shielding data presented in this section is divided into magnetic shielding, electric shielding and plane wave shielding because of their fundamentally different behavior.

2.2.1.1 Magnetic Shielding Effectiveness

The penetration of magnetic fields through aircraft enclosures is most serious at low frequency. Figure 2.4 shows the magnetic shielding effectiveness of composites and metals shaped into flat plates and illuminated by a uniform magnetic field. The shielding in the low frequency limit is determined by the conductivity and shield thickness alone. The metals have highest conductivity and shield most; the composites, having less conductivity, shield correspondingly less.

For an enclosure geometry (parallel plates, cylinder or sphere) the magnetic shielding decreases with frequency sharply to a breakpoint where there is essentially no shielding at all. In Figure 2.4 the magnetic shielding effectiveness of an enclosure is compared to that of a flat plate. Only at about 100 MHz is enclosure shielding as good as that of the plate. The shielding effectiveness also depends upon the shield geometry through the volume-to-surface ratio $\frac{V}{S}$. Figure 2.5 illustrates the shielding effectiveness of an enclosed geometry as a function of $\frac{V}{S}$; a higher $\frac{V}{S}$ yields a better shielding effectiveness for uniform magnetic fields. The breakpoint where magnetic shielding drops to a very small value is shown in Figure 2.6 for a uniform magnetic field. The breakpoint is lower in frequency for higher conducting materials. Consequently metals, such as aluminum and titanium, have the breakeven point lowest in frequency followed by composites.

SHIELD THICKNESS CORRESPONDS TO 8 PLY COMPOSITE
MATERIAL AT 0.00525 IN/PLY

SHIELD CONDUCTIVITY = 10^4 mohs/m

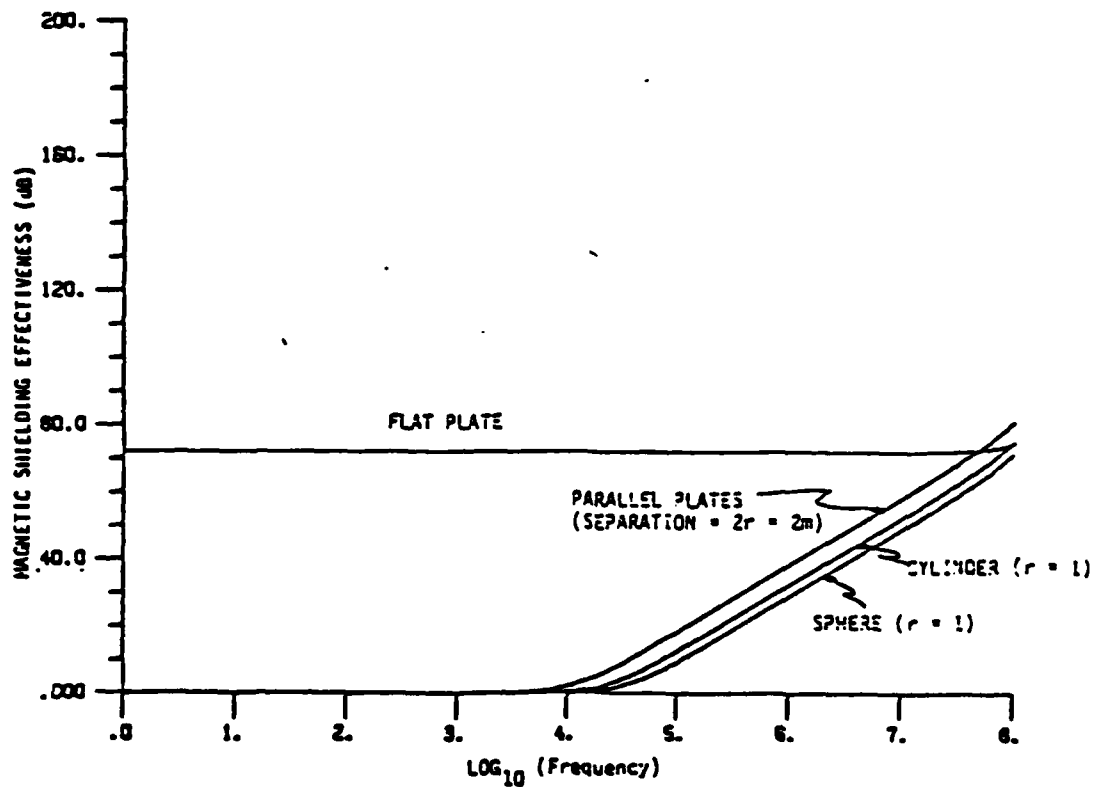


Figure 2.4 Magnetic Shielding Effectiveness With A Uniform Incident Magnetic Field (3)

SHIELD THICKNESS CORRESPONDS TO 8 PLY COMPOSITE
MATERIAL AT 0.00525 IN. THICK

SHIELD CONDUCTIVITY = 10^4 mhos/m

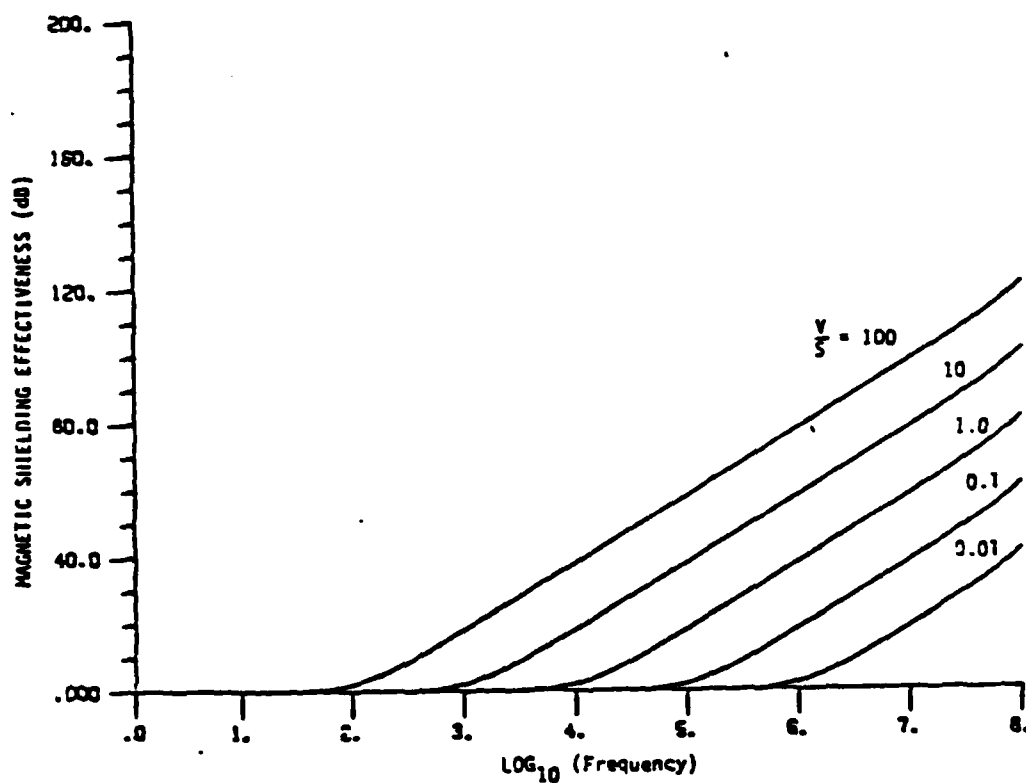


Figure 2.5 Magnetic Shielding Effectiveness of an Enclosure under a Uniform Magnetic Field as a Function of Volume-to-Surface Ratio (3)

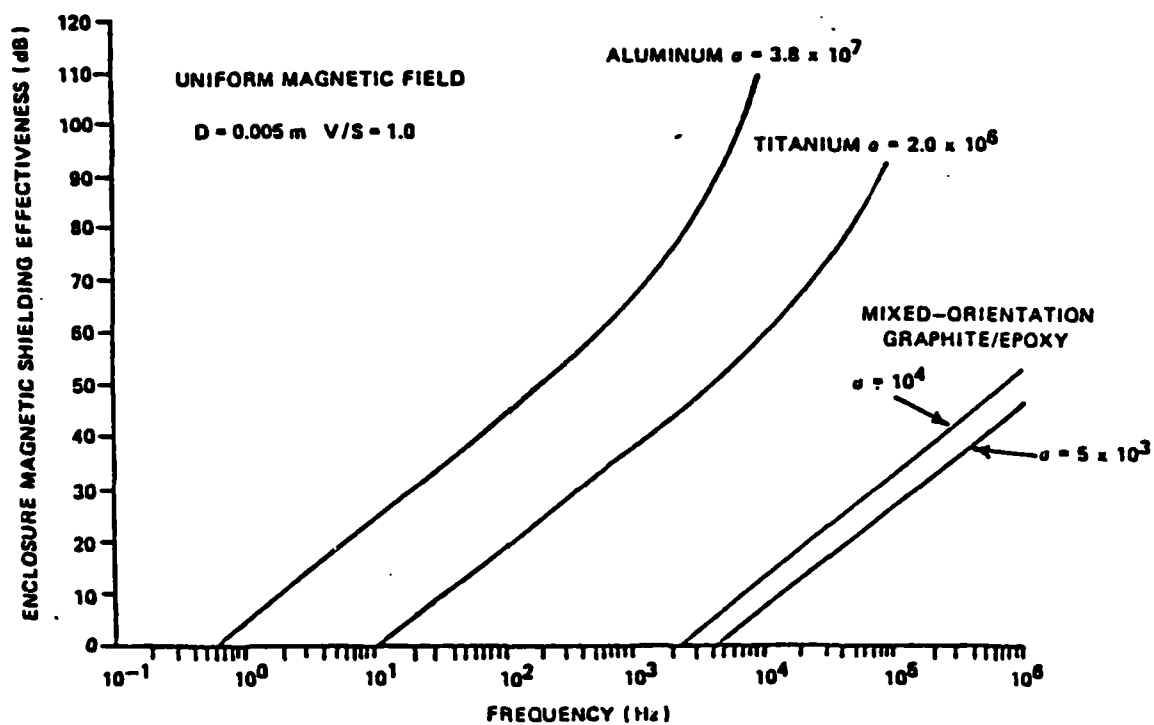


Figure 2.6 Magnetic Shielding Effectiveness Breakpoint Behavior for Enclosures⁽³⁾

The magnetic shielding effectiveness can be improved by using metallic coating to protect against lightning and surface charging effects. Figures 2.7 and 2.8 show the measured magnetic shielding effectiveness of 12- and 24-ply graphite/epoxy both bare and protected using various lightning protection schemes. Considerable improvement in magnetic shielding is possible with proper lightning protection.

The magnetic shielding effectiveness is also sharply dependent on the external field. In Figure 2.9 the shielding for an infinite flat plate is shown for both a uniform and non-uniform magnetic field. The nonuniform field shielding drops with frequency to zero very fast while a uniform field levels out at a high value.

Figure 2.10 illustrates measurements of shielding effectiveness made with a nonuniform magnetic field produced by a loop antenna for several flat graphite/epoxy composite laminate structures. The results indicate essentially no shielding below 1 MHz. Figure 2.11 magnetic shielding effectiveness for a non-uniform magnetic field for various metals and composites (8-, 12- and 24-ply). The metals (aluminum and titanium) shield best and are followed by graphite. Boron has essentially no shielding in non-uniform fields up to 100 MHz.

Figure 2.12 illustrates the use of surface transfer impedance to calculate magnetic shielding effectiveness for a flat plate under both a uniform and nonuniform field, and for a volume in a uniform field. The advantage is that, the transfer impedance is a characteristic of the material only, not of its shape or of the external field incident on it.

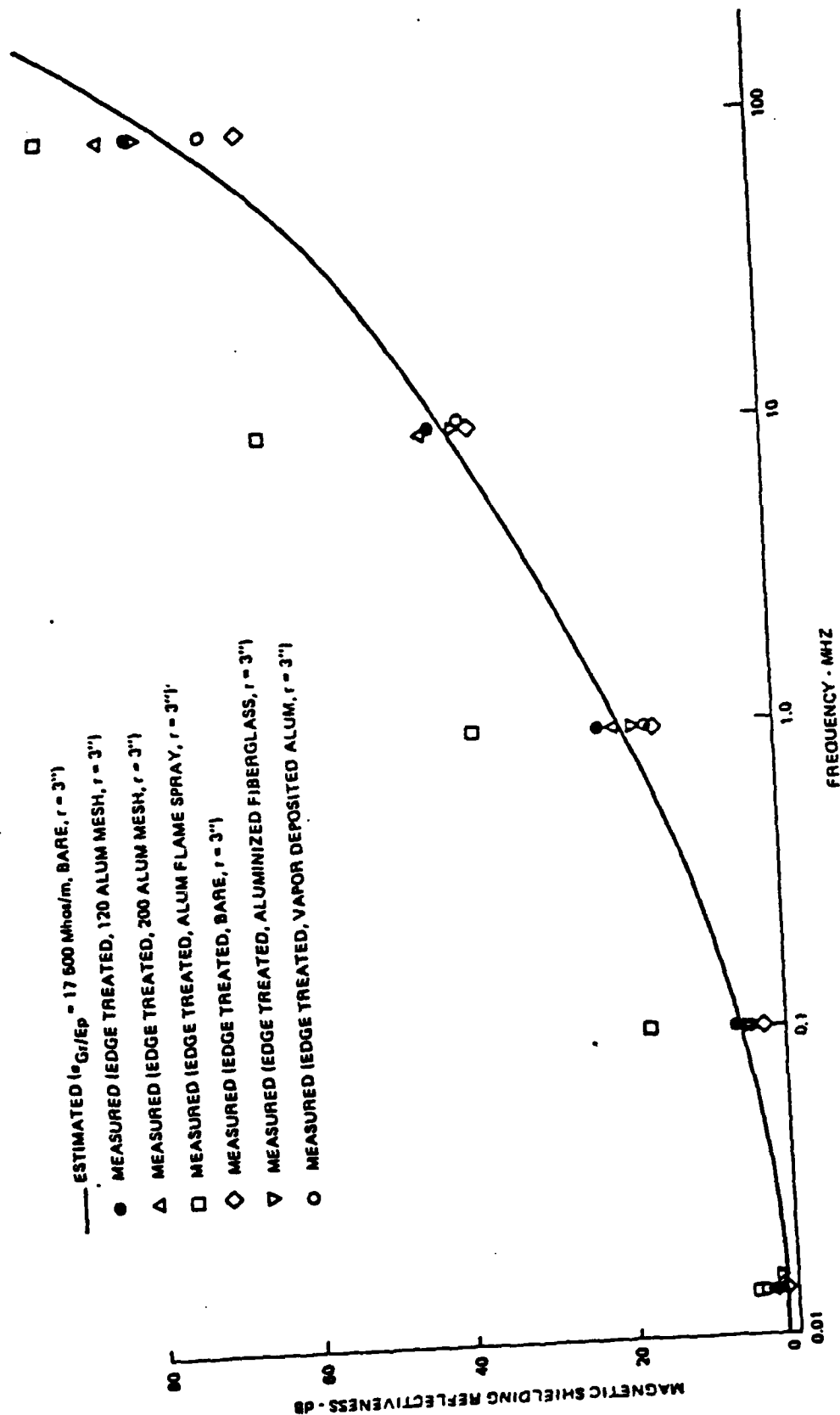


Figure 2.7 Magnetic Shielding of 12 ply (0°, 45°, 90°) Graphite/Epoxy Bare and With Protection (6)

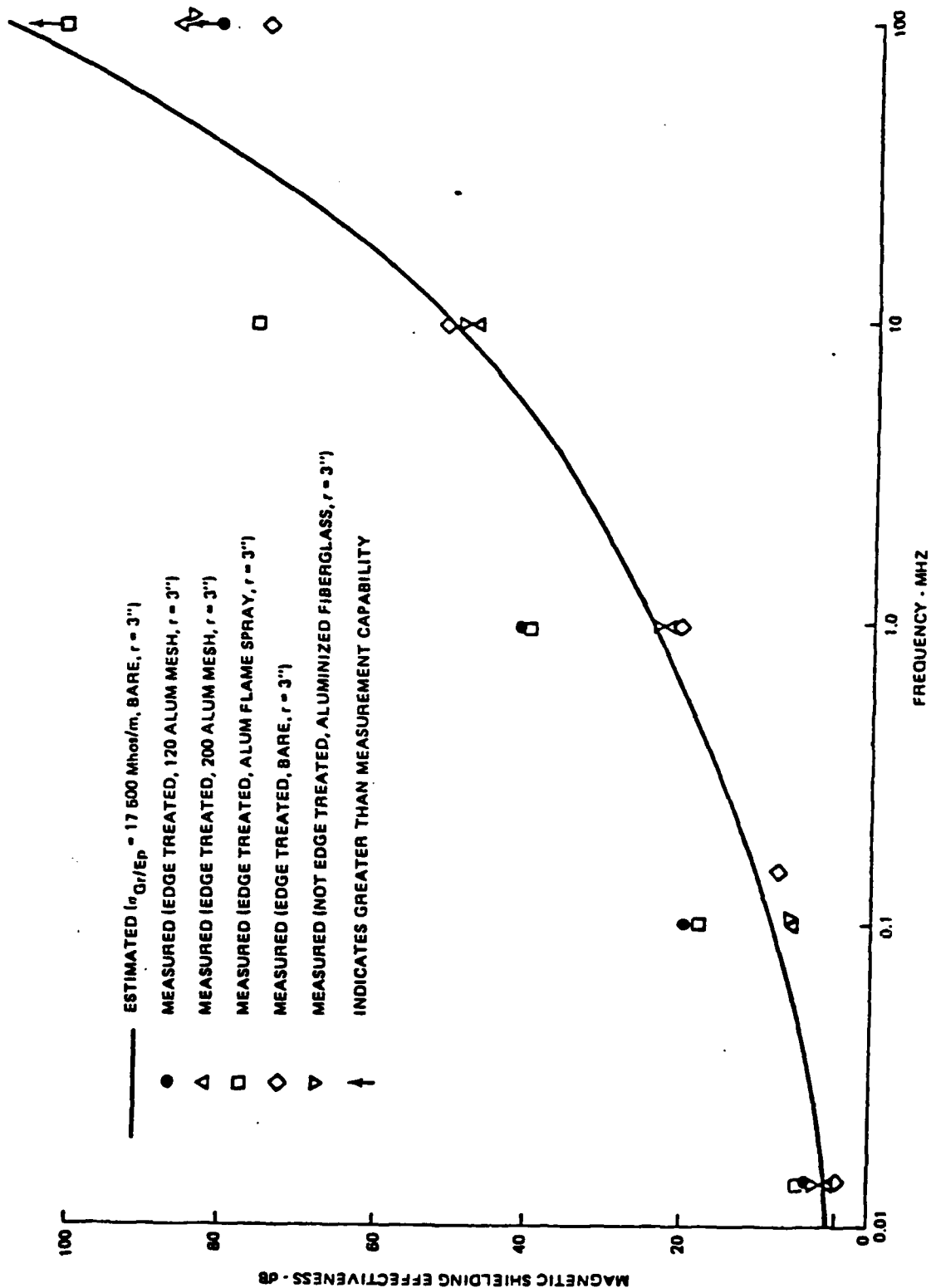


Figure 2.8 Magnetic Shielding For 24 Ply ($0^\circ, \pm 45^\circ, 90^\circ$) Graphite/Epoxy Bare and With Protection (6)

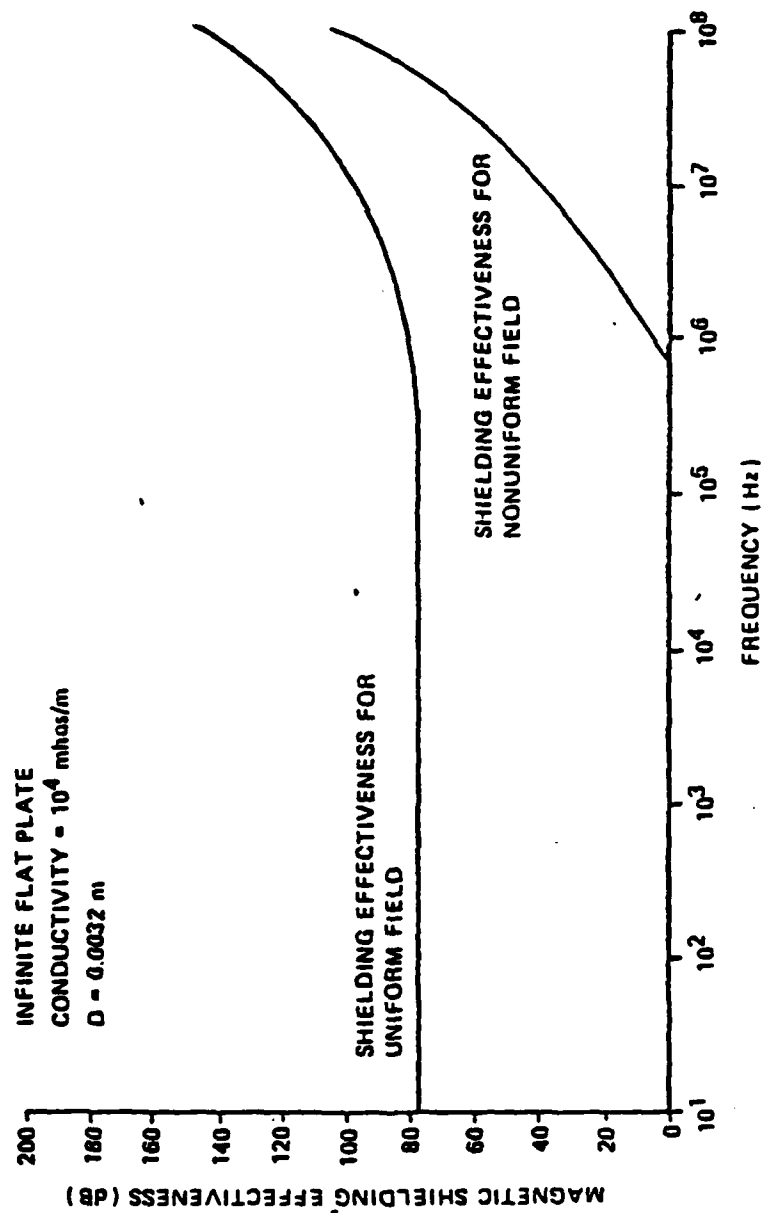
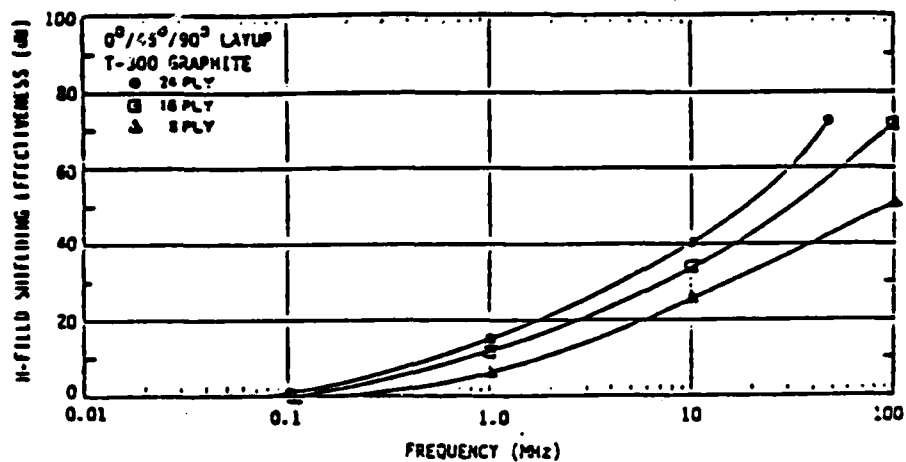
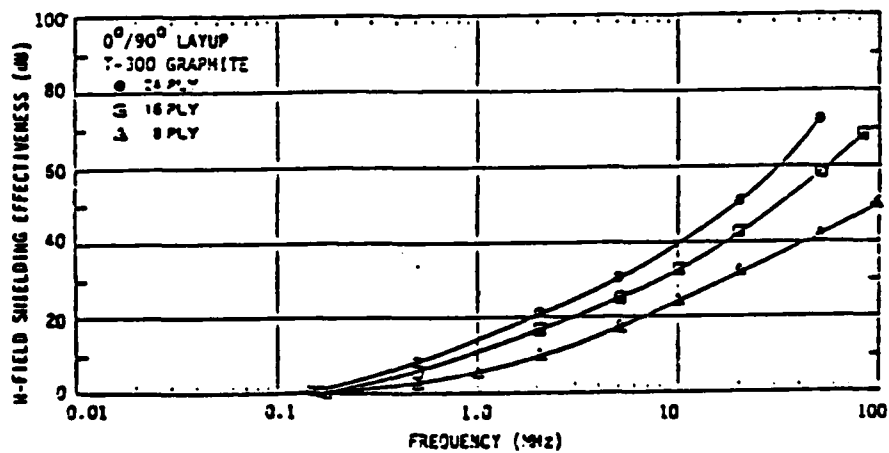


Figure 2.9 Magnetic Shielding Effectiveness for a Mixed-Orientation Graphite/Epoxy Composite Enclosure under a Uniform Field as a Function of Volume-to-Surface. Conductivity = 10^4 . Shield Thickness = 0.003 m (3)



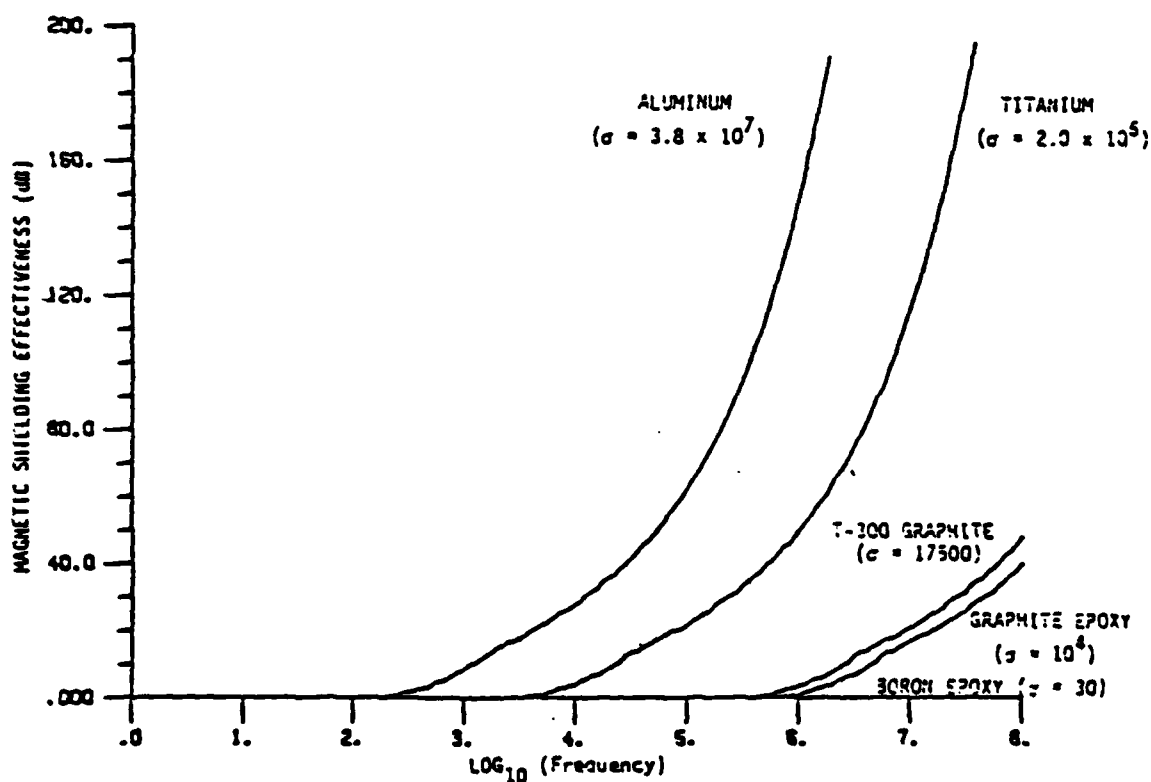
(a) 0°/45°/90° Layup



(b) 0°/90° Layup

Figure 2.10 Infinite Flat Plate with a Nonuniform Incident Magnetic Field Test Results (3)

LOOP DIAMETER = 1 in.
 ANTENNA-PLATE SEPARATION = 1 in.
 PLATE THICKNESS CORRESPONDS TO 8 PLY COMPOSITE
 MATERIAL AT 0.00525 IN/PLY



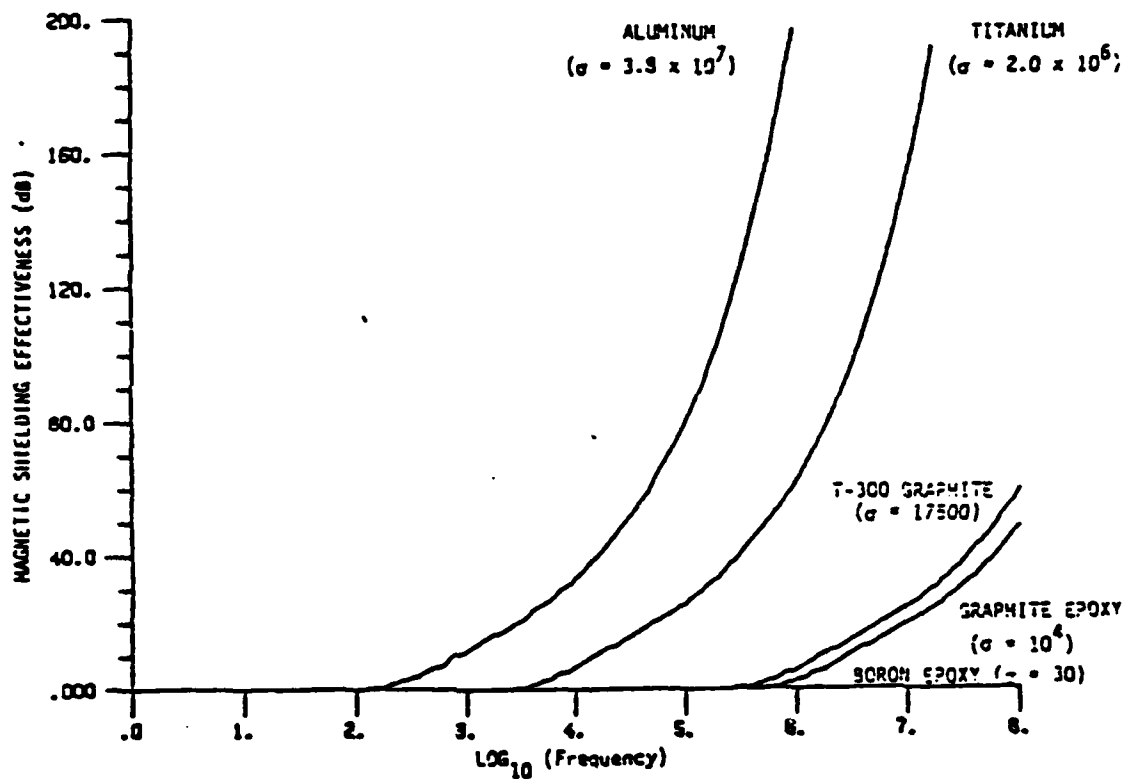
(a) Plate Thickness = 0.0032 m

Figure 2.11 Magnetic Shielding Effectiveness of a Flat Plate under a Non-uniform Magnetic Field generated by a Loop Antenna Parallel to the Plate (Sheet 1 of 3)(3)

LOOP DIAMETER = 1 in.

ANTENNA-PLATE SEPARATION = 1 in.

PLATE THICKNESS CORRESPONDS TO 12 PLY COMPOSITE
MATERIAL AT 0.00525 IN/PLY



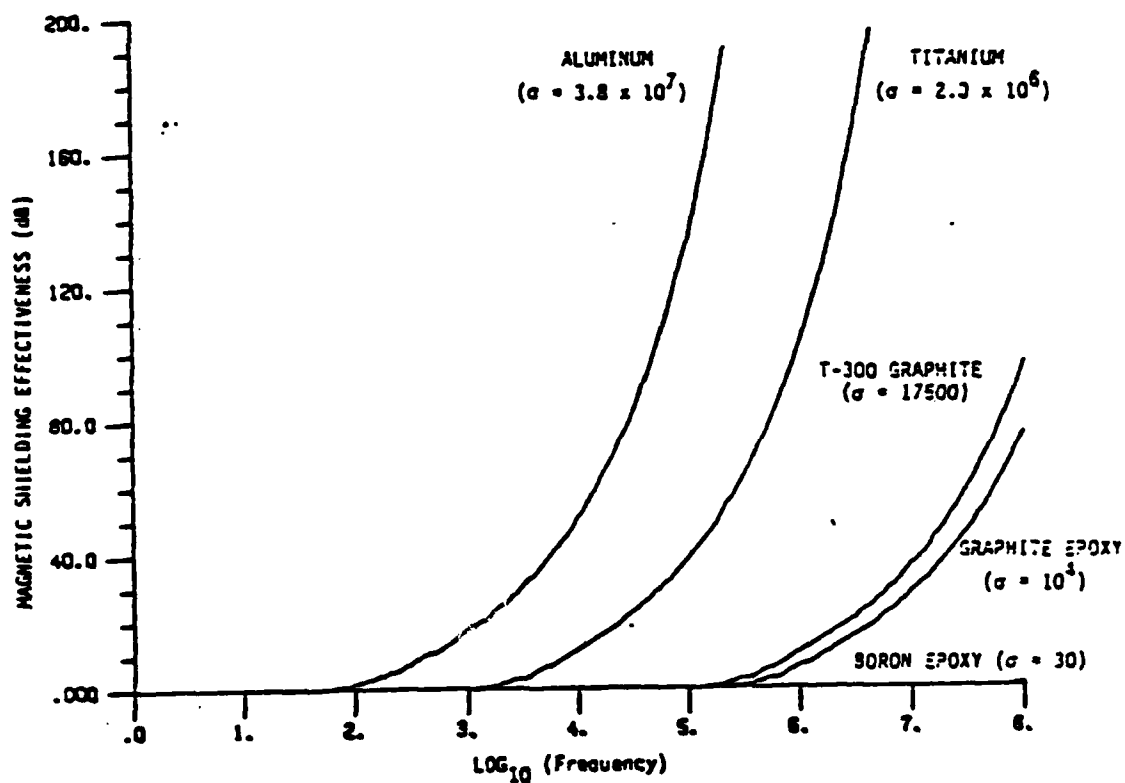
(b) Plate Thickness = 0.00214 m

Figure 2.11 Magnetic Shielding Effectiveness of a Flat Plate under a Non-uniform Magnetic Field generated by a Loop Antenna Parallel to the Plate (Sheet 2 of 3) (3)

LOOP DIAMETER = 1 in.

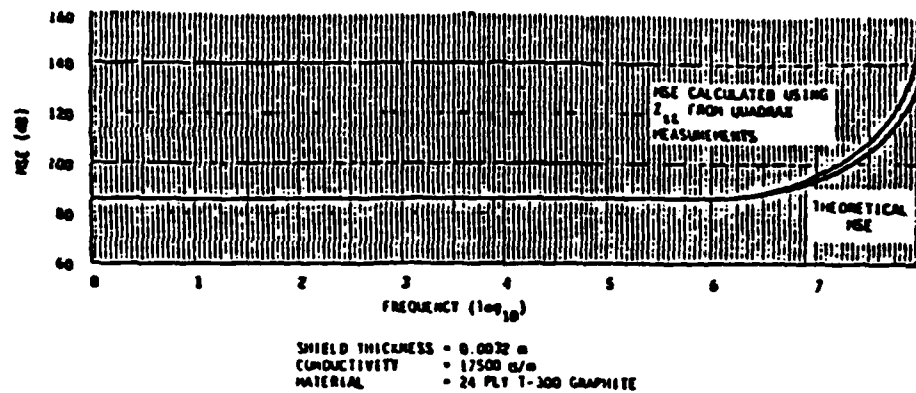
ANTENNA-PLATE SEPARATION = 1 in.

PLATE THICKNESS CORRESPONDS TO 24 PLY COMPOSITE
MATERIAL AT 0.00525 IN/PLY

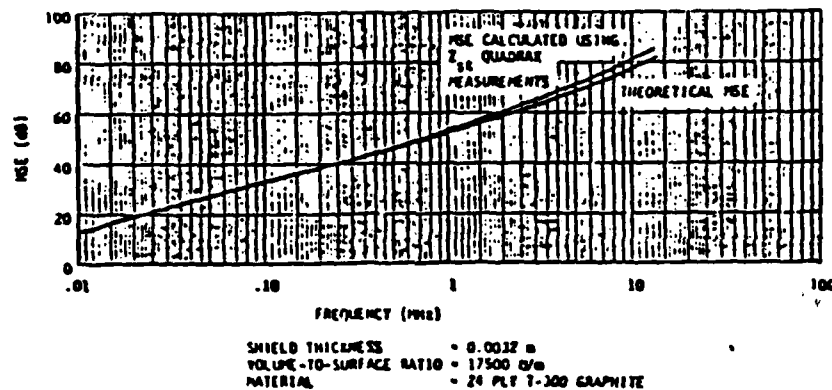


(c) Plate Thickness = 0.00107 m

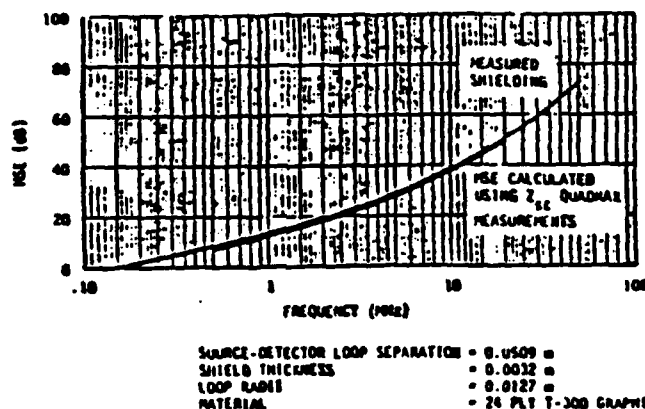
Figure 2.11 Magnetic Shielding Effectiveness of a Flat Plate under a Non-uniform Magnetic Field generated by a Loop Antenna Parallel to the Plate (Sheet 3 of 3)(3)



(a) Flat Plate under a Uniform Magnetic Field



(b) Volume under a Uniform Magnetic Field



(c) Flat Plate under a Nonuniform Magnetic Field

Figure 2.12 Shielding Effectiveness using Surface Transfer Impedance⁽³⁾

2.2.1.2 Electric Shielding Effectiveness

Figure 2.13 shows the electric shielding effectiveness for an 8-ply graphite/epoxy enclosed shield compared to an aluminum structure. Because the low frequency shielding is primarily reflective loss, the electric shielding effectiveness decreases with frequency at high frequency, absorption (which increases with frequency) becomes more important. In between, the electric shielding effectiveness goes through a minimum as shown in Figure 2.13 for aluminum.

Electric shielding effectiveness also depends on the volume-to-surface ratio, $\frac{V}{S}$, of the enclosure. The higher the ratio, the less electric shielding. This behavior is shown in Figure 2.14 for 8-ply graphite/epoxy.

E-field shielding for 12- and 24-ply graphite/epoxy panels which are bare and protected is shown in Figures 2.15 and 2.16. The frequency range is from 10 kHz to 1 GHz.

2.2.1.3 Plane Wave Shielding Effectiveness

Some limited data on low frequency plane wave shielding effectiveness is given in Figures 2.17 and 2.18 for 12-ply and 24-ply graphite/epoxy composite panels.

2.2.2 High Frequency Shielding

Most measurements to date appear to confirm the opinion that composites tend to behave like metals at frequencies above 1 GHz. The best data to date on high frequency composite shielding was taken by Boeing⁽¹⁰⁾ using anechoic chamber techniques. The frequency range was from 1 GHz to 18 GHz and the composite panels were 2-ply and 4-ply laminates. The trend is clearly towards higher shielding as frequency increases.

VOLUME-TO-SURFACE RATIO = 1

SHIELD THICKNESS CORRESPONDS TO 8 PLY COMPOSITE
MATERIAL OF 0.00525 IN/PLY

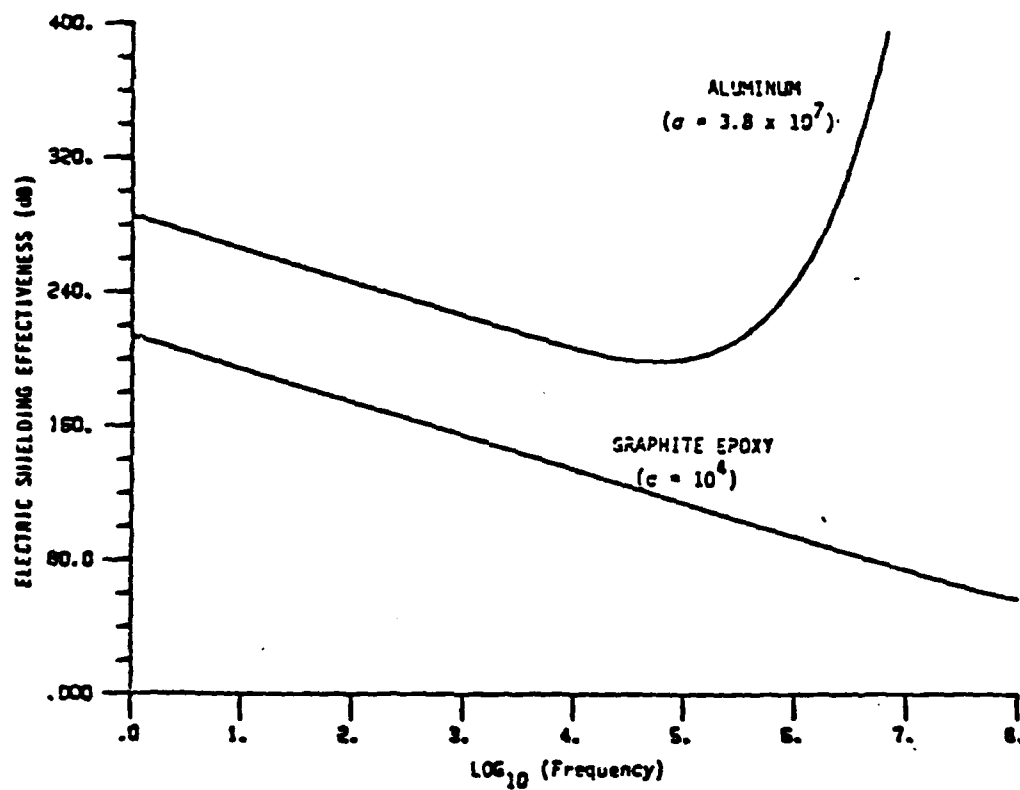


Figure 2.13 Electric Shielding Effectiveness of an Enclosure under a Uniform Electric Field⁽³⁾

Shield Conductivity = 10^4 mhos/m

Shield Thickness corresponds to 8-ply
composite material at 0.00525 in/ply

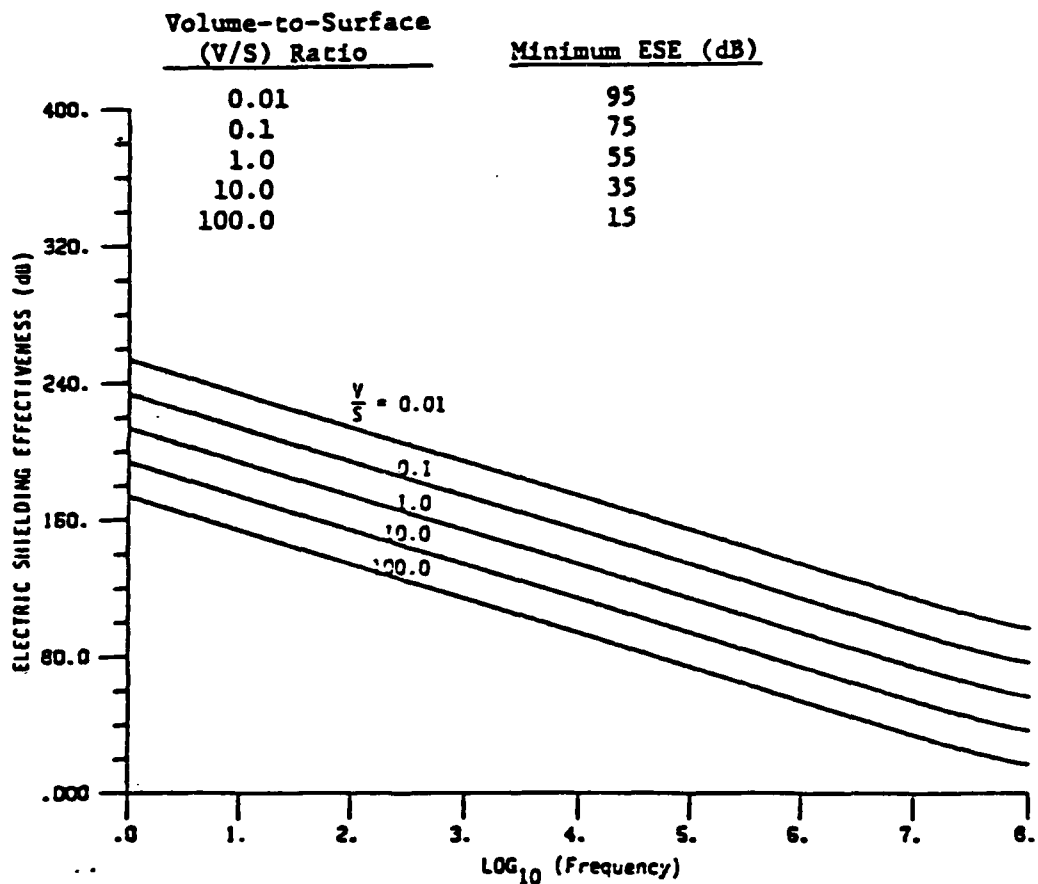


Figure 2.14 Electric Shielding Effectiveness of an Enclosure under a Uniform Electric Field as a Function of Enclosure Volume-to-Surface Ratio (3)

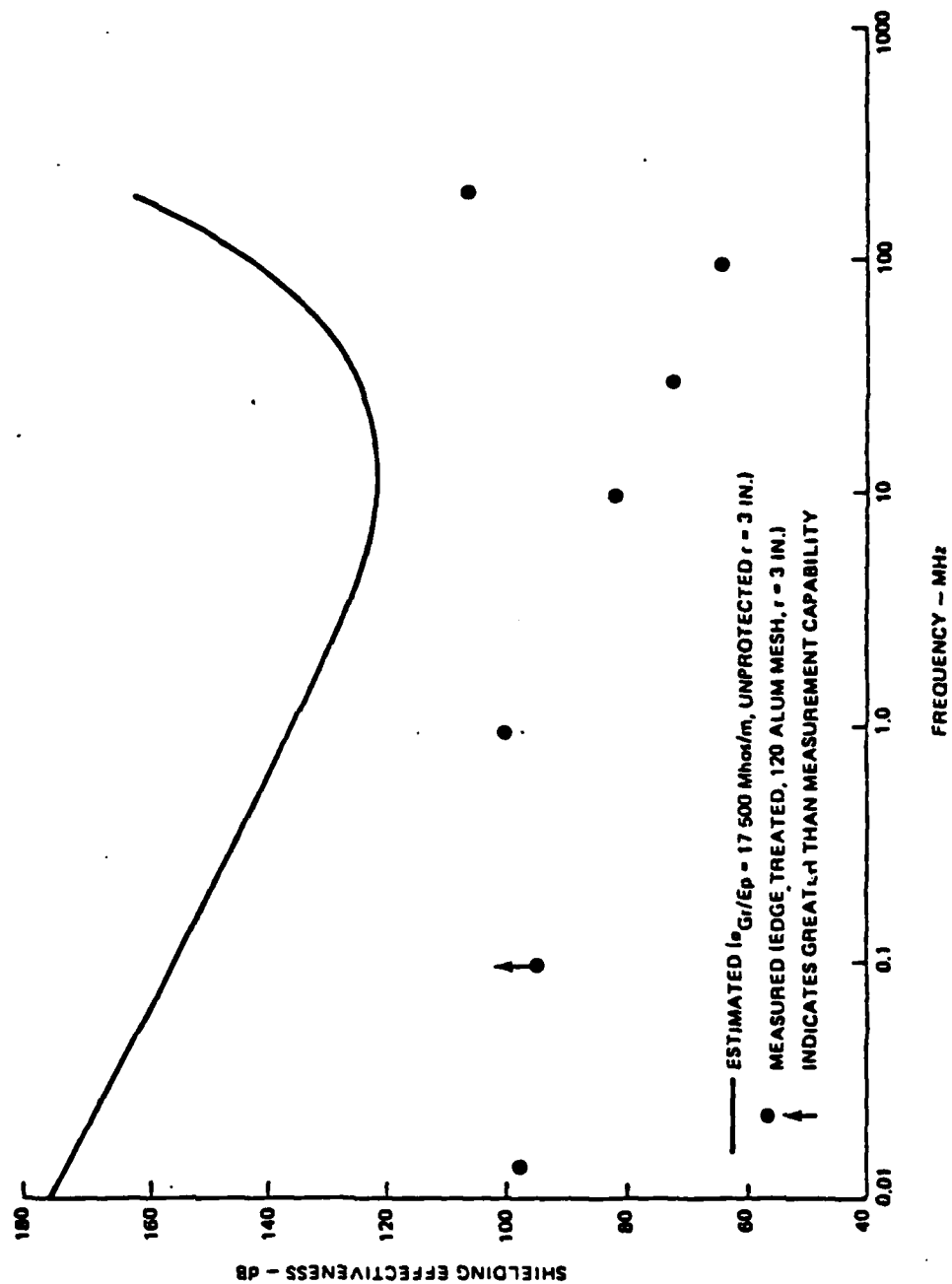


Figure 2.15 E-Field Shielding for 24-ply Graphite/Epoxy Composite Panel (6)

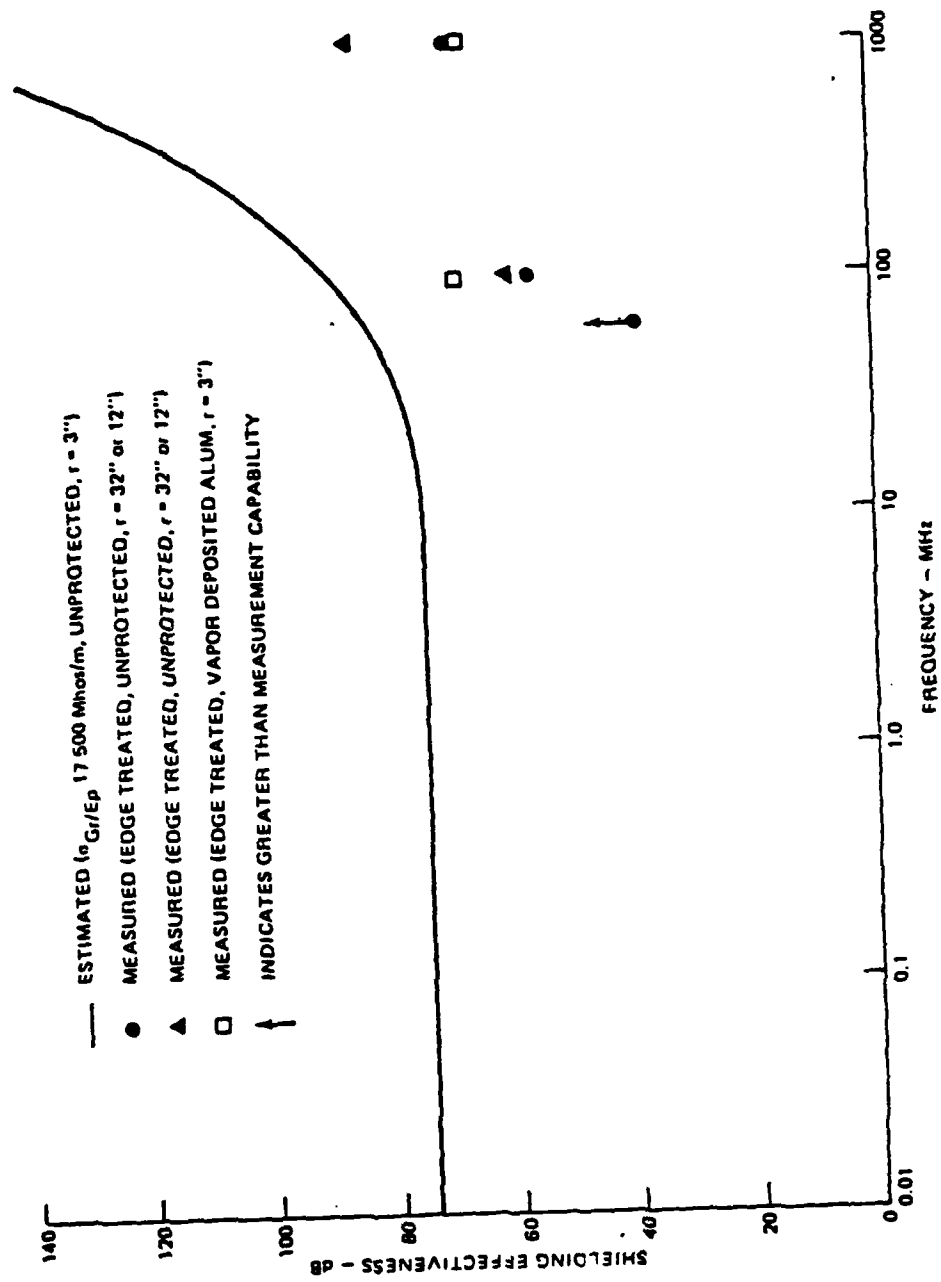


Figure 2.17 Plane-Wave Shielding Effectiveness For 12-ply Graphite/Epoxy Composite Panel (3)

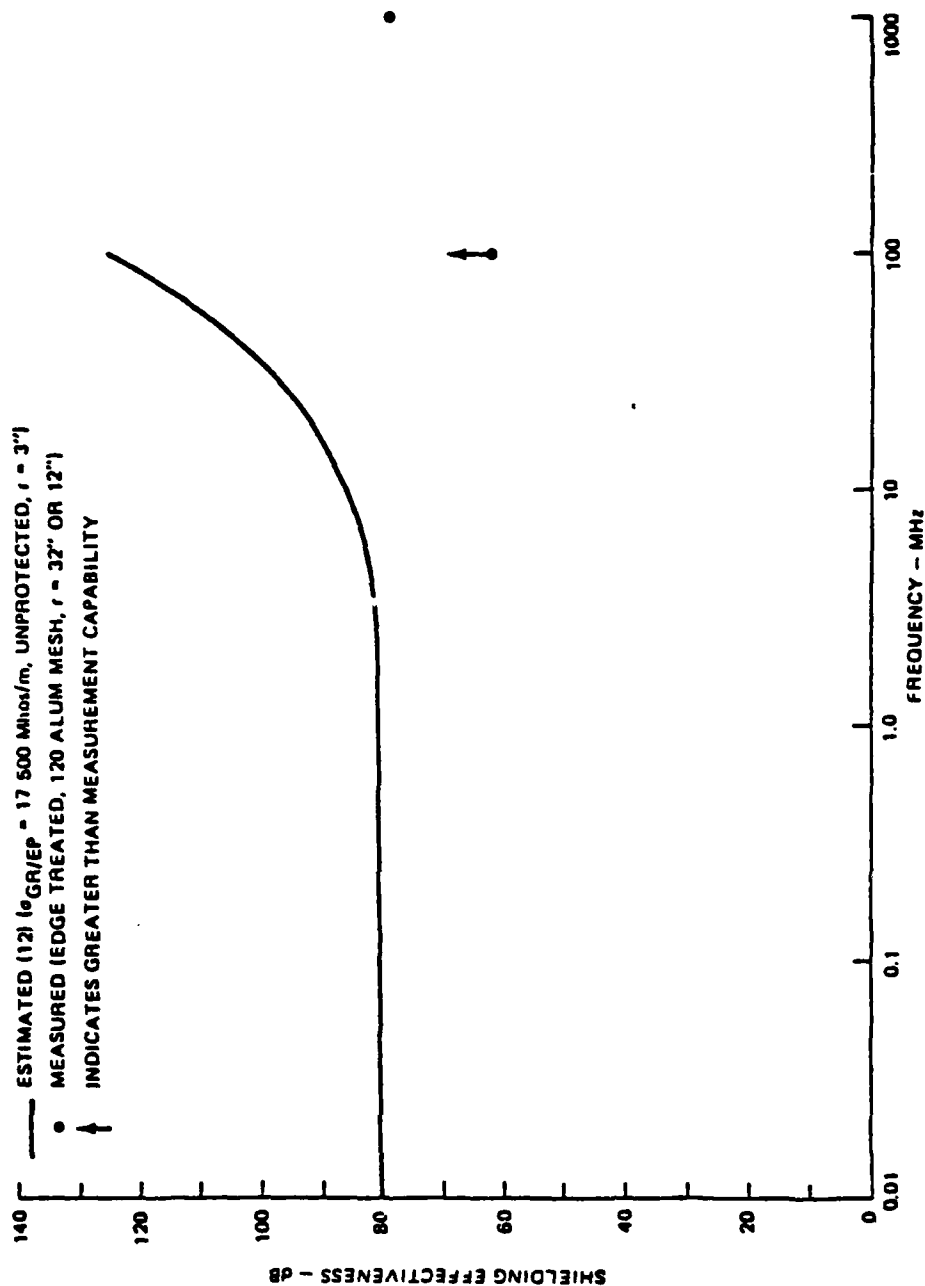


Figure 2.19 Plane-Wave Shielding Effectiveness for 24-ply Graphite/Epoxy Panel (3)

2.3. Composite Joint Coupling

In this section a theoretical overview is given of joints in airframe skins with measured joint admittances. Measured changes in shielding effectiveness are given for composite panels with joints.

2.3.1 Theory

External EM fields will induce currents on the surface of both metal and composite aircraft. The existence of a joint in the aircraft skin results in a voltage drop across the joint as shown in Figure 2.19. The external field induces a surface current J_s on the skin which produces a field E_s across the joint. The joint voltage drop is then

$$V_J = \int_a^b E_J \cdot dl = \frac{J_s}{Y_J} \quad (2-16)$$

where Y_J is the joint admittance per unit joint width.

Three common types of joint construction are shown in Figure 2.20. The measured joint admittances for these joints are given in Figure 2.21. These joint admittances range from a few mhos/m to a few hundred mhos/m depending on the joint type. Joint 2 with Y_J 15 mhos/m is typical of the joints currently used in aircraft. The joint admittance is rather insensitive to frequency over a large frequency range.

A theoretical model can be developed for the simple infinite butt joint shown in Figure 2.22a modelled as a uniform slot of width W . An equivalent transmission line circuit for the butt joint is shown in Figure 2.22b which results in the following

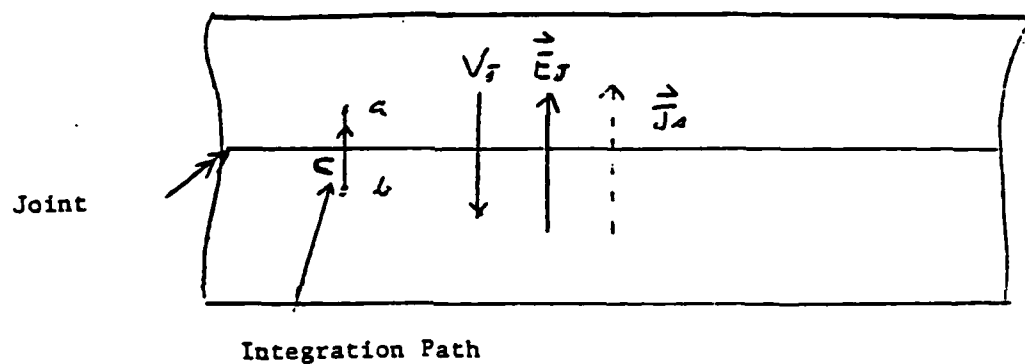
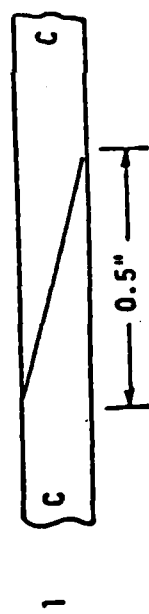
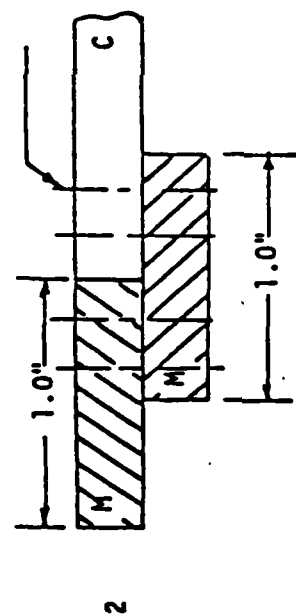


Figure 2.19 Joint Coupling⁽³⁾

CYLINDER WAS FABRICATED EXTRA LONG, CUT, MACHINED AND SECON-
DARILY BONDED WITH EA-934
ADHESIVE.



1/8 DIA RD. HD. RIVET C TO M
1/8 DIA BOLT M. TO M.



CYLINDER CENTER TOWARDS BOTTOM
OF PAGE. METAL RINGS FABRICATED
FROM ALUMINUM SHEET, CUT, ROLLED
AND WELDED. THE RIVETS OR BOLTS
WERE PLACED IN A CIRCUMFERENTIAL
ROW APPROXIMATELY ONE INCH APART
AND ALTERNATING 1/8 INCH TO EITHER
SIDE OF THE CIRC. CTR LINE.

FIRST THREE STEPS (4 PLY PER
STEP) WERE PRECURED (COMPACTED).
EA-934 APPLIED TO SANDED COMPOSITE
STEPS, AND THEN LONGITUDINALLY
SLIT METAL RING MANEUVERED INTO
PLACE. REMAINING COMPOSITE STEPS
WERE APPLIED TO EA-934 COATED
METAL RING IN PLACE. METAL RING
WAS FABRICATED FROM 2024 ALUMINUM.

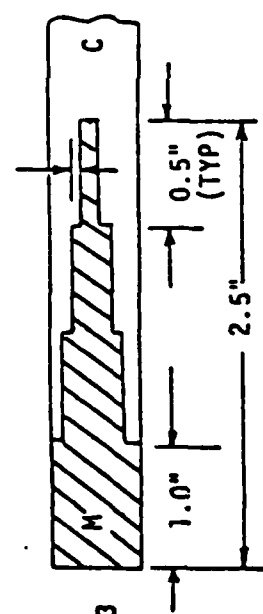


Figure 2.20 Structural Joints
(3, 5)

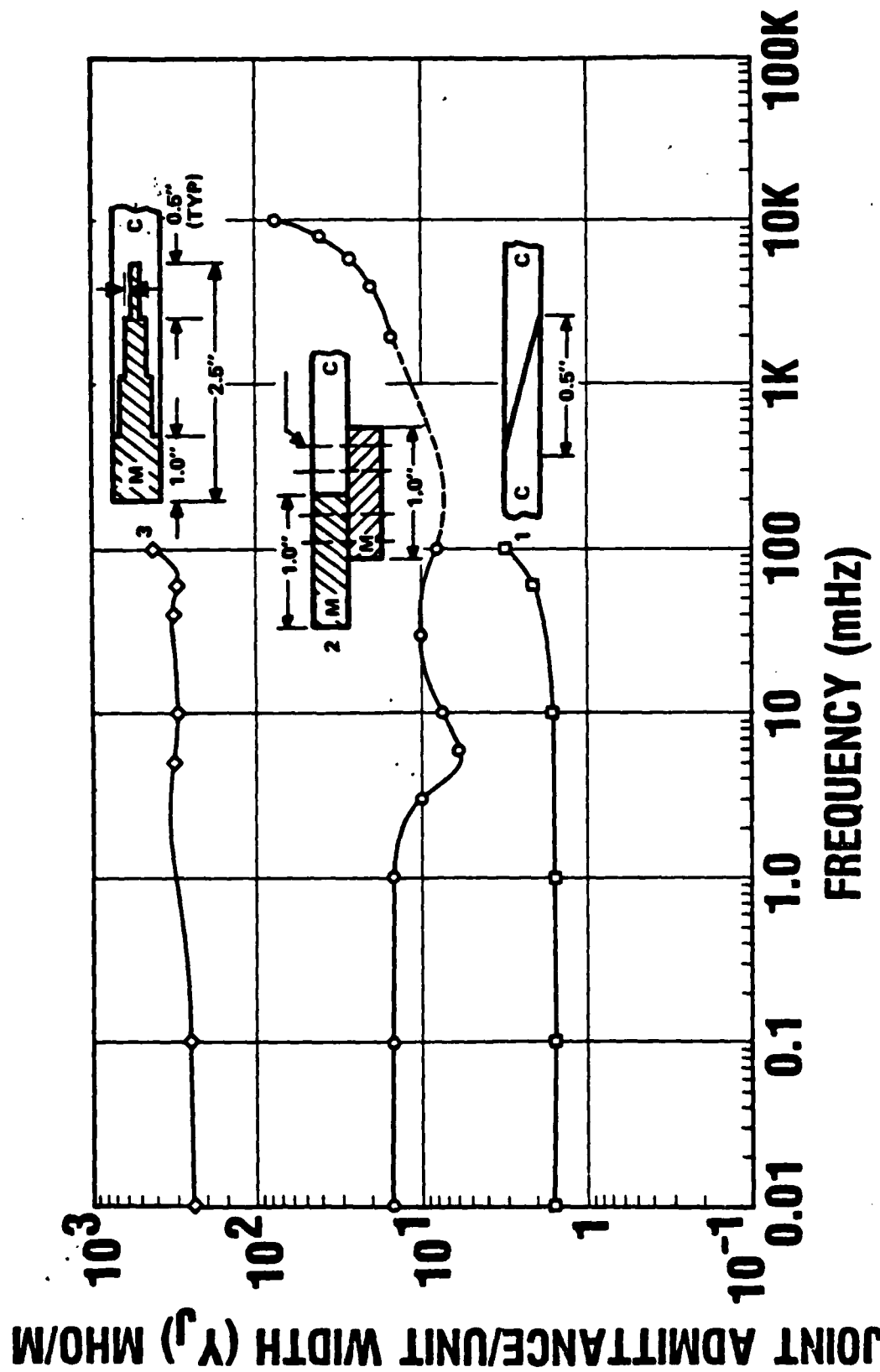


FIGURE 2.21. JOINT ADMITTANCE/UNIT WIDTH AS A FUNCTION OF FREQUENCY.

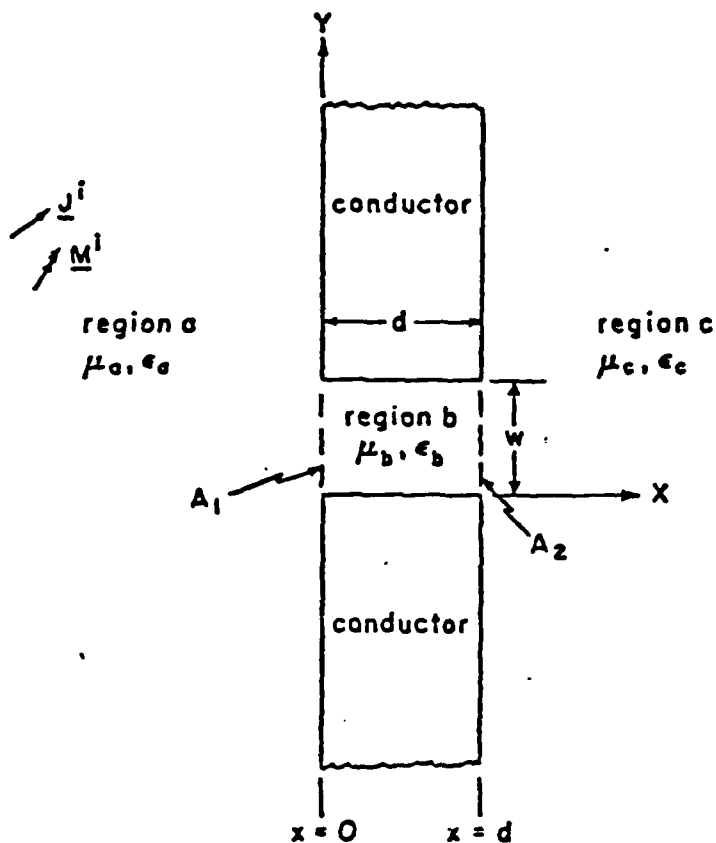


Figure 2.22a Uniform Slot of Width w in a Perfectly Conducting Screen of Thickness d (8)

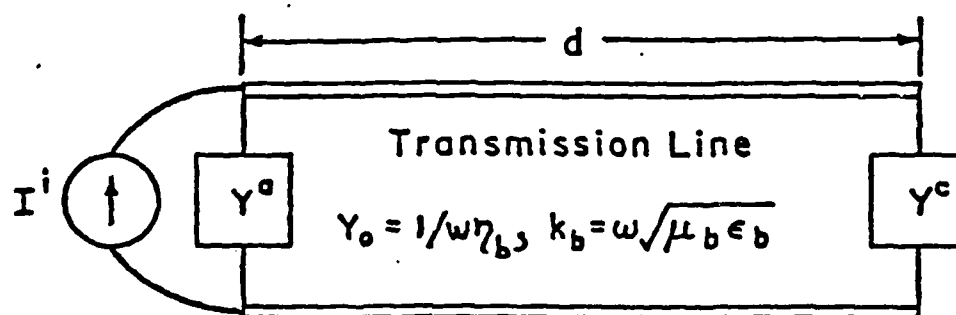


Figure 2.22b Equivalent Circuit for a Narrow Slot in a Thick Conducting Screen (3)

expression for Y_J :

$$Y_J = (Y^a + Y^c) \cosh Y_b d + (Y_o + \frac{Y^a Y^c}{Y_o}) \sinh Y_b d \quad (2-17)$$

Here Y^a and Y^c are the admittances of a thin slot looking into Region a and Region c as in Figure 2.22a and Y_o is given in 2.22b. For a highly lossy slot, equation (2-17) becomes

$$Y_J \approx \frac{\sigma_b d}{W} \quad (2-18)$$

independent of frequency. This is the behavior shown by the measured joint admittances in Figure 2.21.

2.3.2 Shielding Effectiveness Plus Joint Admittance

A part of its Protection Optimization Program, Grumman has performed measurements on graphite/epoxy panels with various types of doublers and fasteners. Tests were made under various conditions, such as tight joints, loose joints or no joints, to verify that degrading the quality of the joint reduces the shielding effectiveness of the composite panels.

The tightly jointed panel shielding effectiveness is shown in Figures 2.23 - 2.25 for magnetic, electric and plane wave shielding as a function of frequency. The results indicate that little difference in shielding resulted from use of different fasteners to join the panels. Two joined aluminum plates were also tested for shielding effectiveness as a standard and performed better than the joined composite panels.

Figure 2.26 shows the magnetic shielding behavior of two joined composite panels; one 12 ply the other a 24-ply. As the joint quality is degraded the magnetic shielding decreases dramatically for high frequencies. The same general trend, although less dramatic, held for electric and plane wave shielding effectiveness (Figures 2.27 and 2.28 respectively).

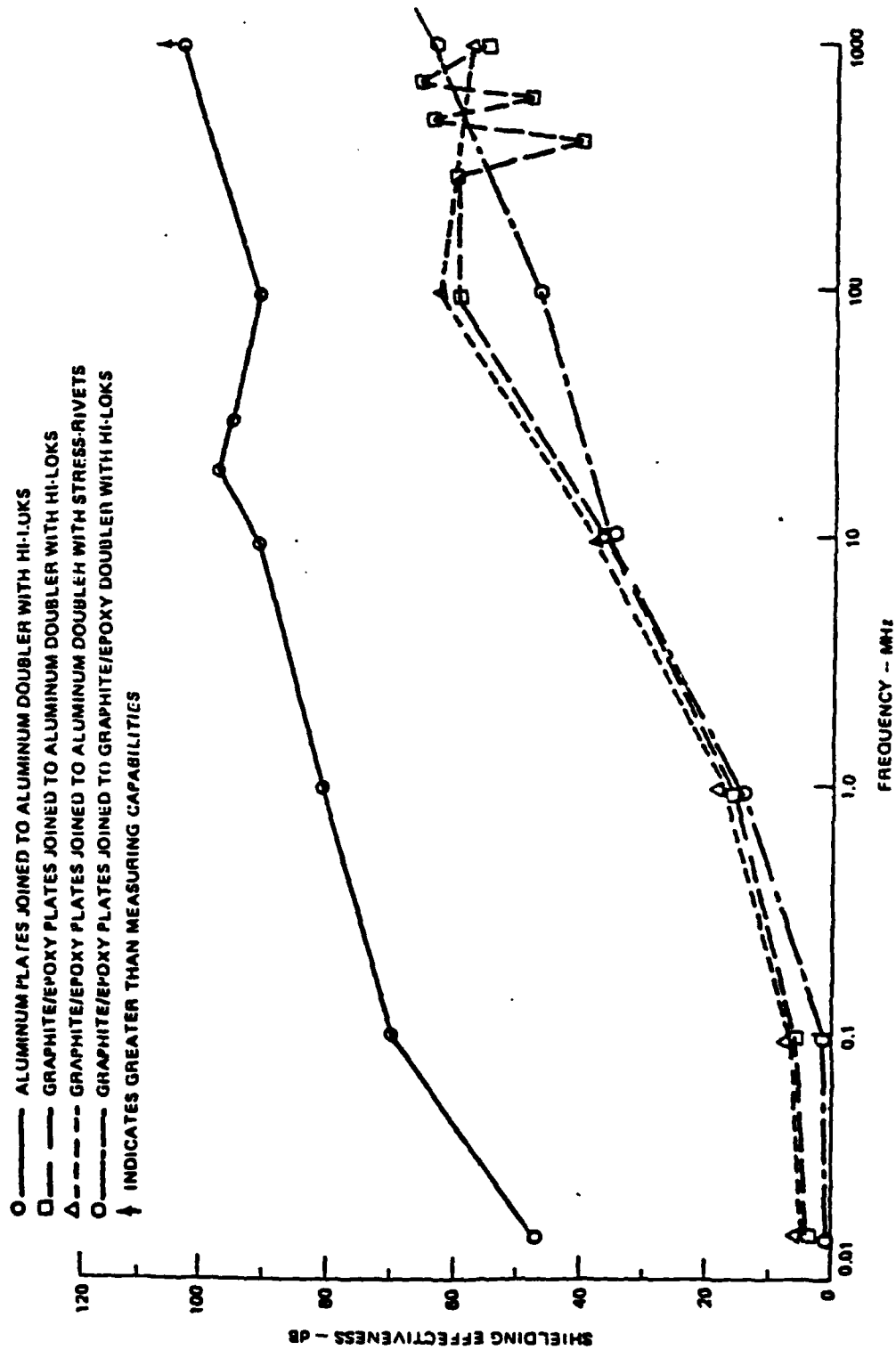


Figure 2.23 Magnetic Shielding Effectiveness For Tightly Joined Panels (6)

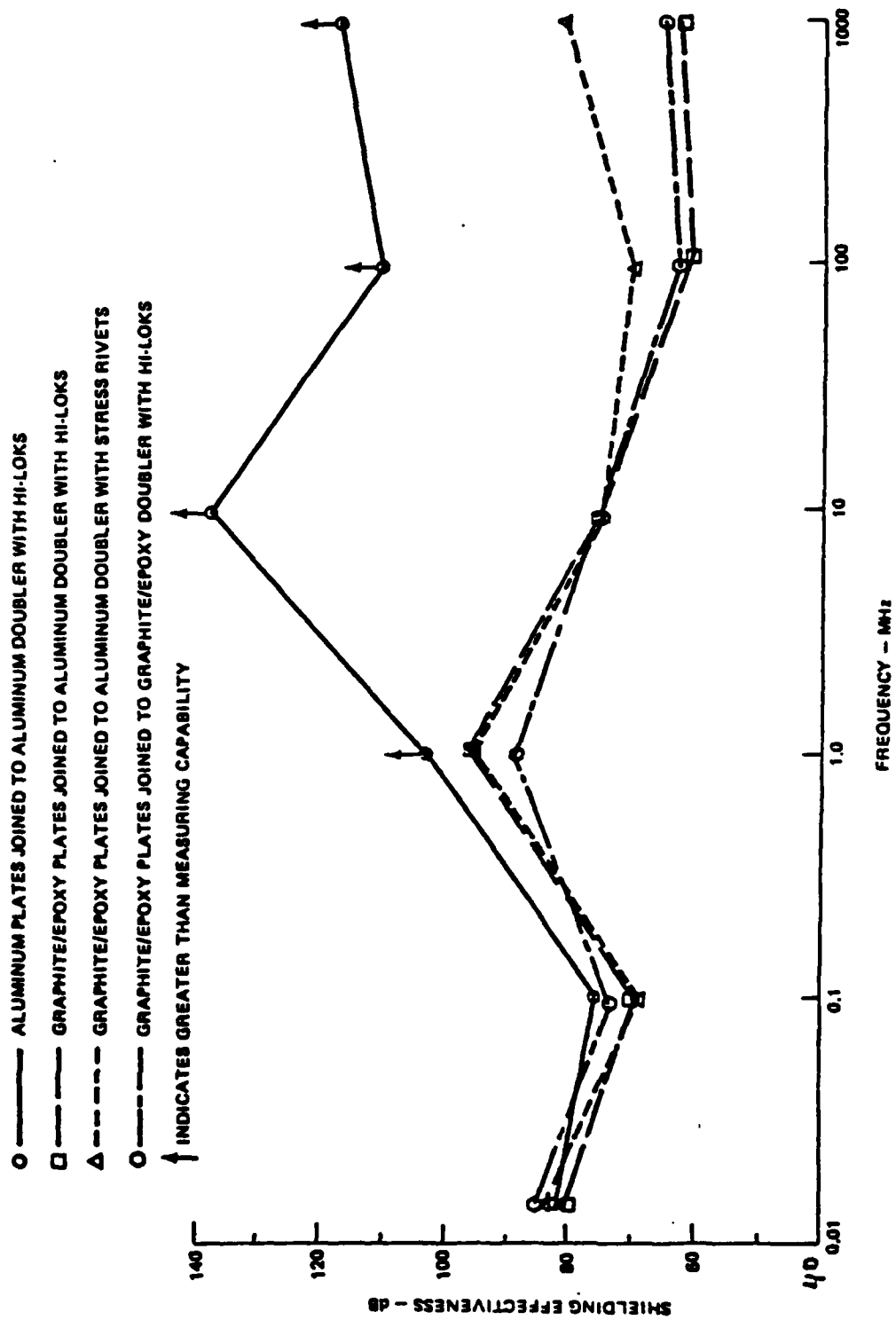


Figure 2.24 Electric Shielding Effectiveness of Tightly Joined Panels (6)

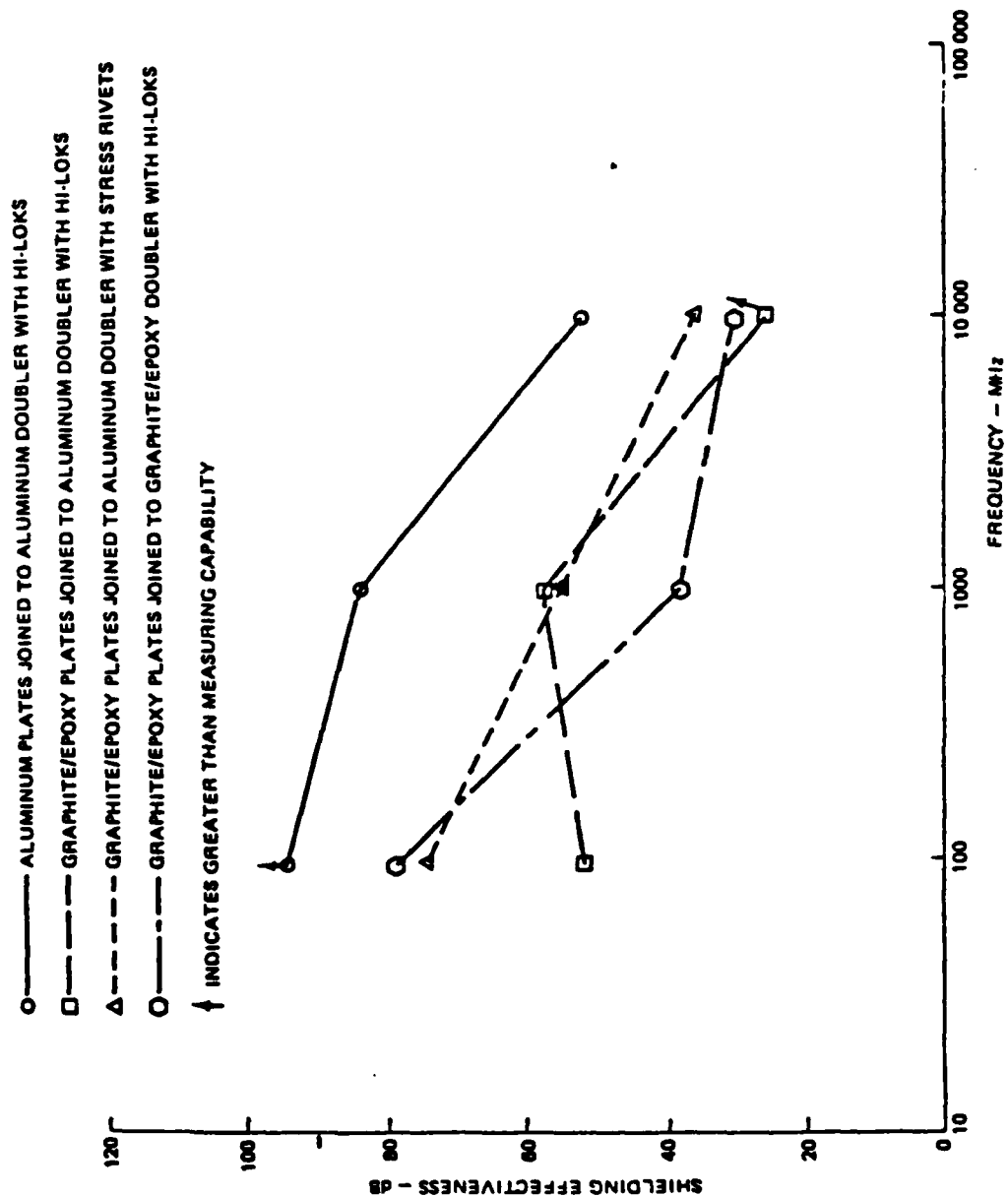


Figure 2.25 Plane-Wave Shielding Effectiveness of Tightly Joined Panels (6)

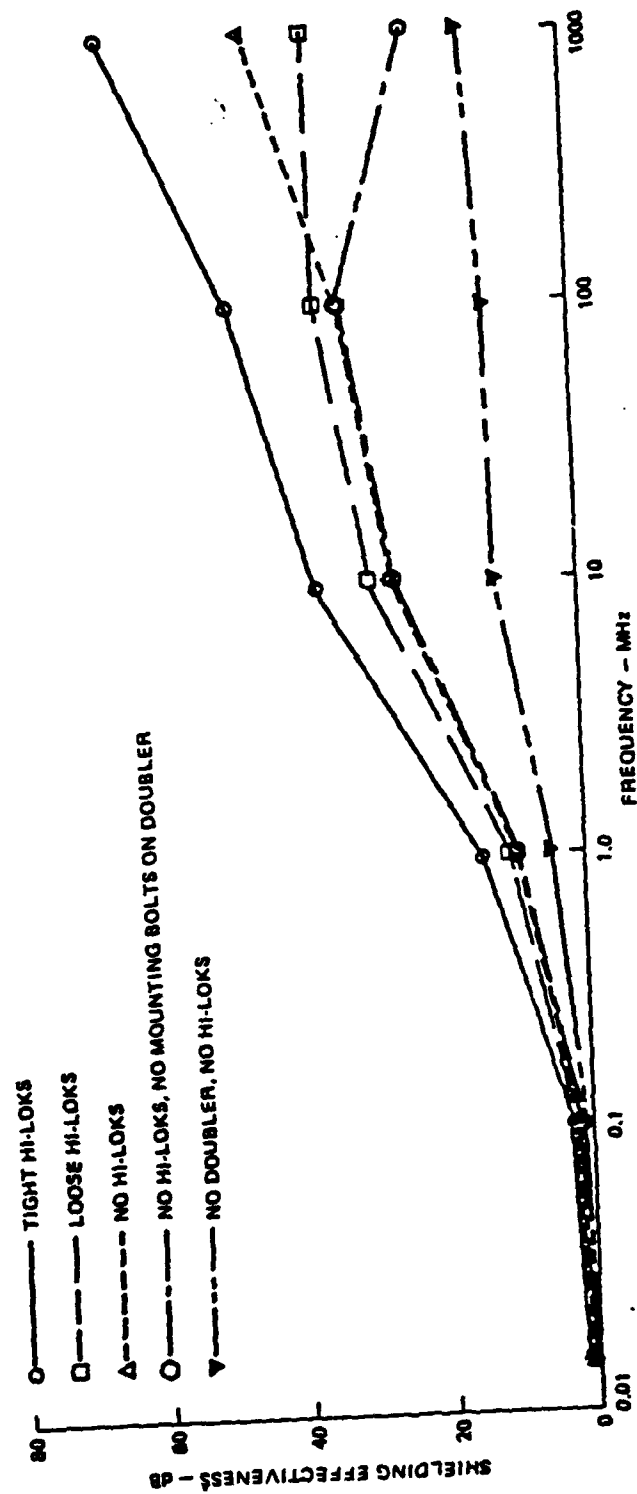


Figure 2.26 Variation of Magnetic Shielding Effectiveness of 12-ply Graphite/Epoxy Panels Joined to 24 Ply Graphite/Epoxy Doublers With Hi-Loks(6)

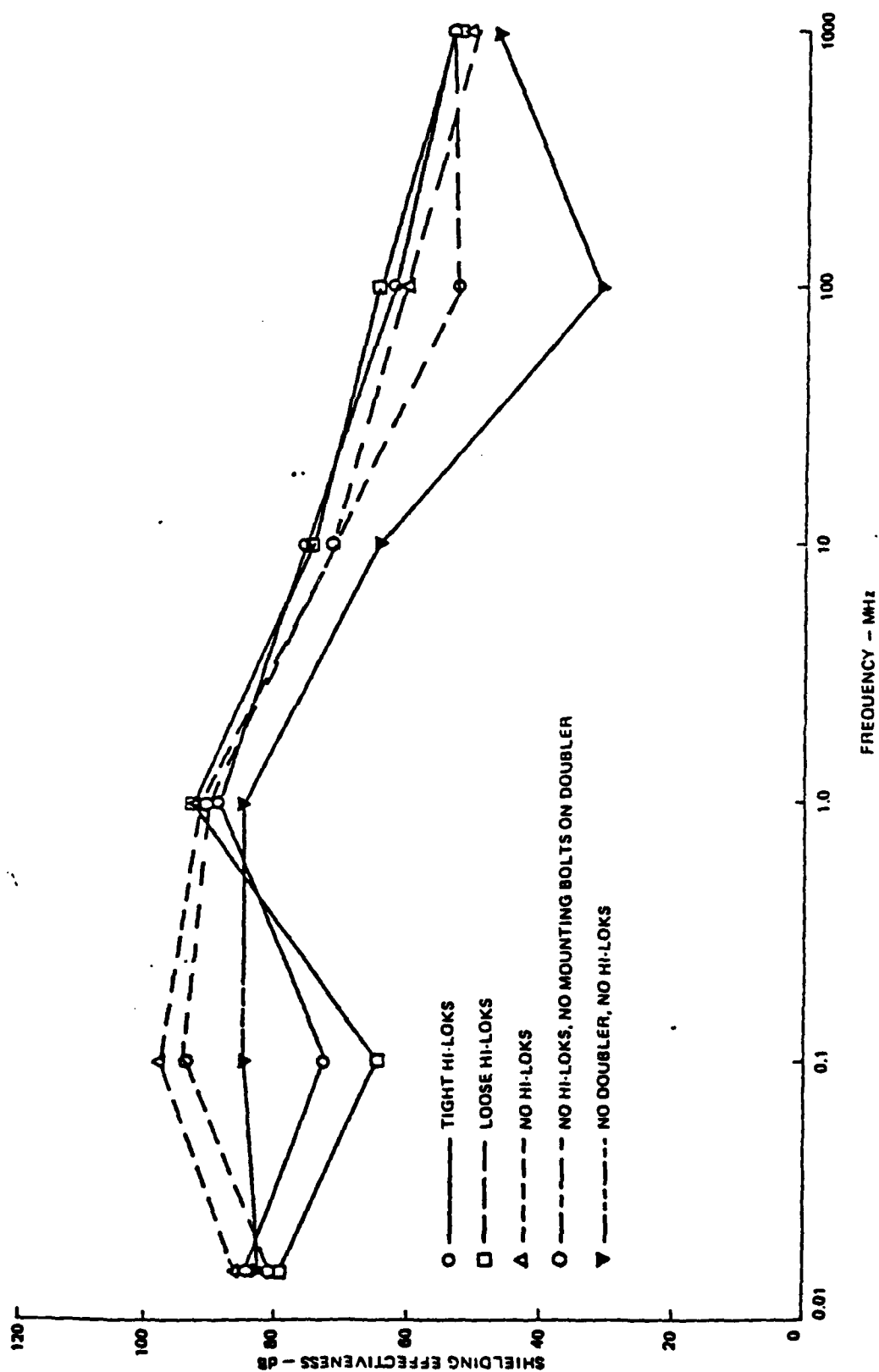


Figure 2.27 Variation of E-Field Shielding Effectiveness of 12-ply Graphite Epoxy Joined to 24 Ply Graphite/Epoxy Doubler With Hi-Loks (6)

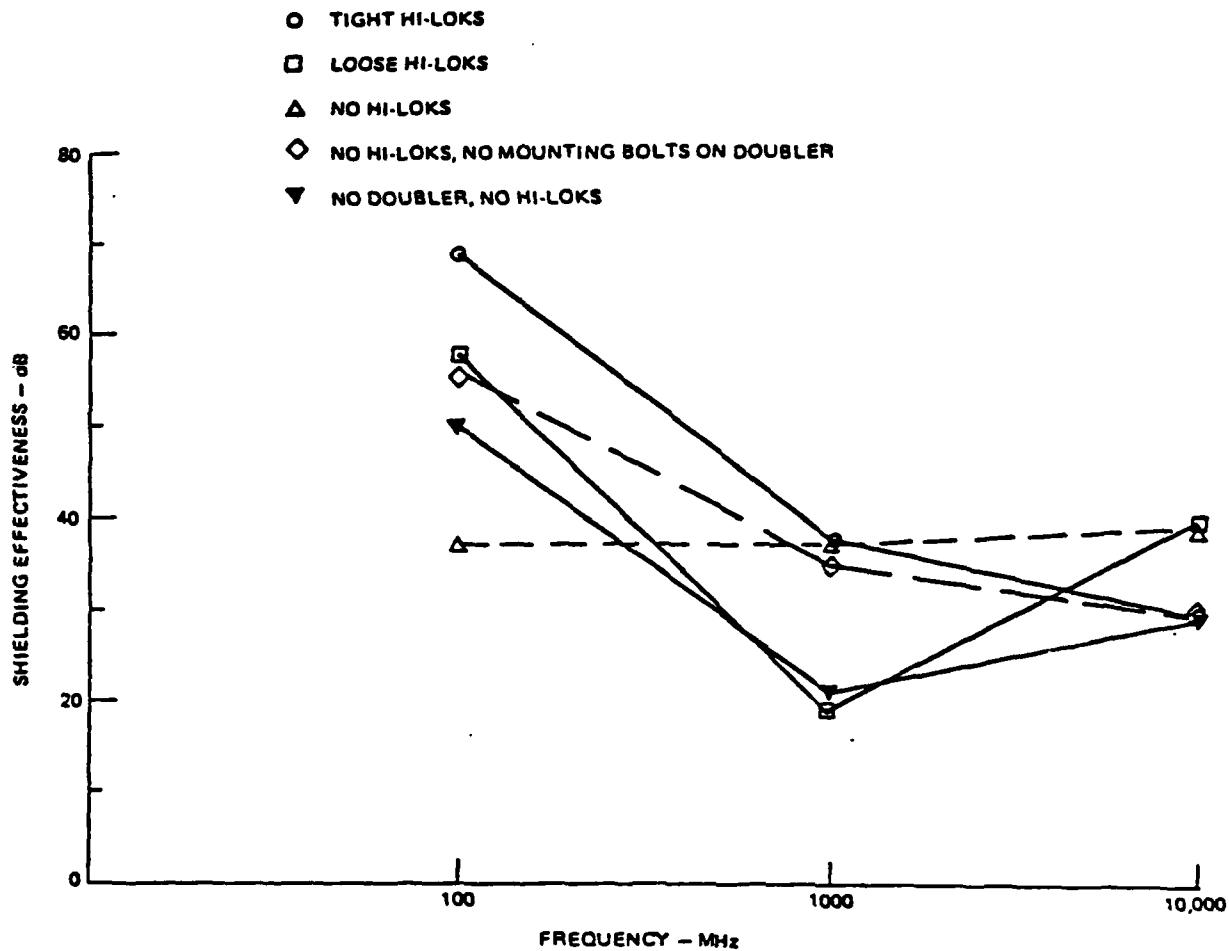


Figure 2.28 Variation of Plane-Wave Shielding Effectiveness for 12-ply Graphite/Epoxy Panels Joined to 24 Ply Graphite/Epoxy Doubler With Hi-Loks (6)

2.4 Ranking and Low Weight Penalties Imposed by Thin Metallic Protective Coatings

Figure 2.1 contrasted the wide range of low frequency transfer impedance values for 2 ply composite panels and 4 mil metallic coatings. A graphite/epoxy panel exhibits a 77db lower transfer impedance than aluminum, Boron/epoxy and Kevlar are 136db and 327db respectively lower. In terms of open circuit diffusion voltage, V_{oc} where $V_{oc} = J_s Z_t$. Figure 2.29 shows the reduction in graphite/epoxy voltage $V_{oc} = J_s Z_t^{g/e}$ provides by a thin metallic sheet. A worse case assumption of metallic layer isolation from the airframe composite material is assumed as the best coatings are aluminum which corrode severely with graphite/epoxy. Figure 2.1 shows copper to exhibit a 325 fold voltage reduction while aluminum foil exhibits a 127 fold reduction. The popular 4 mil aluminum flame spray coating is far down in the voltage reduction due to its 10-20 fold lower conductivity caused by oxides and less aluminum content than present in foil.

In order for these coatings to be a viable corrective measure they must not impose a significant weight penalty in order for composite to remain weight attractive. Figure 2.30 ranks the coating weight penalties. The aluminum coatings exhibit the least weight penalty as one would expect from the primary aerospace material.

Figure 2.31 ranks the protective coatings in order of the amount of voltage they provide per unit of 1 square foot of weight aluminum foil, copper foil and aluminum flame spray rank significantly higher than all other protective coatings. The high conductivity low weight as an aluminum foil cause it to be the best-followed by copper due to its conductivity and aluminum flame spray due to its very low weight. Aluminum flame spray must be used with caution. Though it ranks third in Figure of Merit 4 mils of it do not offer the sizeable voltage reduction of aluminum foil or copper foil. This can be compensated by increasing the flame spray thickness without incurring a significantly larger

weight penalty. Figure 2.31 also indicates that an approximately 2.5 higher conductivity in aluminum flame spray would make it competitive with aluminum foil at a lower weight penalty. The metallic coating benefits of:

- o EM Protection
- o Laser Protection
- o Heat Protection
- o Water Vapor Absorption Reduction
- o Ability to build better more reliable joints
- o Airframe structural integrity protection when servicing the aircraft

make coatings a desirable solution to composite electromagnetic problems. An aluminum foil coating protection combined with box device protection offers total electromagnetic protection and aids many other aircraft disciplines. The Naval Air Systems Command is requiring application of the protection on its upcoming composite aircraft and helicopter procurements

AD-A115 132

ATLANTIC RESEARCH CORP ALEXANDRIA VA F/G 11/4
NOTEBOOK ON ELECTROMAGNETIC PROPERTIES OF COMPOSITE MATERIALS B--ETC(U)
SEP 81 D R PFLUG, J A BIRKEN, R A WALLENBERG N00019-80-C-0157
NAVAIR-AIR-518-9 NL

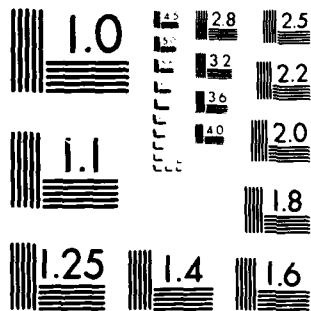
UNCLASSIFIED

2 of 2

REF ID: A115132



END
DATE
FILMED
7 82
DTIC



MICROCOPY RESOLUTION TEST CHART
NATIONAL BUREAU OF STANDARDS 1963-A

2.5 References

1. J.R. Moser, "Low Frequency Shielding of a Circular Loop Electromagnetic Field Source," IEEE Trans. Elec. Comp., Vol. EMC-9, No. 1, pp 6-18, March 1967.
2. S.A. Schelkunoff, Electromagnetic Waves, Van Nostrand, 1943.
3. R. Wallenberg, et. al, Advanced Composite Aircraft Electromagnetic Design and Synthesis, Interim Report, SRC-TR-79-490, April 1980.
4. D. Strawe, L. Piszher, Interaction of Advanced Composites With Electromagnetic Pulse (EMP) Environment, The Boeing Co.
5. F. Force, et. al., Investigation of Effects of Electromagnetic Energy on Advanced Composite Aircraft Structure and Their Associated Avionic Electrical Equipment, Phase D, Vol 1, The Boeing Co., Final Report, September 1977.
6. Protection Optimization For Advanced Composite Structures, Fourth Quarter Report, Grumman Aerospace Corp., June 1978.
7. J.A. Birken, "In Depth Studies of Composite Material Electromagnetic Performance," NATO AGARD Conference Proceedings, No. 283, Electromagnetic Effects of (Carbon) Composite Materials Upon Avionic Systems, June 1980.

3.0 ELECTROMAGNETIC THREATS

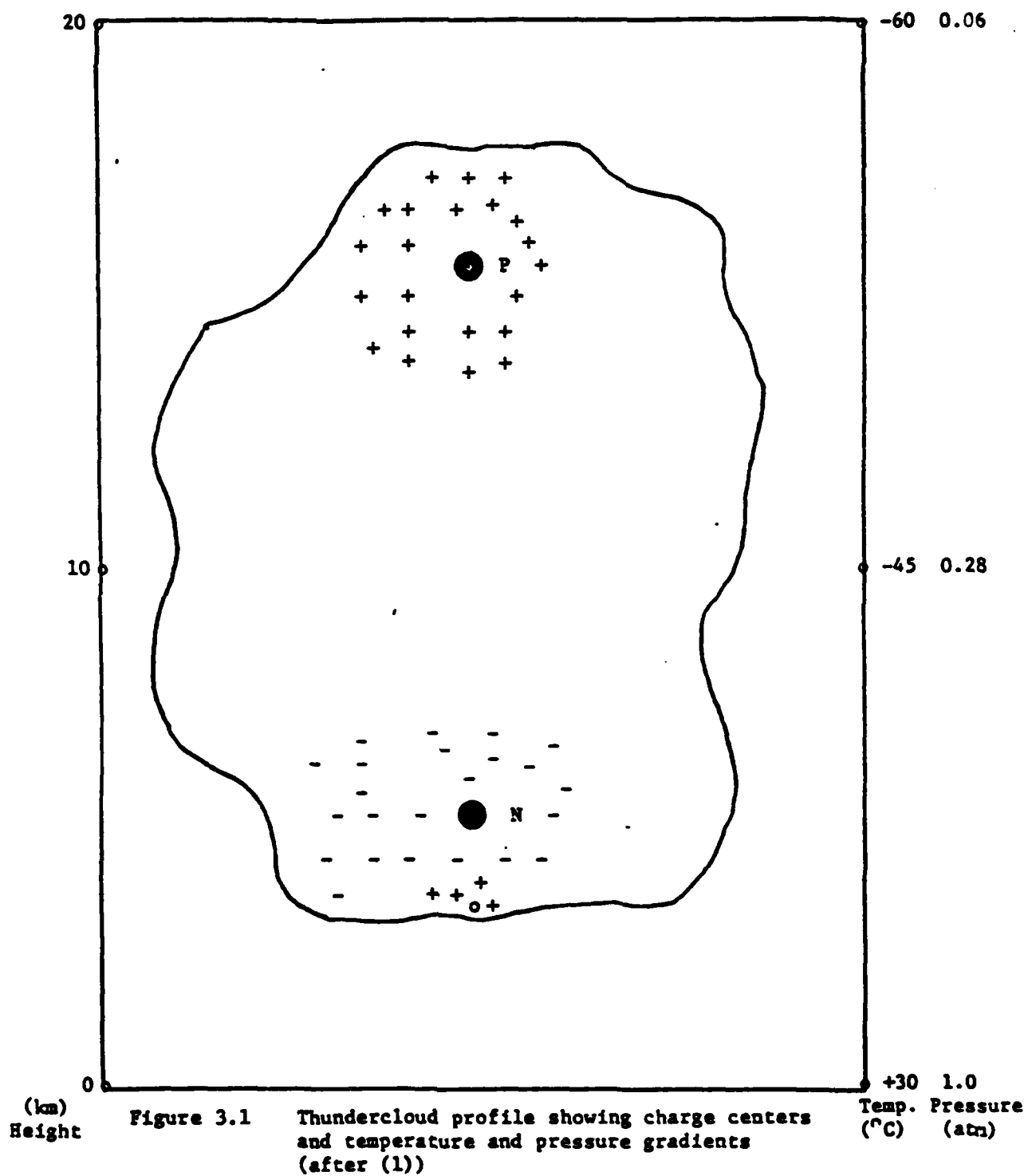
The ability to operate successfully under adverse conditions is an extremely important consideration in the design of aircraft using composite material. The adverse conditions discussed in this section are electromagnetic in origin and are termed electromagnetic threats. Certain threats, such as lightning and precipitation static, occur naturally in the environment or as a result of normal system operation. Others, such as high powered RF from radars, nuclear electromagnetic pulse, or high energy lasers are man-made and originate from both friendly and hostile sources. Each threat is described in detail and an assessment made of its possible impact on system performance.

3.1 Natural Threat

In this section the naturally occurring threats of lightning and precipitation static are discussed. A general description is given for each threat; certain mathematical models are presented that describe the main threat mechanisms, and a brief assessment is made of the impact of the threat on system performance.

3.1.1 Lightning

Lightning may be generally described as a sequence of transient, high current electrical discharges in the atmosphere. The lightning flash that is usually observed is in reality several individual lightning strokes separated by 40 milliseconds or more. Lightning is most commonly associated with thunderstorm activity but may occur in sandstorms, snowstorms, dust clouds from erupting volcanos, or even in clear air.⁽¹⁾ Only discharges from thunderclouds to ground will be discussed since most available experimental data pertains to this situation.



3.1.1.1 The Lightning Process - Overview^(1,4,5,6)

A thundercloud is a dynamic mixture of water droplets, water vapor and ice under the influences of a temperature gradient, a pressure gradient and a gravitational field. The various processes occurring within the cloud cause a separation of electrical charge to occur with large positive charge generally accumulating at the cloud top and large negative charge generally accumulating at the cloud bottom. A cloud profile illustrating charge separation versus the temperature and pressure gradients involved is shown in Figure 3.1. The charge distributions are usually described in terms of major or minor charge centers in the cloud. These centers act as equivalent sources which reproduce the measured E and H fields external to the cloud but do not necessarily coincide with the actual charge distribution. The magnitudes of the charge centers are typically ± 40 coulombs for major centers and ± 10 coulombs for minor centers. The detailed mechanism of the charge separation process is not known but is probably similar to the familiar triboelectric or thermoelectric frictional charging processes. The potential difference between major charge centers is on the order of 10^8 volts. This voltage will give a cloud energy of 4×10^9 joules which represents an upper bound on the energy available for the lightning process.

Lightning will occur whenever the separation of charge in the thundercloud produces an electric field sufficient to cause electrical breakdown of the air gap between cloud and ground. The good weather electric field intensity at the ground is 100 volts/m while the uniform field intensity needed to cause electrical breakdown of dry air at normal atmospheric pressure is 300 kV/m. For non-uniform fields, the field intensity for breakdown will always be less. The electric fields that produce lightning discharges are very non-uniform, being relatively strong at the cloud base and relatively weak at the ground.

There are two mechanisms that are thought to occur in the discharge process. In the first mechanism, which is dominant for uniform fields, the free electrons existing in the air gap are accelerated by the electric field and interact with atoms and molecules in the air to produce additional electrons and ions through electron-impact ionization and photoionization. These growths of electron and ion densities are termed avalanches. Numerous avalanches will eventually lead to breakdown of the air gap.

A second mechanism becomes dominant for non-uniform fields. Luminous pulses of ionization, called streamers, propagate out at high velocity from the high field region to the low field region. The streamer head contains an intense electric field capable of producing ionization in the surrounding air allowing the streamer to propagate rapidly. The streamer that initiates the lightning process is unique in that it propagates in a characteristic stepping fashion. This streamer, called the stepped leader, typically propagates at a velocity of 1.5×10^5 m/sec in steps 50m long with a pause of 50 microseconds between steps about 5 coulombs of charge are deposited along the leader channel, which may be 3 km long and a few meters wide, in about 20 msec. The detailed physics of the stepped leader is not well understood although several theories have been proposed.⁽¹⁾ Many utilize the concept of a non-luminous pilot leader which precedes and guides the luminous stepped leader.

As the stepped leader propagates downward, the high field in the leader head causes upward moving streamers to be launched from ground or a sharp object. Such streamers will be initiated for ground electric field intensities of 10^6 volt/m or greater. When the upward and downward leaders meet, a conducting channel is formed. The leader head is effectively grounded while the leader tail is still at high potential. The result is a very luminous, positive discharge up the leader channel called the first return stroke. Tremendous energy (typically 5×10^8 joules) is delivered to the leader channel in a few microseconds. A large fraction of this energy causes the leader channel to expand and its temperature to rise (up to $30,000^\circ\text{K}$). A cylindrical shock wave is produced which is the main source for thunder. A small fraction (about 1%) of the energy produces the electromagnetic spectrum. The return stroke current is characterized by a rapid rise in current peak value (up to 100 kamps within 10 microseconds), a slow decline (to one-half the peak value in 40 microseconds) and a propagation velocity of 5×10^7 m/sec. The stroke lasts typically 70 - 100 microseconds.

After the return stroke has traversed the channel, current up to hundreds of amperes will continue to flow for several milliseconds. During this time tens of coulombs of charge may be transferred to the channel. This continuing current is thought to be an important mechanism for maintaining ionization along the conducting channel for subsequent return strokes.

If sufficient charge is made available to the channel from the thundercloud in a time of 100 milliseconds or less, a streamer called a dart leader will traverse the channel. This streamer precedes a subsequent return stroke and is similar to a stepped leader except that the stepping process is usually absent. Subsequent return strokes are usually of less intensity than the first return stroke but otherwise similar in characteristics. The total set of strokes constitutes the lightning flash seen by the eye and is typically a fraction of a second in duration.

Lightning flashes vary widely in their properties depending on lightning type and location on the earth. Table

3.1 lists a range of values for the various components of a lightning flash as found in the literature. The values in this table are meant to give a feeling for the orders of magnitude involved and to serve as a guideline. The total lightning discharge process is illustrated in Figure 3.2 in the time domain. The waveform is not to scale but serves to illustrate the trend of the data given in Table 3.1 and to summarize the preceeding discussion.

3.1.1.2 Radiated Lightning Spectrum^(4,6,7)

Two measured lightning spectra are shown in Figures 3.3a - 3.3b and include the contributions of many investigators. The measured range is from a few kHz to a few GHz. The spectra are normalized respectively to 10 km and one statue mile and have bandwidths of 1 kHz. The frequency range of maximum signal amplitude is 5-10 kHz and the amplitude decreases roughly inversely as the frequency. Beyond a few GHz the spectrum has not been measured.

3.1.1.3 Lightning Near Fields^(2,4)

For points reasonably near the discharge channel, the near fields of the lightning are dominant. The near electric field is produced by the charge deposited along the stepped leader channel. As estimate for this field can be given by considering the electric field produced by a uniform line of charge of finite length. Such a field is given by

$$E = - \frac{\rho}{2\pi\epsilon_0} \left(\frac{1}{D} - \frac{1}{(L^2+D^2)^{1/2}} - \frac{L^2}{(L^2+D^2)^{3/2}} \right) \quad (2-1)$$

where ρ is the charge density; L is the length of the leader channel in meters; and D is the distance from the channel in meters. As an order of magnitude estimate, for ρ equal to 1 coulomb per km, L equal to 2.5 km, and D equal to 100m, the field is 200 kV/m which is close to the measured value of 100 kV/m.

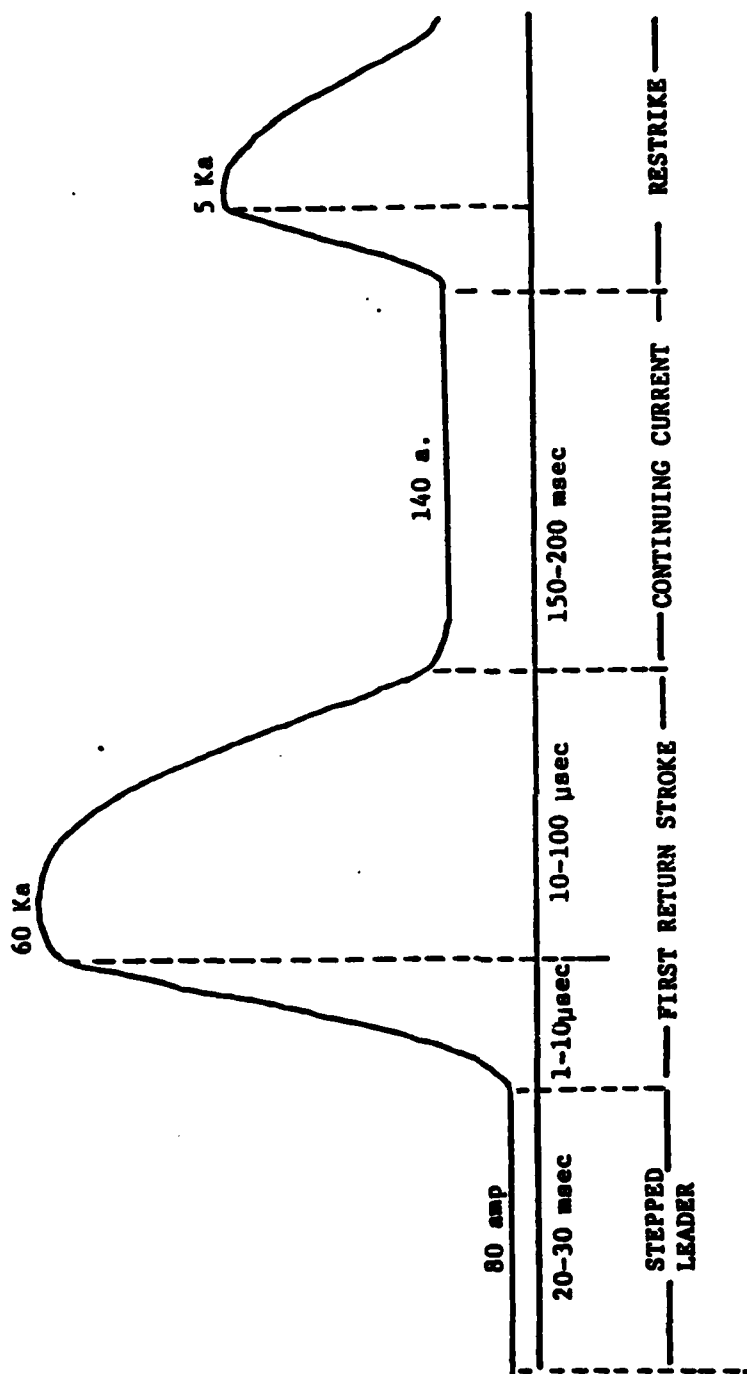


Figure 3.2 Current Waveform (not to scale) for a lightning flash to ground (5)

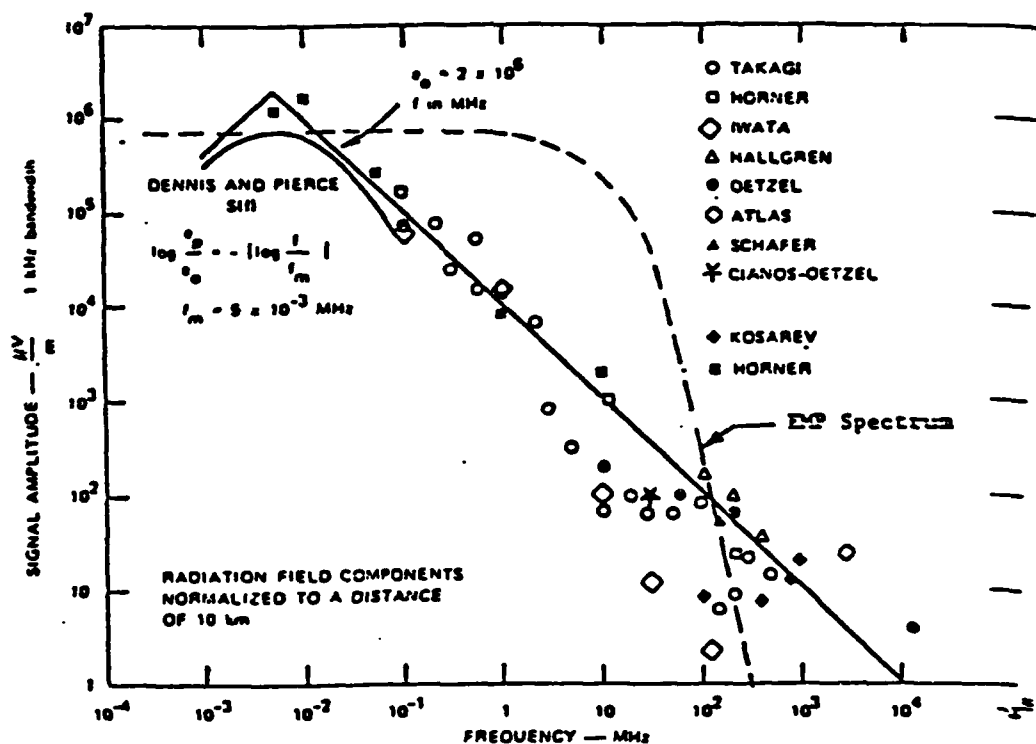


Figure 3.3a Radiated lightning spectrum normalized to 10 km (an EMP spectrum is included for comparison) (4,6)

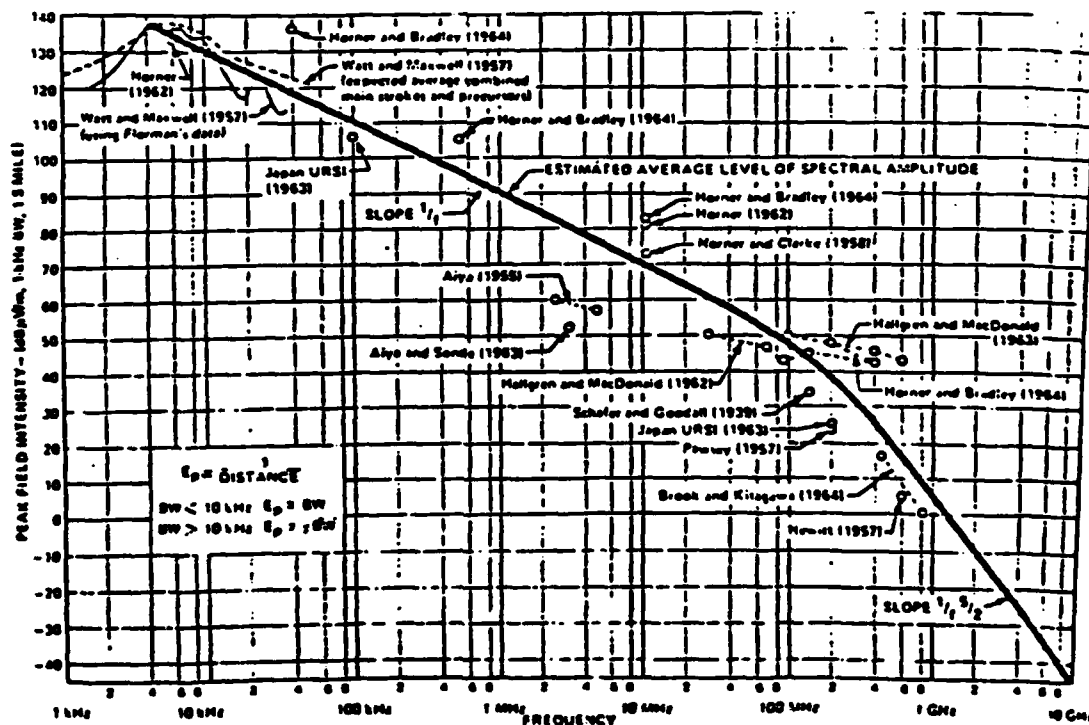


Figure 3.3b Radiated lightning spectrum normalized to one statute mile (6,7)

Table 3.1 Representative Characteristics for Cloud-to-Ground Lightning Flashes (1)

	Minimum	Average	Maximum
Stepped Leader			
Step Length (m)	3	50	200
Time Between Steps (μsec)	30	50	125
Velocity of Propagation (m/sec)	1×10^5	$1-5 \times 10^5$	2.6×10^6
Charge Deposited on Channel (cou)	3	5	20
Dart Leader			
Velocity of Propagation (m/sec)	1×10^6	2×10^6	2×10^7
Charge Deposited on Channel (cou)	0.2	1	6
Return Stroke			
Velocity of Propagation (m/sec)	2×10^7	5×10^7	1.4×10^8
Rate of Current Rise (Ka/μsec)	1	10-20	100
Time to Peak Current (μsec)	0.25	2	30
Peak Current (Ka)	3	10-20	140
Time to Current Half-Value (μsec)	10	40	250
Charge Transferred (cou)	0.2	2.5	20
Channel Length (km)	2	5	14
Continuing Current			
Current Duration (msec)	58	160	400
Current Value (a)	30	140	500
Charge Transferred (cou)	7	26	110
Total Flash			
Strokes per Flash	1	3-4	26
Time Between Strokes (msec)	3	40-80	300
Duration of Flash (sec)	0.01	0.2	2
Charge Transferred (cou)	3	25	90

The magnetic near field is produced primarily by the large return stroke current which forces the magnetic field to lag behind the electric field. The magnetic near field can be estimated by considering a current moving along a thin cylindrical column. This model for the current gives the magnetic field

$$H = \frac{I}{2\pi D} \left[\frac{L}{(L^2 + D^2)^{1/2}} \right] \quad (3-2)$$

where I is the return stroke current and L and D are as in (3-1).

Several expressions for the current waveform of the return stroke current have been proposed and are in common usage.⁽⁵⁾ One very simple waveform that is often used is the simple triangular function shown in Figure 3-4. This function has a quick rise to a maximum and a slow decay which are the basic requirements for the stroke current waveform.

The waveform defining the Space Shuttle Lightning Protection Criteria is shown in Figure 3-5 and consists of several straight lines bounding the various parts of the actual waveform. The result is a more detailed expression for the current which is still simple.

Analytic expressions commonly used for the waveform are double and quadruple exponentials. A triple exponential is also occasionally used, but this waveform forces the current to jump discontinuously. One double exponential function is given by

$$I(t) = I_0(e^{-\alpha t} - e^{-\beta t}) \quad (3-3)$$

$$I_0 = 206 \text{ ka}$$

$$\alpha = 1.7 \times 10^4 \text{ Hz}$$

$$\beta = 3.5 \times 10^6 \text{ Hz}$$

The waveform for this double exponential is shown in Figure 3-6.

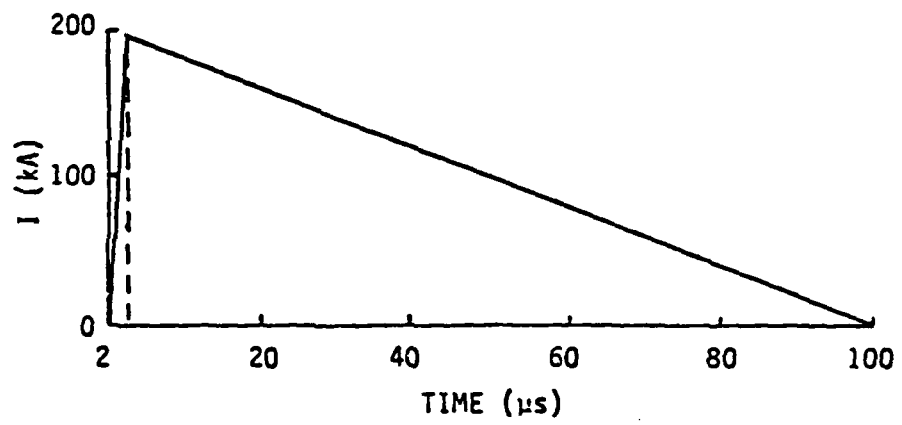


Figure 3.4 Triangular lightning current waveform⁽⁵⁾

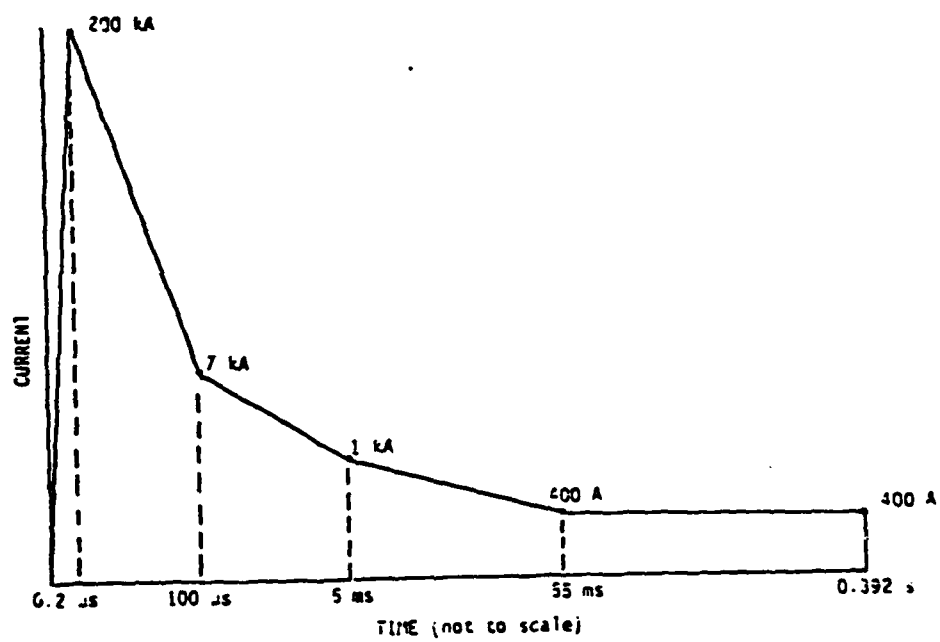


Figure 3.5 Space shuttle lightning current waveform⁽⁵⁾

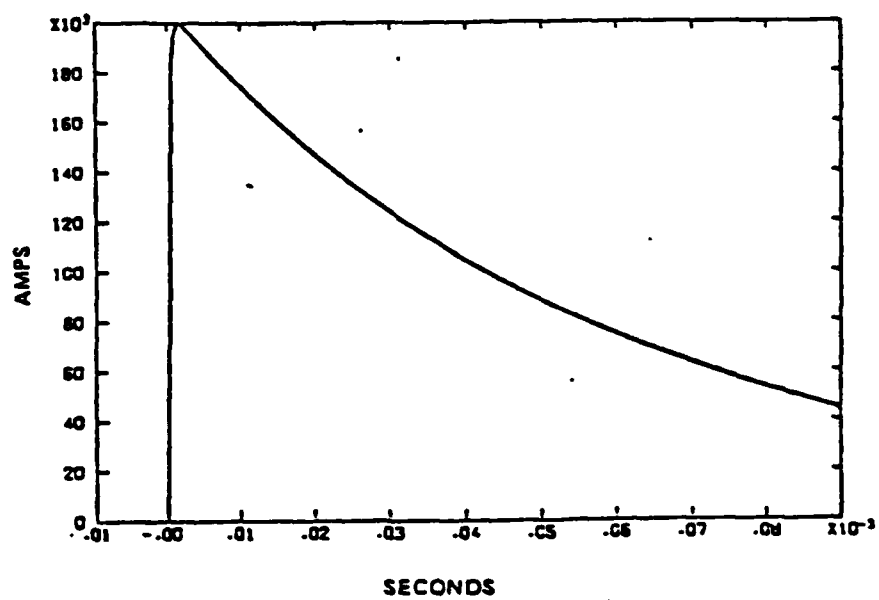


Figure 3.6 Double exponential lightning current waveform⁽⁵⁾

A triple exponential waveform is

$$I(t) = I_0(e^{-\alpha t} - e^{-\beta t}) + I_1 e^{-\gamma t} \quad (3-4)$$

where

$$\begin{aligned} I_0 &= 30 \text{ ka} \\ I_1 &= 2.5 \text{ ka} \\ \alpha &= 2 \times 10^4 \text{ Hz} \\ \beta &= 2 \times 10^5 \text{ Hz} \\ \gamma &= 2 \times 10^3 \text{ Hz} \end{aligned}$$

and a quadruple exponential function is

$$I(t) = I_0(e^{-\alpha t} - e^{-\beta t}) + I_1(e^{-\gamma t} - e^{-\delta t}) \quad (3-5)$$

where

$$\begin{aligned} I_0 &= 30 \text{ ka} \\ I_1 &= 2.5 \text{ ka} \\ \alpha &= 2 \times 10^4 \text{ Hz} \\ \beta &= 2 \times 10^5 \text{ Hz} \\ \gamma &= 1 \times 10^3 \text{ Hz} \\ \delta &= 2 \times 10^4 \text{ Hz} \end{aligned}$$

The waveform for the triple exponential function is shown in Figure 3.7 and the one for the quadruple exponential function is in Figure 3.8. The double exponential in (3-4) has a maximum current of 206 ka and actually represents a "worst case" situation. The triple and quadruple exponential functions have maximum currents of 30 ka and are more typical of the average current in the return stroke.

The frequency domain representations of these waveforms are interesting and are given in Figures 3.9 - 3.12. The last figure shows the superposition of all the waveforms and indicates general agreement with the overall waveform for a lightning flash given in Figure 3.3.

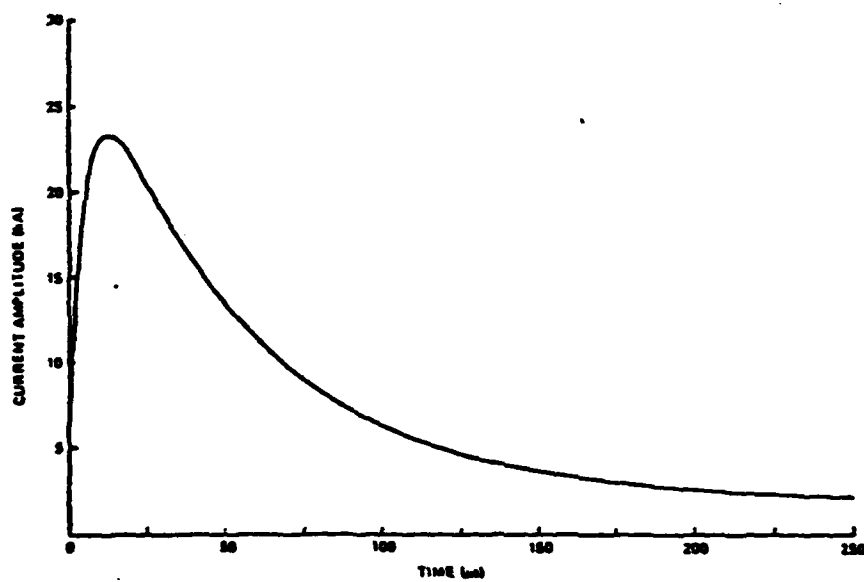


Figure 3.7 Triple exponential lightning current waveform⁽⁵⁾

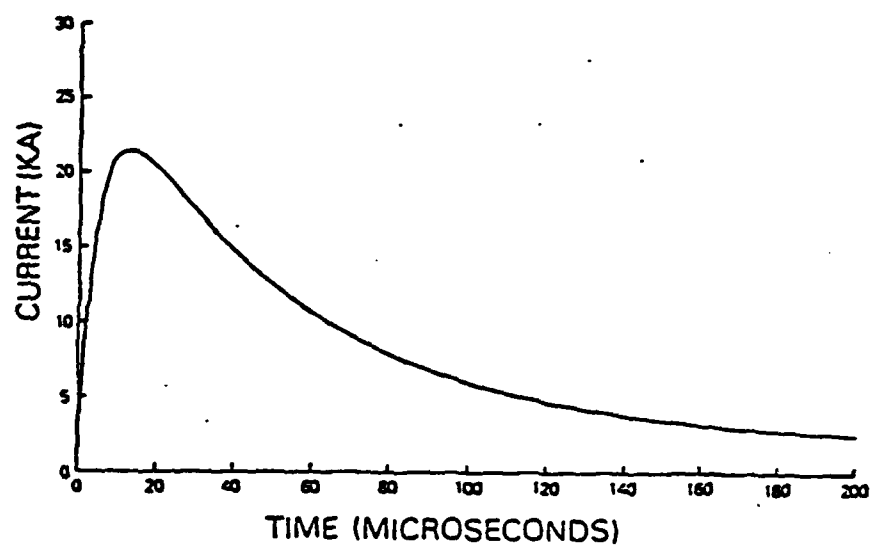


Figure 3.8 Quadruple exponential lightning current waveform⁽⁵⁾

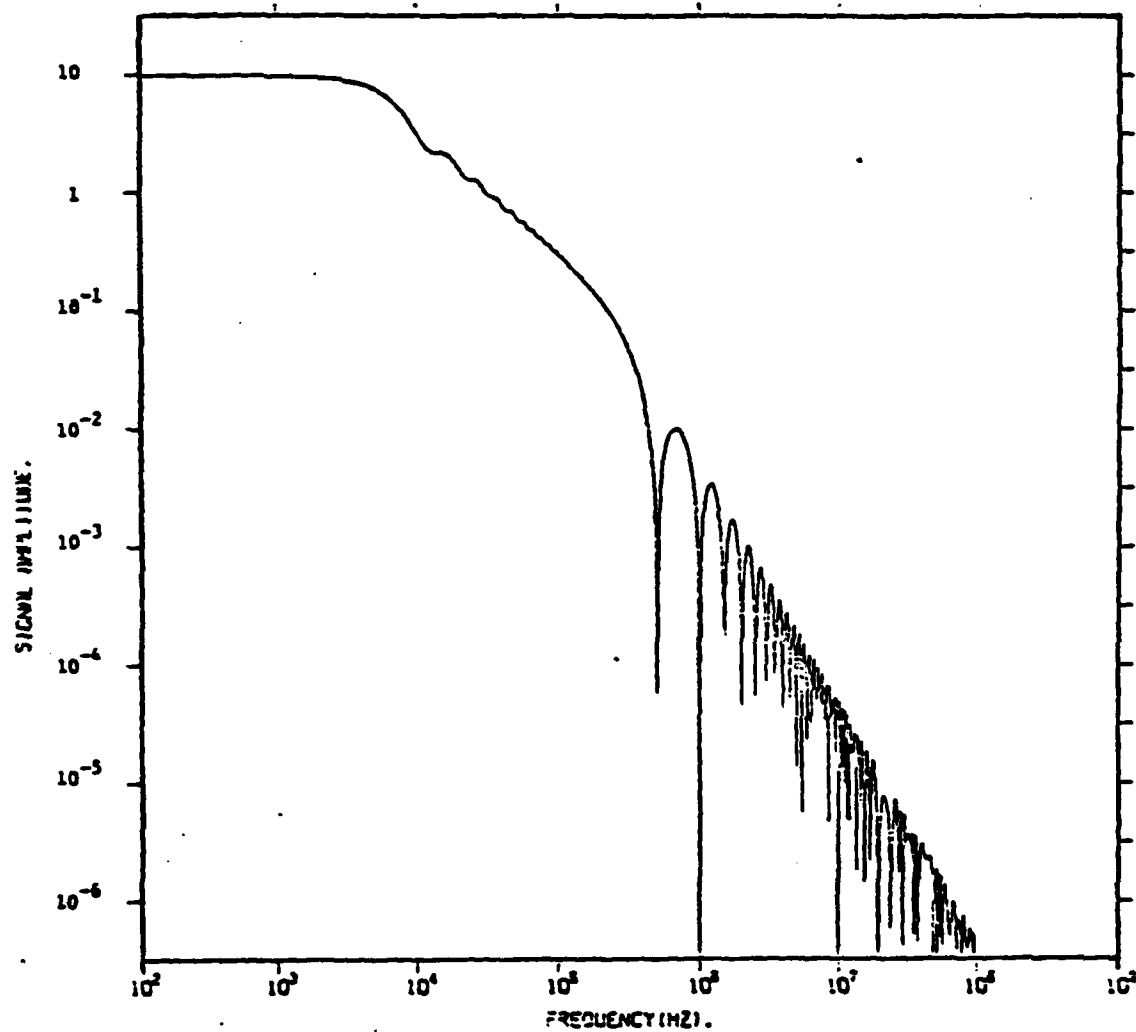


Figure 3.9 Spectrum of triangular current lightning waveform⁽⁵⁾

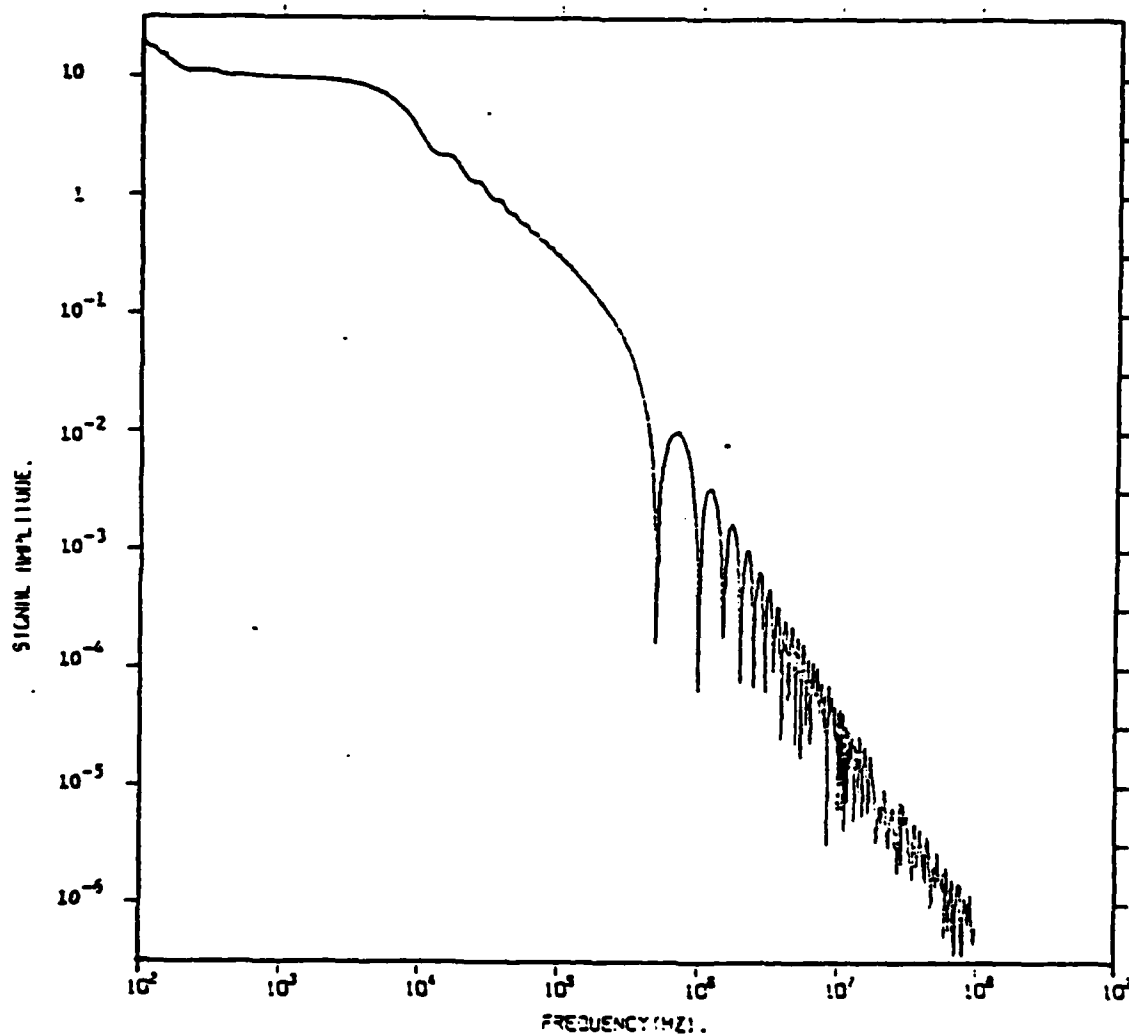


Figure 3.11 Spectrum of Space shuttle current lightning waveform⁽⁵⁾

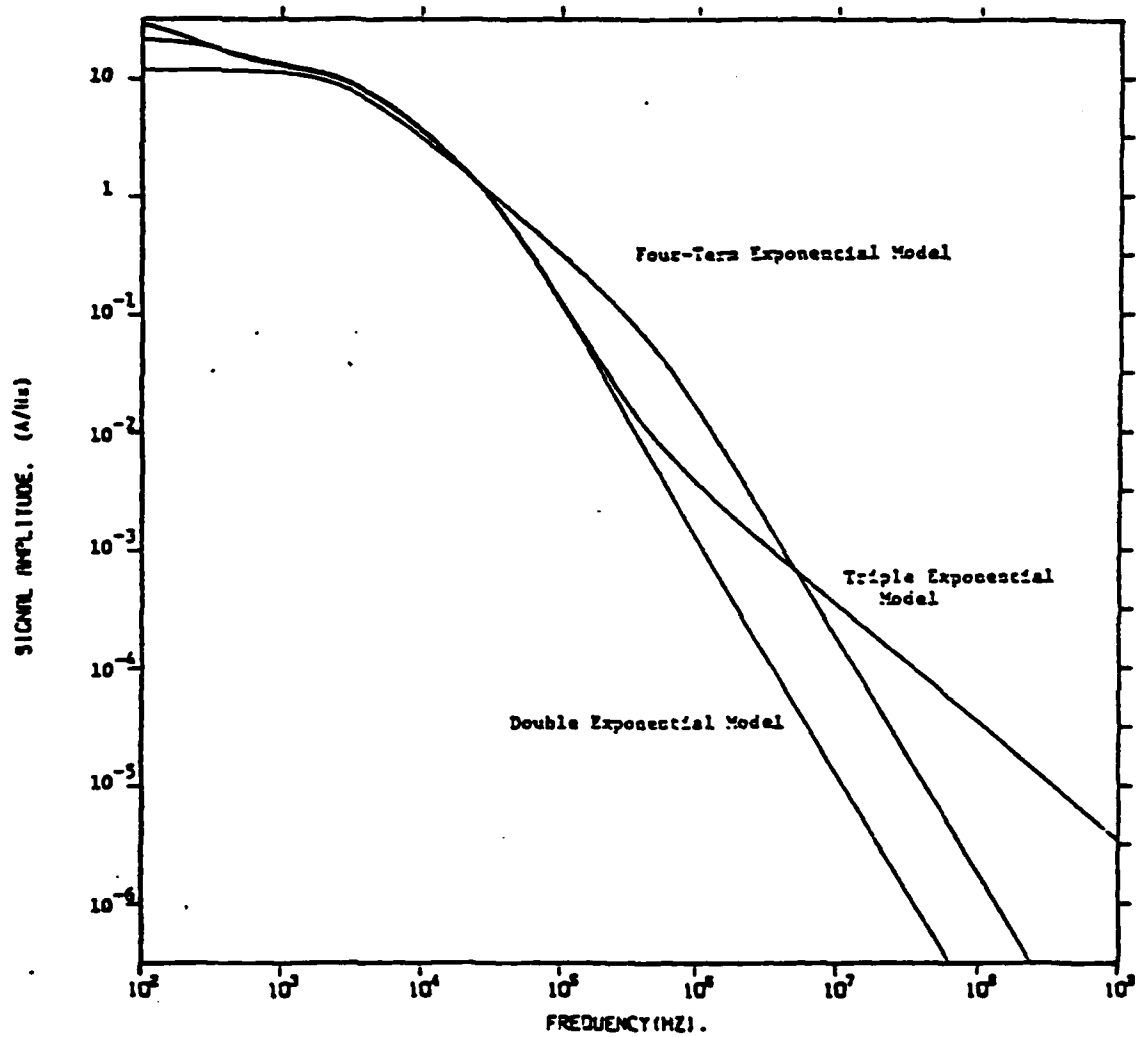


Figure 3.10 Exponential current lightning waveforms⁽⁵⁾

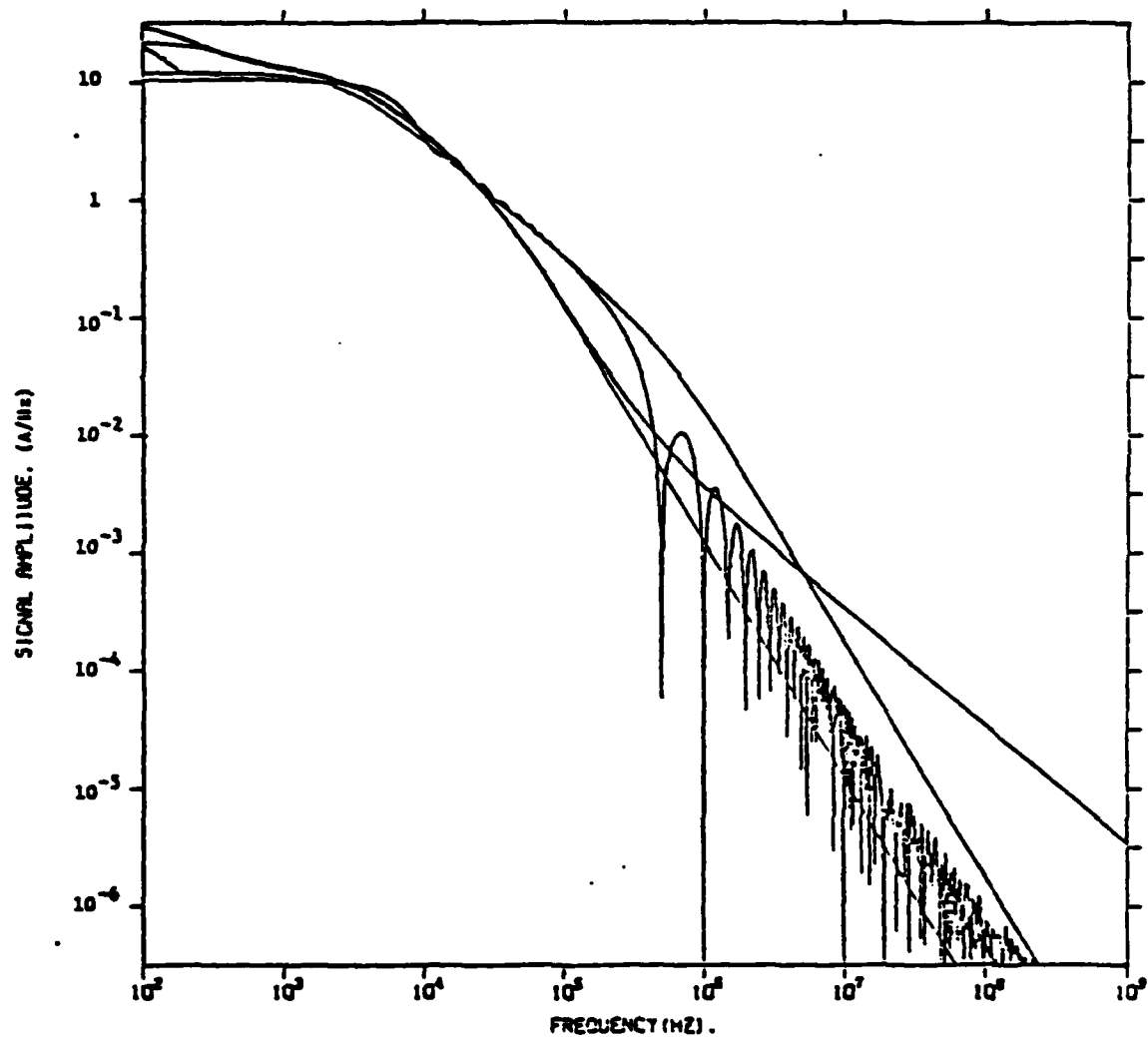


Figure 3.12 Superposition of all lightning current waveforms (5)

3.1.1.4 Lightning Threat Assessment

The threat to composite aircraft from lightning results from either a direct strike or a near miss. Both categories of lightning threat will be discussed separately since different threat mechanisms are involved.

A direct strike on an aircraft takes place when the stepped leader channel becomes attached to the aircraft structure. The aircraft then becomes part of the path traversed by the return stroke. As noted in Section 3.1.1.1 and illustrated in Figure

3.2 , the return stroke is characterized by very high currents and explosive shock waves. Tremendous heat will be generated in the aircraft structure due to the finite conductivity of the structure material. Because of their lower conductivity compared to aluminum and other metals, structures made from composites are more susceptible to physical damage (pitting and puncture points) and even complete burnout of the aircraft. Other vulnerable structures include radomes, canopies, external antennas and special composite panels. The shock waves will produce, in addition, extreme mechanical forces and shock wave heating in the aircraft structure.

In addition to physical damage, composite structures are vulnerable to the high electric and particularly magnetic fields that are generated from a near miss or a direct strike. Because unprotected composite structures tend to offer less EM shielding than metal structures, the electromagnetic fields can more easily penetrate and couple to the internal aircraft avionics. Low power integrated circuits on modern aircraft are particularly sensitive to induced transients of this type. The result of such coupling can then be disruption and/or catastrophic failure of the aircraft avionic systems.

3.1.2 Precipitation Static

3.1.2.1 Overview

The motion of an aircraft or missile through the atmosphere will cause the vehicle to be struck with dust, sleet, hail and other material particles. Continuous particle bombardment of the vehicle will cause charge (positive or negative) to separate from the particles. The result is a net charge transfer from the particles to the vehicle creating a possibly large electric potential. The charging rate depends primarily on the vehicle geometry, velocity, and the nature of the colliding particles. Generally charging is greatest for smaller vehicles with high velocities and for dust and ice crystals. If the surface is sufficiently conducting, the excess charge will move to areas of high field, usually trailing edges or points of the vehicle. For sufficiently high charging rates, corona discharge into the atmosphere will occur. These discharges are in the form of short pulses and are a major source of EM noise in avionic systems. These pulses can be modeled as⁽⁵⁾

$$f(t) = Ae^{-\alpha t} \quad (3-6)$$

Both the amplitude A and the decay constant α depend upon the atmospheric pressure p , as a function of altitude. The atmospheric pressure p is given by

$$p = 760 \exp - \frac{h+0.002h^2}{25} \quad (3-7)$$

where h is in kilofeet and p is in torrs. The parameters A and α in (3-6) are chosen to be

$$A = 7.90569 \times 10^5 p^{0.25} \quad (3-8)$$

$$\alpha = 2.7777 \times 10^{-2} p \quad (3-9)$$

to give a good fit to the exponential data for A and α . The noise spectrum is then given by

$$S = A\left(\frac{\gamma}{\pi}\right)^{1/2}(\omega^2 + \alpha^2)^{-1/2} \quad (3-10)$$

where γ is the number of pulses per minute. This parameter is also a function of atmospheric pressure and good values of γ are given by

$$\gamma = 3.83767 \times 10^3 p^{0.48} \quad (3-11)$$

The noise spectrum is shown in Figures 3.13a - 3.13b. In the first figure, the impact of altitude on the spectrum is shown for several altitudes. In the second figure, the noise level of the spectrum is shown as a function of discharge current for a fixed altitude (sea level).

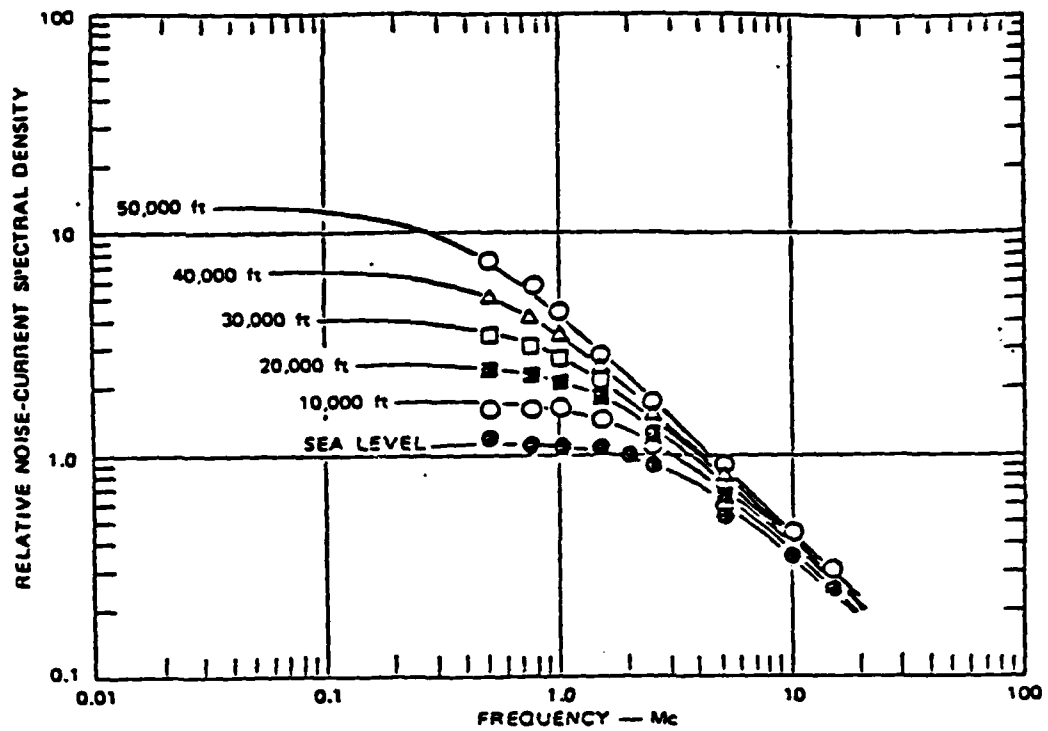
When electric charge is deposited on dielectric media such as radomes, windshields, or structures of intermediate conductivity such as composite structures, the motion of the charge is restricted due to the non-conducting characteristics of these surfaces. For high enough potentials, streamer discharges will occur in the surface. The current for a streamer discharge can be modeled as a double exponential function of the form⁽⁵⁾

$$I(t) = I_m(ae^{-\alpha t} + be^{-\beta t}) \quad (3-12)$$

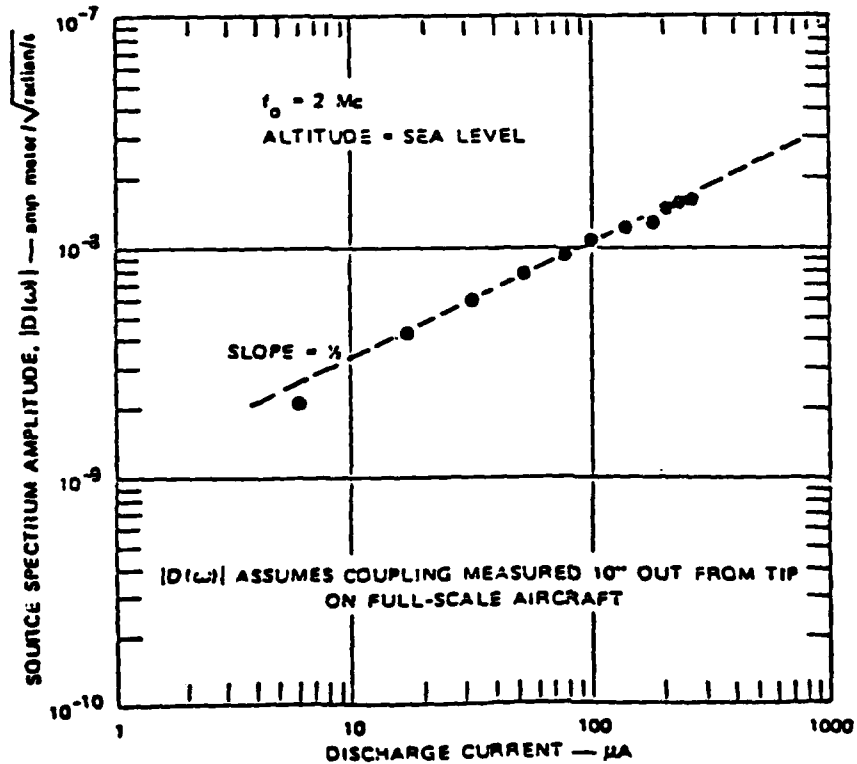
where

$$\begin{aligned} I_m &= 0.01 \text{ amp} \\ a &= 0.597 \\ \alpha &= 1.67 \times 10^7 \text{ Hz} \\ b &= 0.403 \\ \beta &= 3.47 \times 10^6 \text{ Hz} \end{aligned}$$

This current discharge is several orders of magnitude smaller than lightning discharges. One effect of such streamer discharges is that the EM fields penetrate the system and couple onto the system avionics. To illustrate the magnitude of this effect, the current induced on a wire located just below the streamer has been calculated for several streamer lengths using a typical coupling factor $\Psi = 3m^{-1}$. The results are shown in Figure 3.14.



(a) NORMALIZED SPECTRUM SHOWING ALTITUDE EFFECTS



(b) RELATIONSHIP OF ABSOLUTE NOISE LEVEL TO DISCHARGE CURRENT

Figure 3.13 Noise spectrum properties (5)

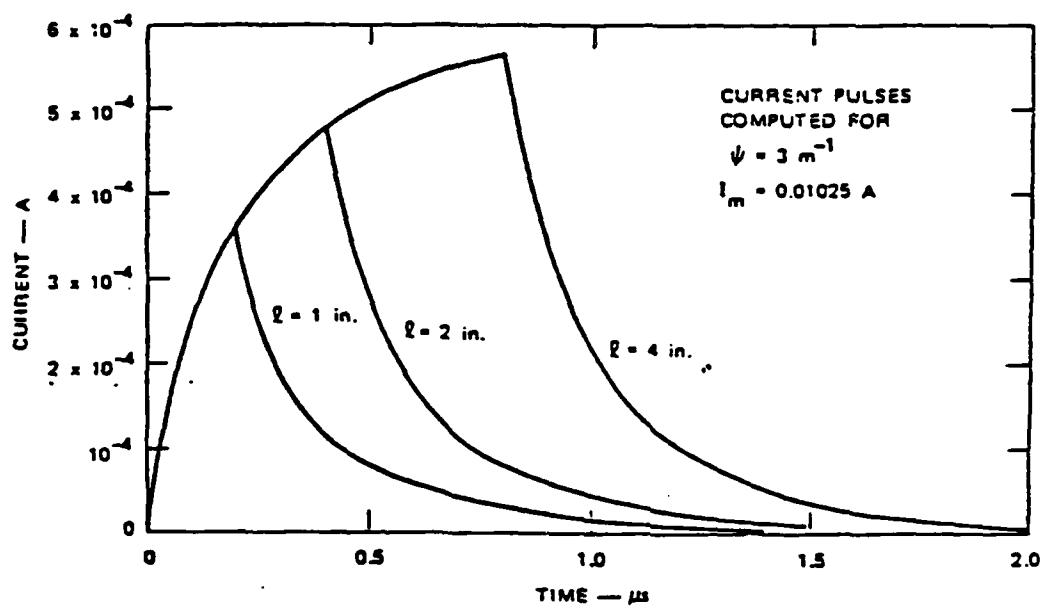


Figure 3.14 Current pulses resulting from streamers of several lengths(5)

3.1.2.2 Precipitation Static Threat Assessment

The threat to composite vehicles from precipitation static results from the broad EM fields radiated during the corona or sparking process. Such fields are a major source of antenna noise. In addition, coupling to avionics can occur by penetration of the fields through composite surfaces and apertures such as radomes or canopies.

3.2 Friend/Foe Threat

In this section, the man-made electromagnetic threats to composite aircraft are described in detail. The threats considered are strong RF sources, nuclear electromagnetic pulse and high energy lasers and particle-beam weapon systems. A general description is given of each threat followed by relevant mathematical models and a threat assessment.

3.2.1 RF Threat

In this section, a realistic but unclassified, electromagnetic environment is presented which might be encountered by a composite aerospace vehicle in an operational scenario. This environment is shown in Figures 3.15 - 3.16 and is expressed in terms of an RF power density as a function of frequency from 10 kHz to 1 GHz. The power density levels were computed assuming mainbeam illumination at a distance of 500 meters from the radiating antenna with the target continuously illuminated.

NO. 940-1410 DISTENEN GRAPH PAPER
 SEMI-LOGARITHMIC
 4 CYCLES X 10 DIVISIONS PER INCH

CUBENE DISTENEN CO.
 NEW YORK, N. Y.

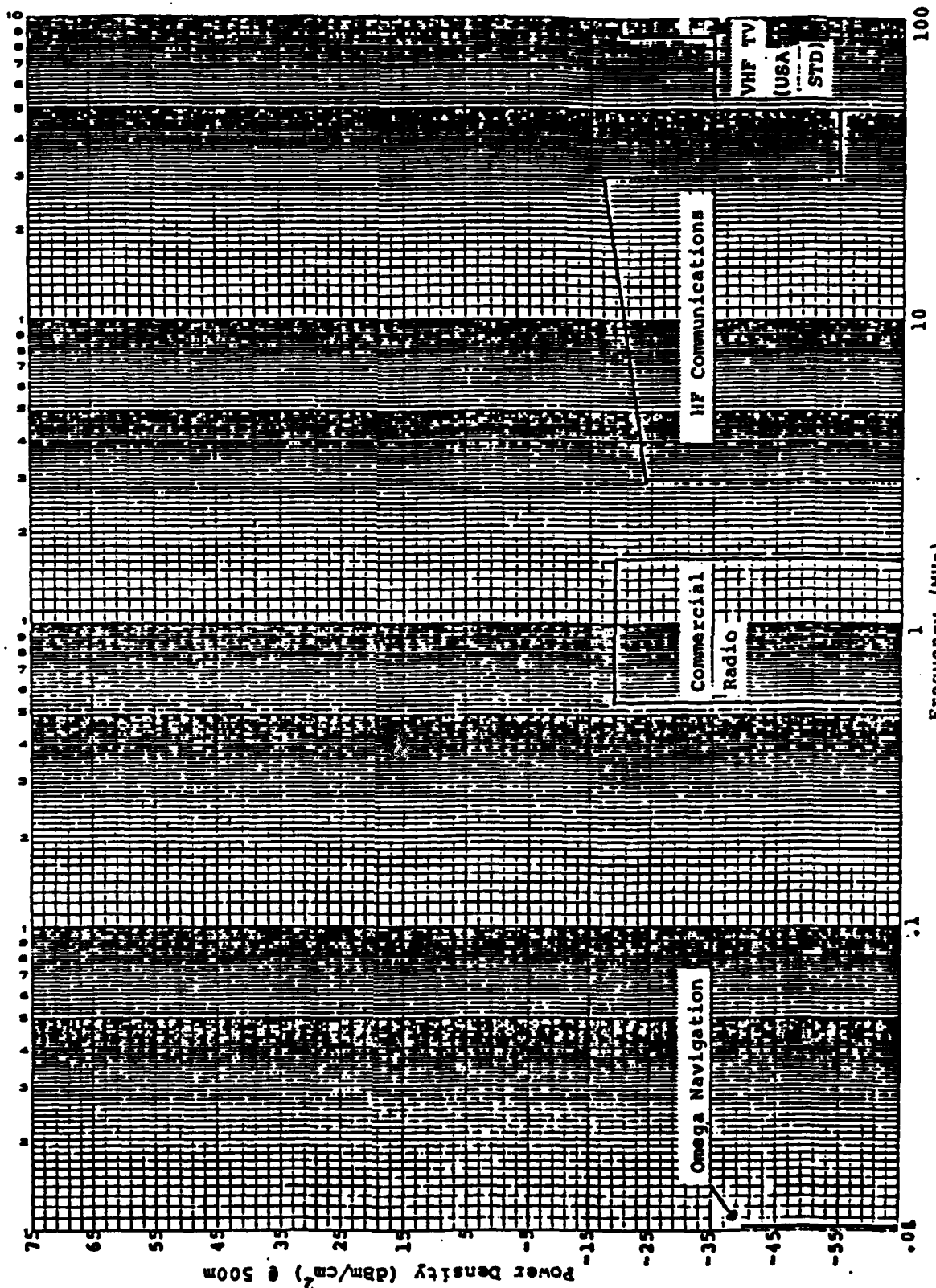


Figure 3.15 RF Environment (10 kHz - 100 MHz)

K-E SEMILOGGRAPHIC 46 4880
 1 SCALE IN DB DIVISIONS
 SUPPL. BY TERRY CO.

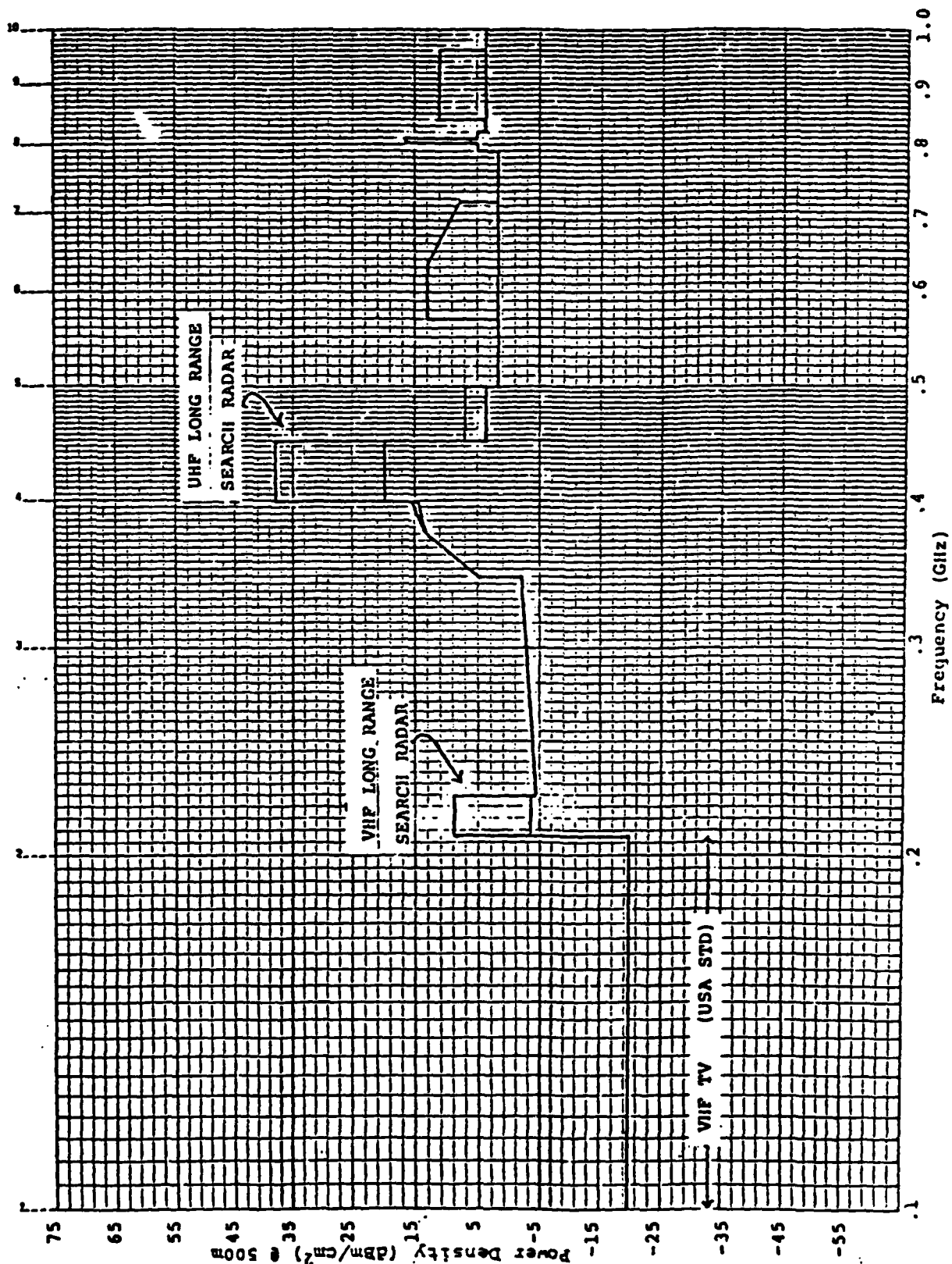


Figure 3.16 RF Environment (100 MHz - 1 GHz)

3.2.2 EMP Threat

3.2.2.1 Overview⁽⁵⁾

The explosion of nuclear weapons in the atmosphere represents a serious electromagnetic threat to composite aircraft. A nuclear explosion produces an EM pulse (EMP) as well as higher frequency components in the visible, x-ray and gamma ray regions of the spectrum. Only the lower frequency EMP will be discussed in this section.

The EM pulse is assumed to arise from a high altitude air burst of the kind commonly discussed in unclassified literature. The electric field from such a pulse can be modeled by a double exponential waveform which, in the time domain, has the functional form

$$E(t) = E_0(e^{-\alpha t} - e^{-\beta t}) \quad (3-13)$$

where

$$E_0 = 58.15 \text{ kV/m}$$

$$\alpha = 6.3 \text{ MHz}$$

$$\beta = 189 \text{ MHz}$$

This waveform has a maximum value of 50 kV/m; a rise to peak time of 0.019 microseconds and a time to half peak amplitude of 0.185 microseconds. The magnetic field is assumed to be given by

$$H = \frac{1}{\eta_0} E \quad (3-14)$$

where $\eta_0 = 377$ ohms and is the free space impedance. The EMP waveform is shown in Figure 3.17. This waveform is similar in appearance to the double exponential waveform for lightning in Section 3.1 but the time scale for EMP is 100 times smaller. This difference in the time scales of the two threats serves to distinguish their impacts on a given aircraft. Because of the time scale difference, there are different frequency components in nuclear EMP than in lightning.

The frequency domain representation of (3-14) is the Fourier Transform given by

$$E(f) = \frac{E_0(\beta - \alpha)}{(\alpha + 2\pi j f)(\beta + 2\pi j f)} \quad (3-15)$$

where f is the frequency. This frequency domain representation of the EMP threat is shown in Figure 3.18. A comparison to the lightning spectrum in Section 3.1 indicates that EMP has a larger number of high frequency components than does lightning.

3.2.2.2 EMP Threat Assessment

The EMP threat to composite aircraft is primarily EM field penetration through composite structures and is similar in many ways to the lightning threat. The EMP spectrum shown in Figure 3.18 shows the existence of many more high frequency components than in the lightning spectrum (see Figure 3.11). Thus EMP amplitudes will tend to be higher than lightning amplitudes for a given common frequency.

3.2.3 High Energy Laser, Nuclear Thermal Radiation and Particle Beam Threat⁽³⁾

Future electromagnetic environments will probably include laser and particle beam weapons. These devices are presently the subject of intensive classified research and development so only a very general overview will be given here.

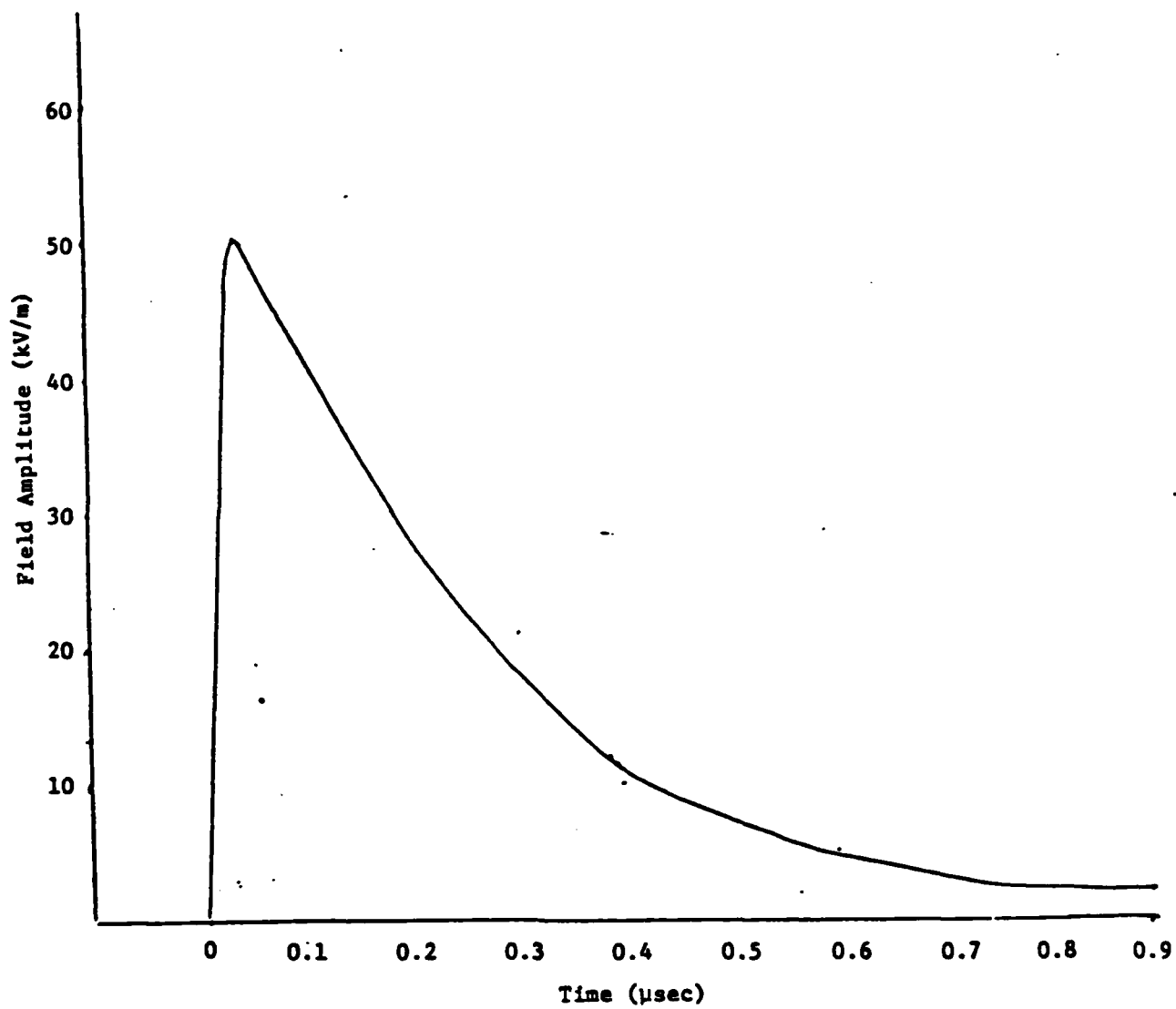


Figure 3.17 EMP Time Domain Waveform (5)

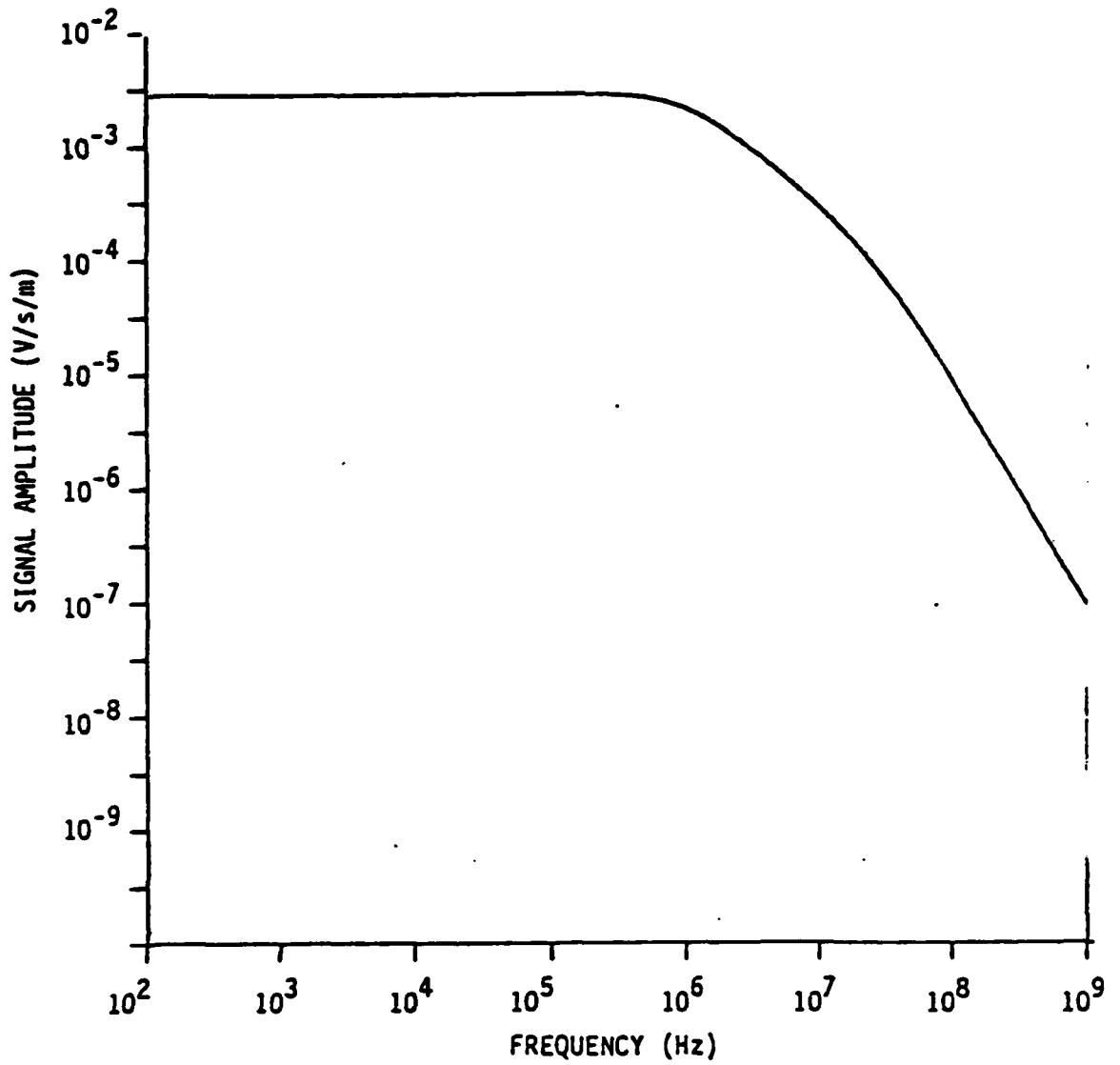


Figure 3.18 EMP in Frequency Domain⁽⁵⁾

A primary candidate for laser weapon systems is the deuterium fluoride laser which operates at 3.8 μ and is capable of several hundred kW (about 500 kW) CW operation. Another prime candidate is the CO₂ laser which operates at 10.6 μ with an output power of 50 - 135 kW. Other chemical lasers are being examined such as the Excimer laser which operates in the μ V region (0.25 - 0.25 μ) and the Free Electron laser tuneable in the vicinity of 3.4 μ at several kW. There are two primary limitations on these laser devices:

1. Thermal blooming which is air heating in the beam that reduces the energy density on the target. The result is an increase in diffraction which defocuses the beam.

2. Aerosol breakdown which is the ionization of particulate matter in the air. A plasma is formed that expands until the entire beam is blocked. This effect occurs at power densities of approximately 10 mW/cm².

Particle beam weapon systems are currently being developed by the U.S. and U.S.S.R. It is expected that the effective ranges of these weapons will be

1. Up to 300 meters - single pulse
2. 4 to 5 km - continuous low PRF
3. Greater than 10 km - continuous pulse propagation

The expected effects on the intended target are

1. Detonation of the high explosive charge in the nuclear warhead carried by the target
2. Disruption of guidance/control/fusing electronics of the target
3. Reduction or voiding of the yield of the nuclear warhead carried by the target.

Energy levels on the order of 100 - 125 joules/gram are required to cause destruction or slumping of nuclear materials, while 210 joules/gram are required to melt lead.

The response of composite structures to thermal pulse heating from a laser, nuclear thermal radiation or a particle beam weapon varies from surface damage to buckling, plastic deformation of the epoxy or complete burn-through with fiber vaporization. This results from the generally⁽³⁾ low thermal conductivity, high absorbtivity, low epoxy combustion temperature and high fiber vaporization temperature of the composite. Figure 3.19 illustrates the backside temperature of a graphite/epoxy substrate as a function of substrate thickness for several energy fluence rates. Drastic strength loss results when steady temperatures reach 400 degrees F.

A summary of the response of a section of graphite/epoxy composite to irradiation by a CW laser is shown in Table 3.2. The composite characteristics that were found to most critically determine laser damage were the laminate lay-up sequence and preload stress factor. Figure 3.20 illustrates the laser energy density necessary to produce a given level of stress in various composite and metal samples for two kinds of failure modes. The energy density necessary to cause heat-related failure is much smaller than the energy density necessary to produce burn-through failure.

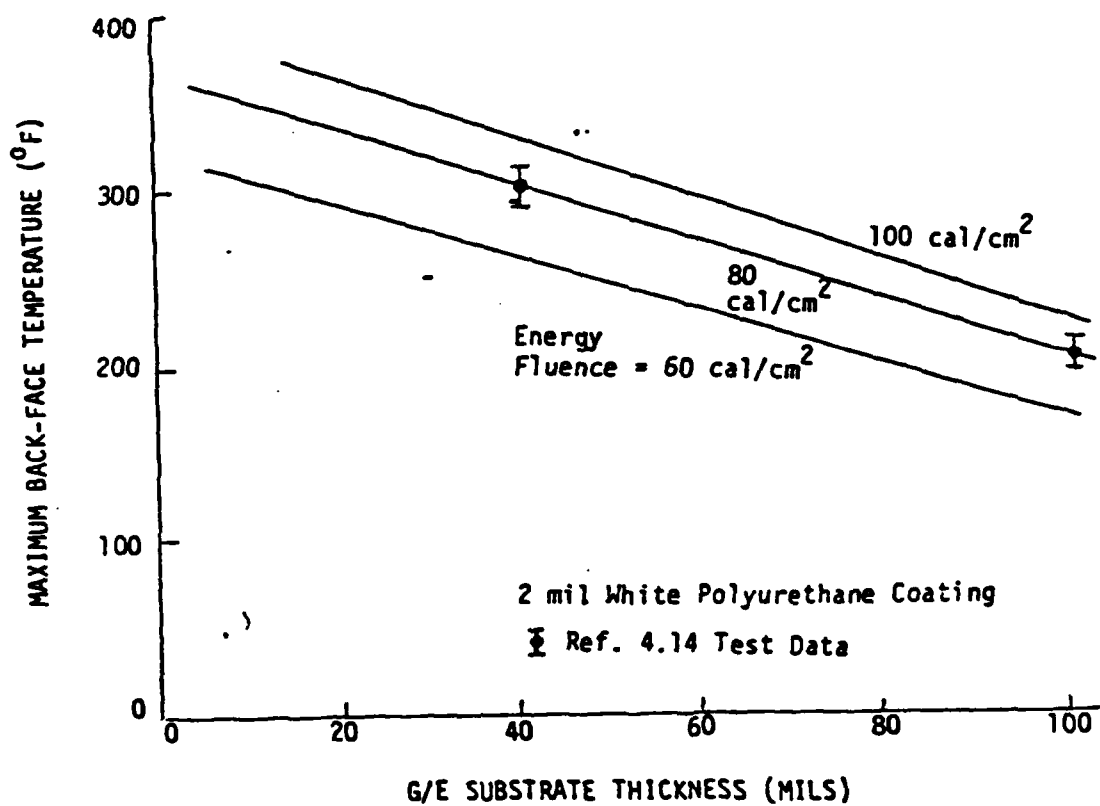


Figure 3.19 Back-face temperature of graphite/epoxy substrate for several thermal pulse fluence levels (3)

Table 3.2 Effect of Variable on CW Laser Response of Graphite/epoxy⁽³⁾

Effect of Variables on CW Laser Response of Graphite/Epoxy

Laser/target variable	Effect of laser damage	
	Burn-through mode ^a	Flood loading mode ^b
Lay-up sequence	No effect	Damage significantly greater when 0° load-carrying ply directly irradiated
Preload stress	Little effect below that stress level causing failure during laser irradiation	Damage increases with decreasing energy fluence and increasing preload stress
Airflow velocity	No effect on penetration rate High airflow velocity reduces structural damage	High airflow velocity reduces structural damage
Beam area	Beam areas $< 4 \text{ cm}^2$ require higher energy levels for penetration	None
Laminate thickness	None	Very little
Fiber/matrix type	None	None
Wavelength	Unknown, all data at $10.6 \mu\text{m}$	Unknown, all data at $10.6 \mu\text{m}$

^aHigh flux, small area irradiation

^bLow flux, large area irradiation

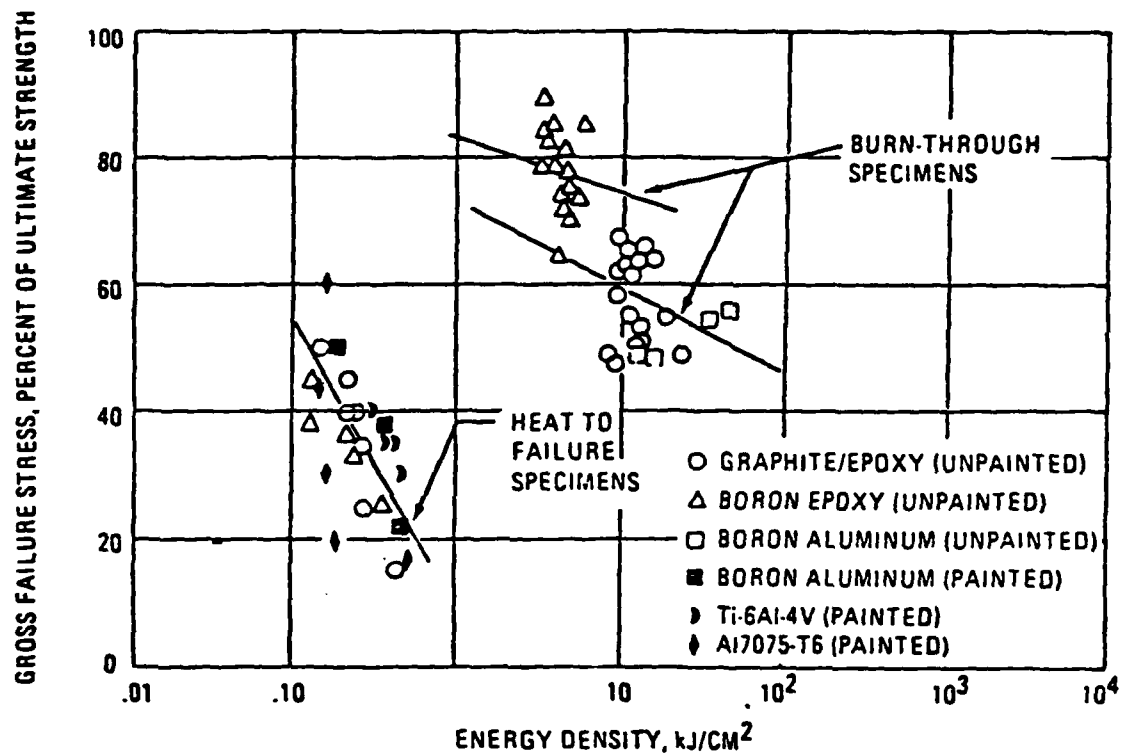


Figure 3.20 Laser energy density necessary to produce a level of stress for two failure modes⁽³⁾

3.3 References

1. Ulman, M.A., Lightning, McGraw-Hill, 1969.
2. Strawe, D., Lightning Source Model Development, Lightning Workshop, NOSC, San Diego California, 1978.
3. Strawe, et. al., Investigation of Effects of Electromagnetic Energy on Advanced Composite Aircraft Structures and their Associated Avionic/Electrical Equipment, Phase II, Volume 1, The Boeing Company, 1977.
4. J. Allen, et. al., A Technology Plan for Electromagnetic Characteristics of Advanced Composites, RADC-TR-76-206, July 1976.
5. Wallenberg, et. al., Advanced Composite Aircraft Electromagnetic Design and Synthesis, Interim Report, Syracuse Research Corp., April 1980.
6. Notebook on Electrical Properties of Composites for Frequencies Above 1 GHz., Atlantic Research Corp., April 1979.
7. Oh, L. L., Measured and Calculated Spectral Amplitude Distribution of Lightning, IEEE Trans. EMC, Nov. 1969.

4.0 Application of Composite Parameter to Existing Aircraft

Figure 4-1 depicts a need to know the ramifications on aircraft design when combining the technologies of:

- Low-level avionic devices
- Composite materials
- High-level threats

to assure adequate protection which allows aircraft to survive/operate in the high-level threat environments of nuclear electromagnetic pulse (NEMP), lightning (LEMP), and radar. Metallic aircraft design has had over 30 years to mature. However, these established design philosophies must be carefully re-examined when incorporating the above cited new technologies. Especially critical is flight crew safety and mission effectiveness as fly-by-wire composite aircraft and computer-controlled weapons systems replace traditional human-actuated mechanical systems.

Loss of aircraft control or mission effectiveness degradation may be categorized by the following:

<u>Category</u>	<u>Determining Parameter(s)</u>
Device upset	V_{OC} , I_{SC}
Device burnout	Energy into device
Airframe damage	Temperature rise and mechanical displacement

The first category is simply a transient condition on a device not resulting in permanent damage, but which may implant erroneous data resulting in incorrect digital system operation. The second condition permanently destroys electronic devices, rendering portions of the avionic system inoperable until replaced. Electronic effects resulting from NEMP and LEMP






	TUBES	DISCRETE TRANSISTORS	INTEGRATED CIRCUITS (IC)	LARGE SCALE INTEGRATED CIRCUITS (LSI)	VERY LARGE SCALE INTEGRATED CIRCUITS (VLSI)
DEVICE	 200V 1 WATT/DEVICE	 TO-18 12V-20V 10-1-10-2 WATT/DEVICE	 FLAT PACK 5V-12V 10-2-10-3 WATT/TRANS	 DIP 5V-7V 10-3-10-4 WATT/TRANS	 CIP CARRIER 15V-2V 10-5-10-8 WATT/TRANS
CAPSULE	GLASS/ METAL/ CERAMIC	METAL/ CERAMIC	METAL/ CERAMIC/ EPOXY	METAL/ CERAMIC/ EPOXY	CERAMIC/ EPOXY
AIRCRAFT	F-8	F-4	F-14	F-18	VSTOL
AIRFRAME MATERIAL	ALUMINUM	ALUMINUM	ALUMINUM/TITAN	GRAPHITE-EPOXY ALUMINUM	GRAPHITE-EPOXY
TIME	PNE-1960's	1950's	1960's	1970's	1980's

Figure 4-1. Aerospace Avionics Device Technology Trends

can cause upset or burnout. In addition, lightning can physically damage airframe sections, which may or may not affect flight safety and mission effectiveness depending on the strike location and aircraft design.

The capability of evaluating the magnitude of these effects during aircraft design or upgrade can

- Realize a 60% electromagnetic "hardening" cost savings
- Shorten the design cycle
- Prevent significant redesign efforts
- Aid contractor in meeting government specifications thereby reducing government/contractor paperwork efforts in modifying specifications
- Increase government/contractor insight prior to hardening testing

The electromagnetic effects on aircraft avionics can be evaluated with the knowledge of six basic frequency dependent functions. These are denoted by $D(f)$ and $T_1(f)$ through $T_5(f)$, which are illustrated in Figure 4-2. Combining these functions determines the amount of electromagnetic protection, $T_6(f)$, required to bring the avionics box open circuit terminal voltage, V_{OC} , to levels which will not upset or burn out the avionics components. The open circuit voltage, V_{OC} , which represents an upper bound for the actual voltage, may be calculated from the relation

$$V_{OC} = D(f)T_1(f)T_2(f)T_3(f)T_4(f)T_5(f)T_6^{-1}(f) \quad (4-1)$$

where:

- $D(f)$ = appropriate threat driving function spectrum
- $T_1(f)$ = material shielding transfer function, Z_t
- $T_2(f)$ = current distribution resulting from the aircraft shape and material distribution
- $T_3(f)$ = joint transfer function = $1 + Z_t^{-1}Y_j^{-1}$
- $T_4(f)$ = cable shielding transfer function

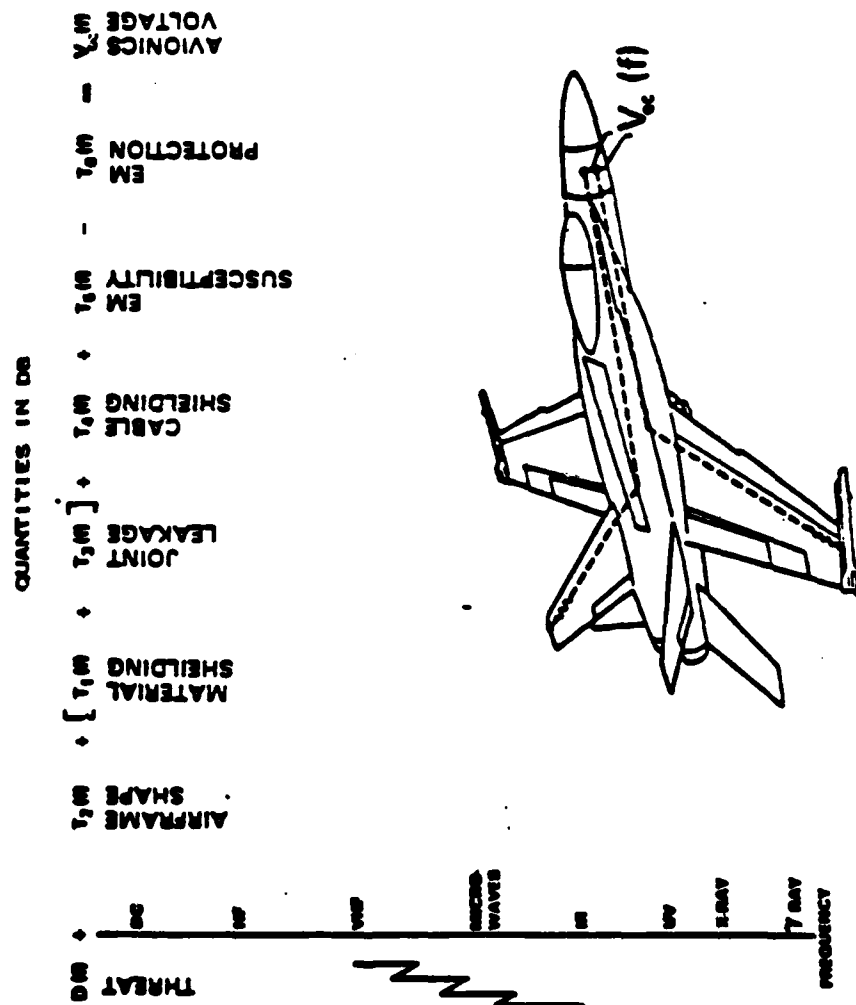





Figure 4-2. Electromagnetic System Parameters

$T_5(f)$ = avionics box terminal penetration characteristic function

$T_6(f)$ = protective transfer function

This section deals only with the threat $D(f)$, the resulting voltage protection; and the resulting weight penalties imposed by the protection.

Figure 4-3 shows peak avionics box terminal open circuit voltage resulting from the electromagnetic threats of

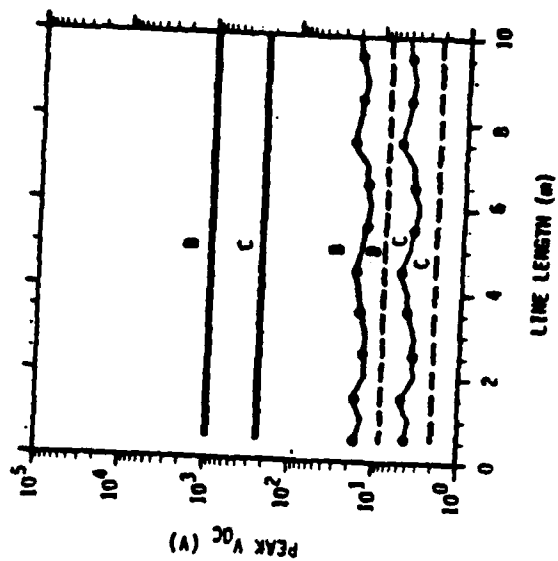
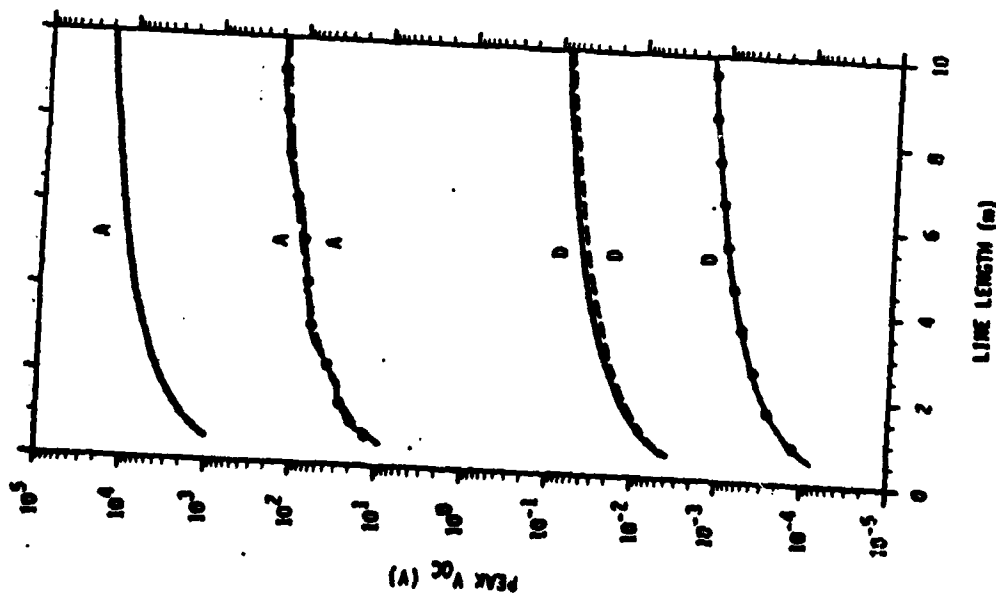
- Direct-strike lightning 
- Near-strike lightning 
- Nuclear electromagnetic pulse 

impinging on an F-14 aircraft having an airframe construction of

- All aluminum
- Aluminum and graphite/epoxy

The open circuit voltage, V_{OC} , is determined by the coupling through composite panels, aluminum panels, and joints which may be summed for total avionics box voltages. An upper bound on the maximum power available at the box terminal is found by computing the short circuit current at the terminals and multiplying by the open circuit voltage. These results are shown in Figure 4-4. It should be emphasized that these results for peak power represent worst-case values because the open circuit and short circuit conditions cannot occur simultaneously.

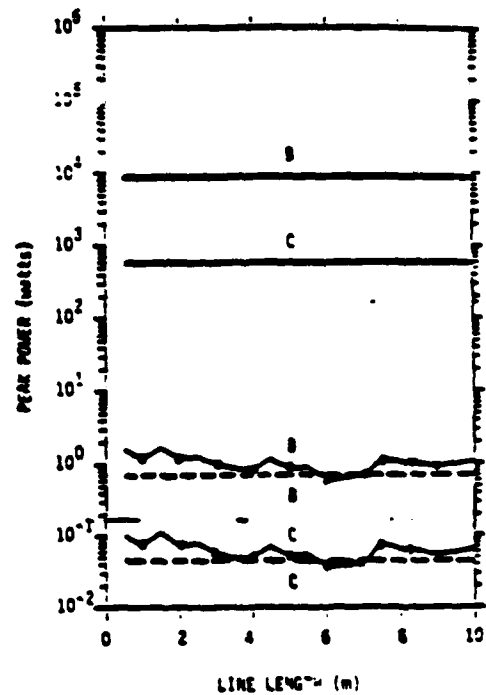
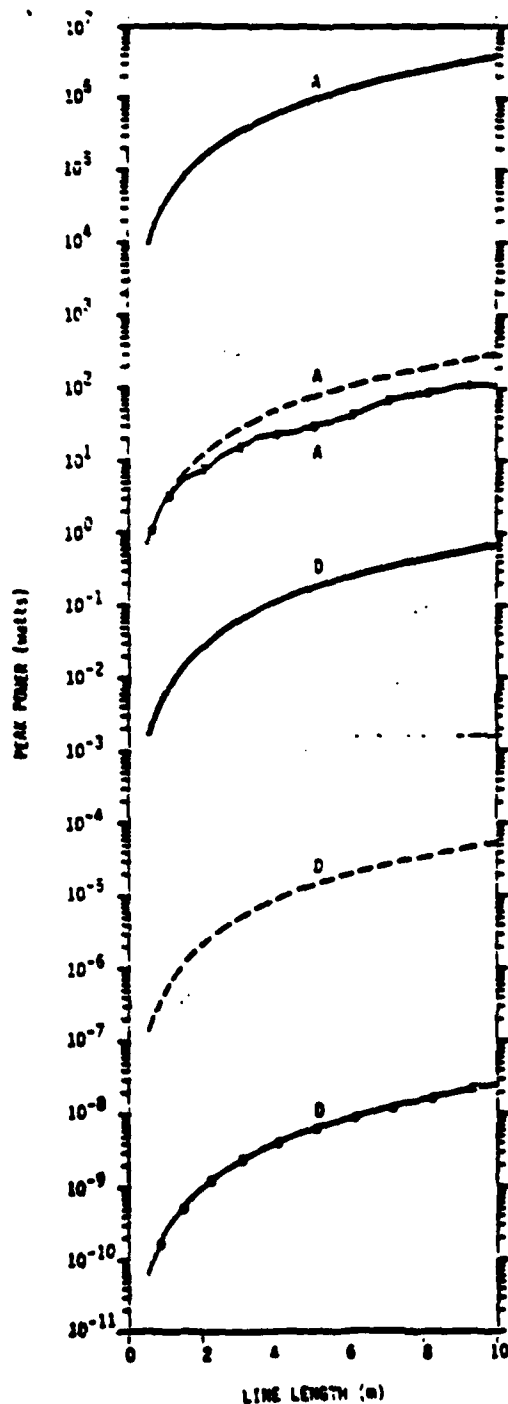
Figure 4-5 shows the Wunsch constant results computed for the cases in Figures 4-3 and 4-4. On the right side of Figure 4-5, representative ranges of Wunsch constants for various semiconductor junction devices are given. Thus, curves exceeding these Wunsch constant ranges indicate that the device junctions are permanently damaged (burned out) if the avionics box provides no further device protection.



- A - Graphite Epoxy Panel Coupling to Single Wire ($\epsilon = 2 \times 10^4$ mho/m, Thickness = 8 ply)
- B - Joint Coupling to Single Wire ($L_j = 1.7m$)
- C - Joint Coupling to Two-Wire Line ($L_j = 1.7m$, $R = 0.5$ in.)
- D - Aluminum Panel Coupling to Single Wire Line ($\epsilon = 3.5 \times 10^7$ mho/m, Thickness = 8 ply)

- - NEPP
- - - Near-Strike Lightning
- Direct-Strike Lightning

Figure 4-3. Peak Open-Circuit Voltage Versus Line Length for Three Threads and Four Coupling-Transmission Line Configurations, $X_0 = 0.05m$, $Z_1 = 100\Omega$



- A - Graphite Epoxy Panel Coupling to Single Wire ($c = 2 \times 10^4$ amp/m, Thickness = 8 ply)
- B - Joint Coupling to Single Wire ($L_j = 1.79m$)
- C - Joint Coupling to Two-Wire Line ($L_j = 1.79m$, $n = 0.5$ in.)
- D - Aluminum Panel Coupling to Single Wire Line ($c = 3.5 \times 10^4$ amp/m, Thickness = 8 ply)

—●— Direct-Strike Lightning
 - - - Near-Strike Lightning

Figure 4-4. Upper Bounds on Peak Power Versus Line Length for Three Threats and Four Coupling-Transmission Line Configurations, $X_0 = 0.05m$, $Z_L = 100\Omega$

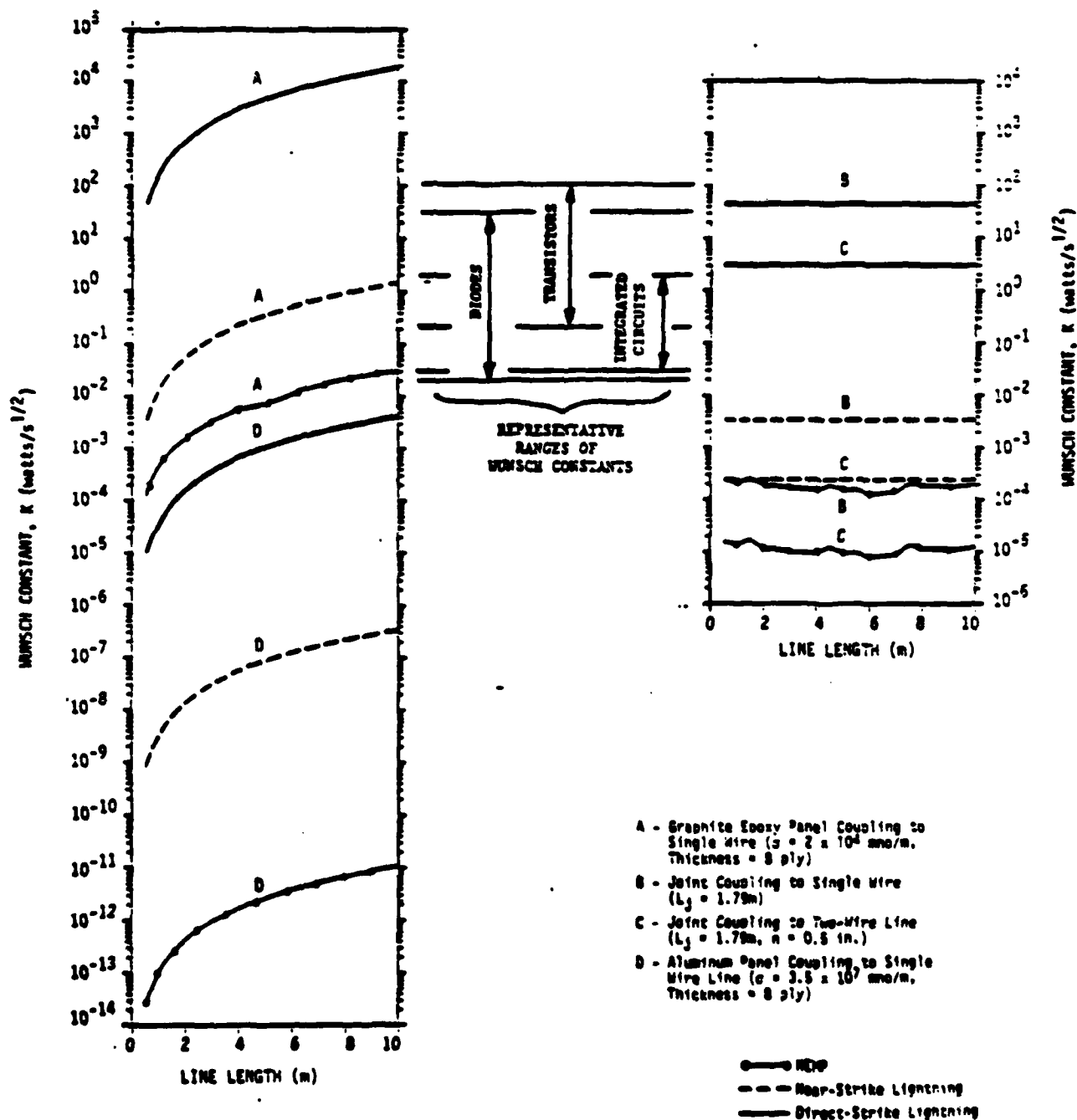


Figure 4-5. Wunsch Constant Versus Line Length for Three Threats and Four Coupling-Transmission Line Configurations, $X_0 = 0.05m$, $Z_L = 100\Omega$

The family of curves in Figures 4-3 through 4-5 were generated from triangular patch surface coupling models of the F-14, which are described in Appendix A, derived from those shown in Figures 4-6 and 4-7. These coupling models evaluate the internal electromagnetic fields that result from the aforementioned electromagnetic threats using knowledge of the precise internal electromagnetic flux distribution in the interior of an aircraft under the approximations discussed in Section 6. Coupling models allow accurate calculation of voltages and powers that exist on internal wires of given internal geometric location.

Figure 4-8 illustrates the outstanding agreement in surface current density, J_s , calculated by the well known THREDE code and the triangular patch surface model used in this report. The early time and peak value difference between the codes is being resolved at present in the full-scale F-14 testing currently underway in the Navy's FAANTIAEL effort.

The significance of threat rise time, τ , on aircraft vulnerability is examined in Figures 4-9 through 4-12. Figure 4-9 shows an increase in skin current density by a factor of 17% for a reduction in threat rise times from 0.1 μ s to 2.0 μ s for near-strike lightning. For the NEMP case shown in Figure 4-10, the peak skin current density increases by a factor of 14 for a decrease in rise time from 0.001 μ s to 0.1 μ s. These increases in peak surface current are due to the higher frequency content in the short rise time threat spectra. However, they have little effect on interior circuit voltages where only joint and panel coupling occurs. This behavior is to be expected in light of the joint admittance and transfer impedance function characteristics shown in Section 3.

Figures 4-12 and 4-13 show the transfer impedance shielding capability of coated panels and the improvement obtainable over an 8-ply panel consisting of graphite/epoxy. The weight penalties imposed by the various coatings is illustrated in Figure 4-14. Finally, a weight shielding figure of merit is shown in Figure 4-15 using the 8-ply composite panel as a baseline.

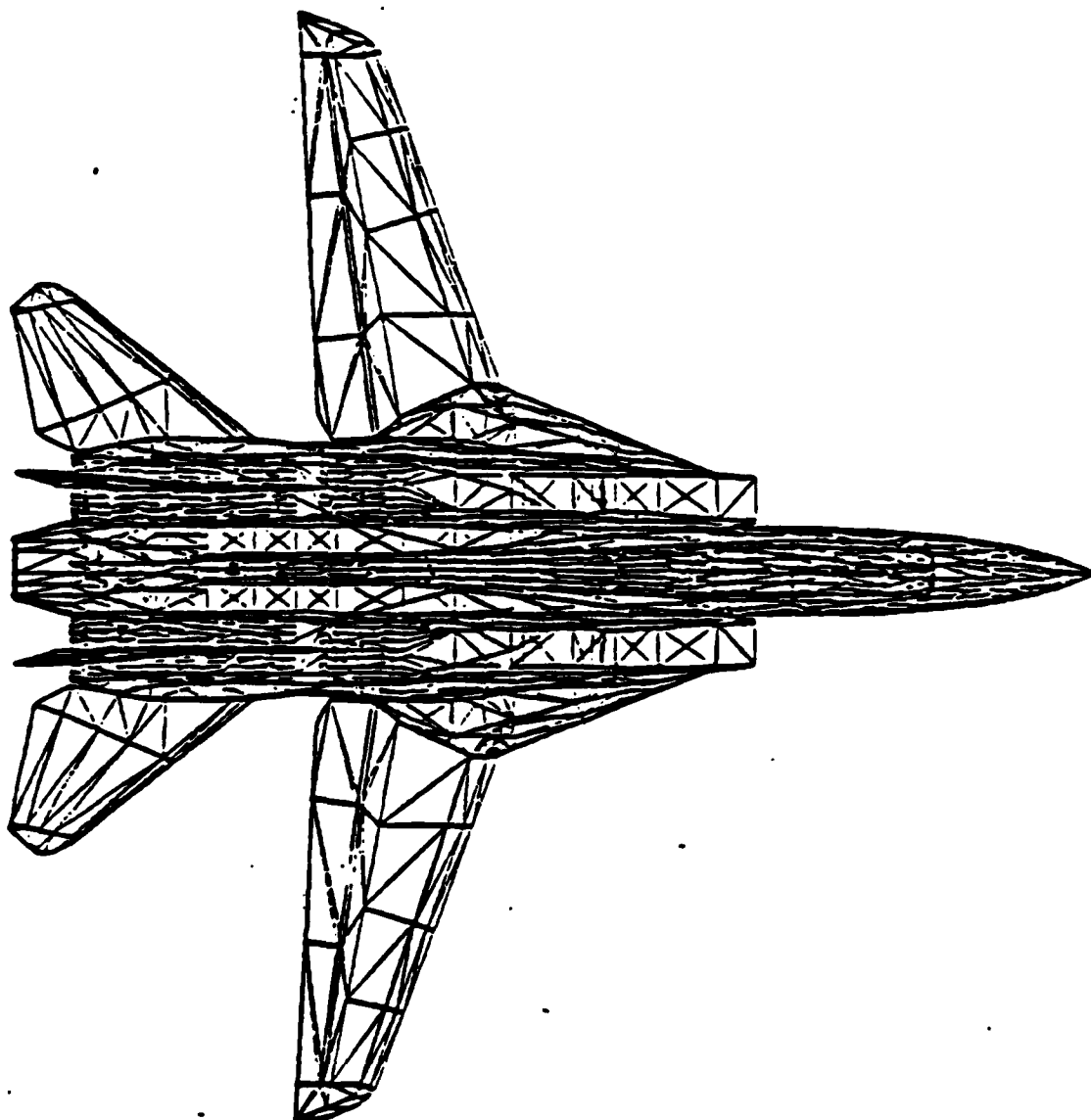


Figure 4-6. Top View of F-14 Using Triangular Patch
Data Base of Reference 4

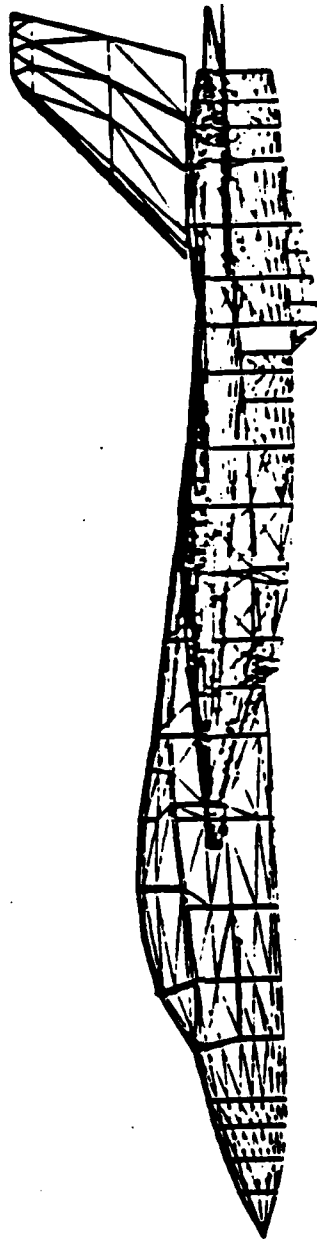
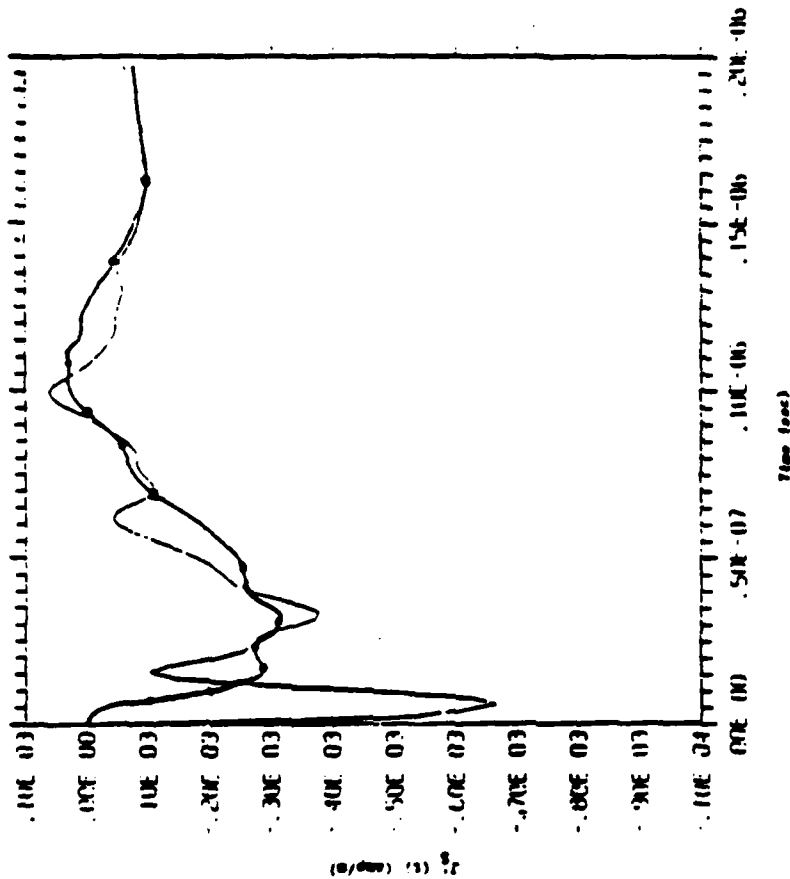
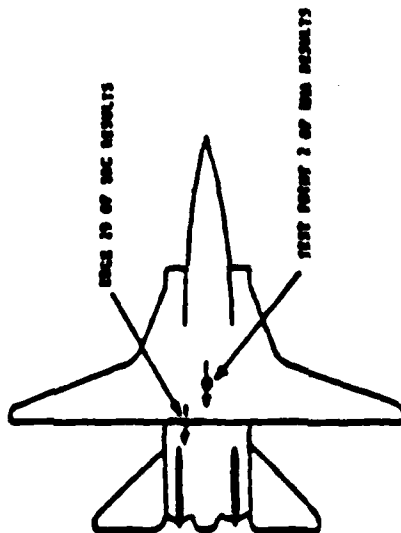


Figure 4-7. Side View of F-14 Using Triangular Patch Data Base
of Reference 4



NOTE: Circles denote values abstracted from EMA results.

(b) Plot of $J_s(t)$ for MEMP Excitation

(a) Surface Current Test Point Locations

Figure 4-8. Comparison of Surface Current Density with MRC/EMA Code and Surface Patch Model Used in This Report

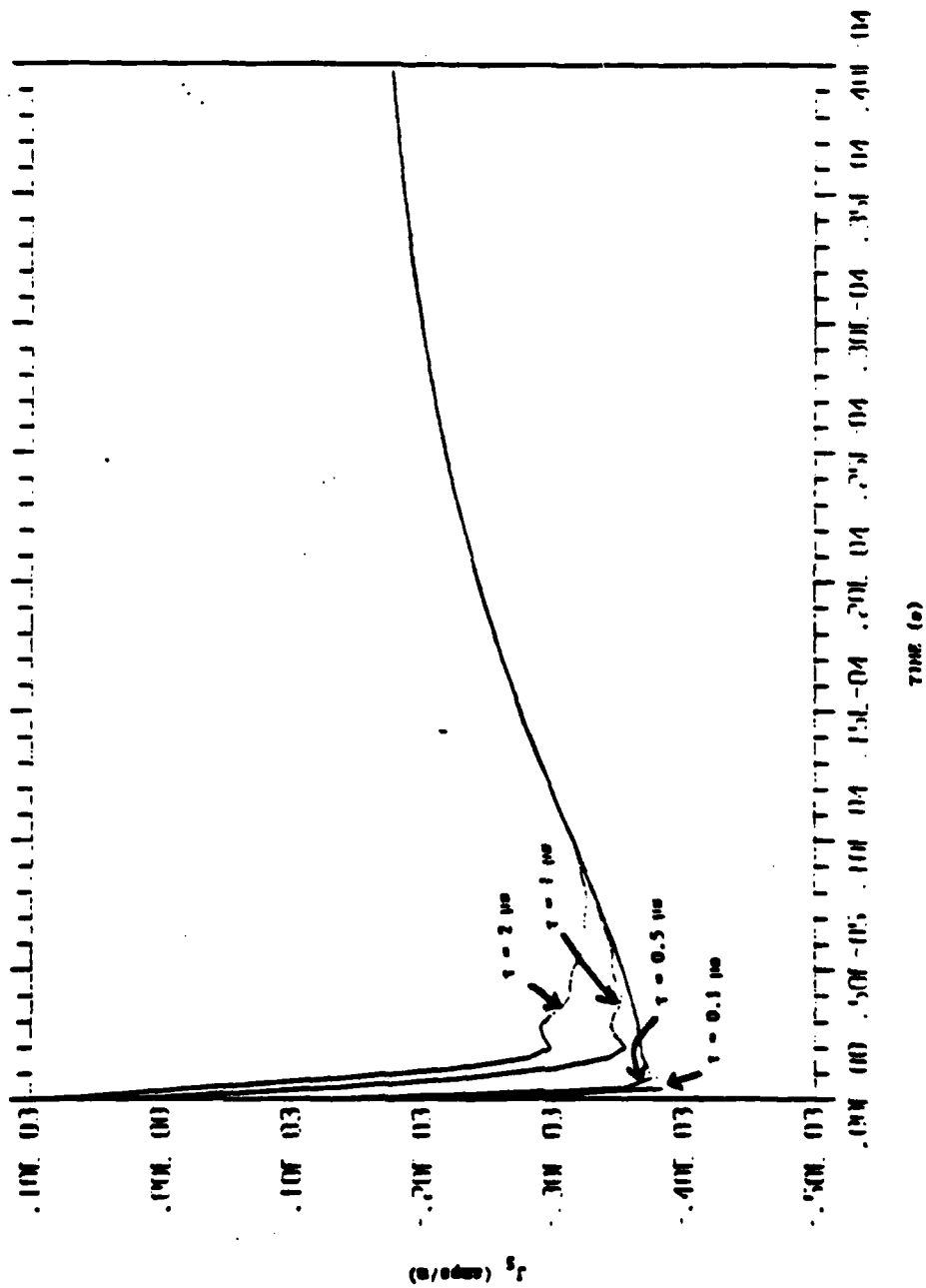


Figure 4-9. J_S^{29} Due to Near-Strike Lightning at 100m for
Different Rise Times

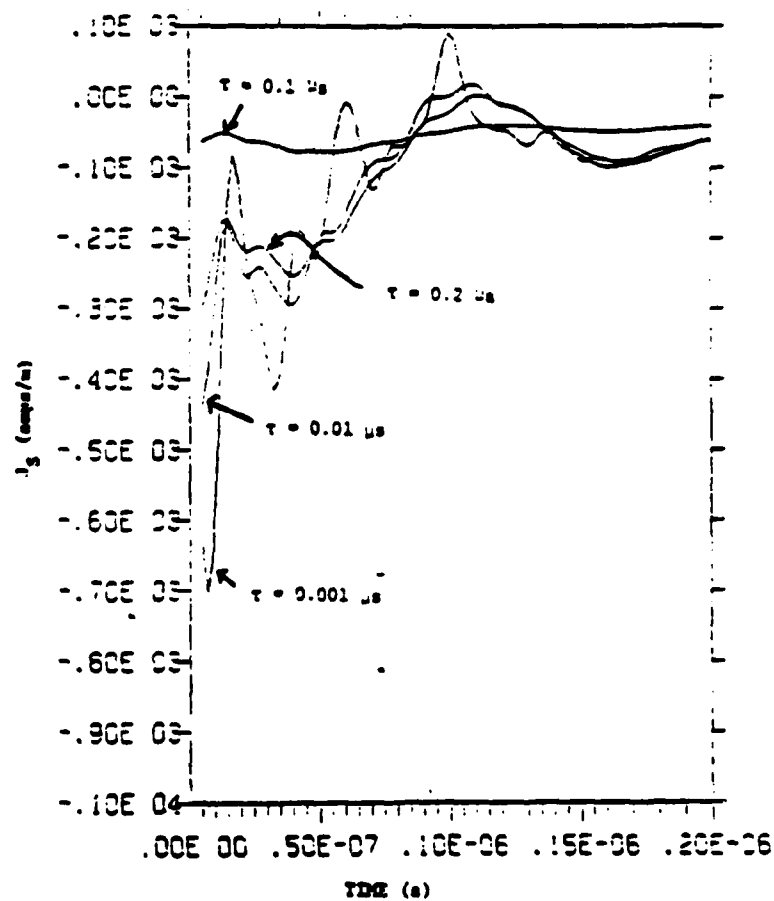


Figure 4-10. Skin Current Density J_s on Edge No. 29 of Triangular Patch Model of F-14 Aircraft for Various Rise Times τ of Incident NEMP

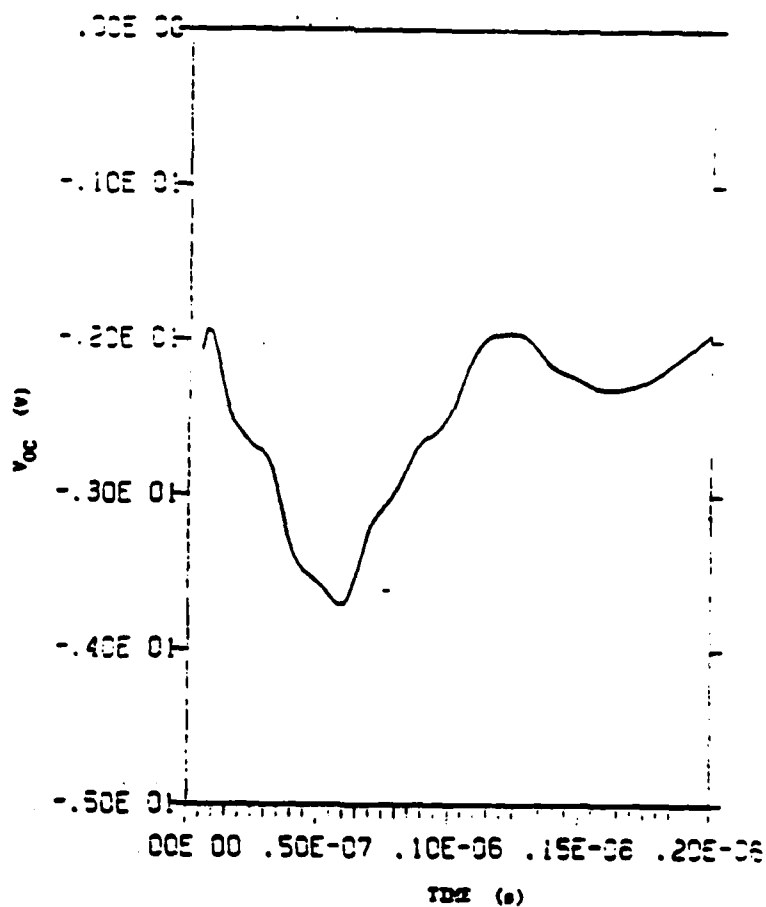


Figure 4-11. Peak $V_{OC}(t)$ for One Wire Line Behind Gr/Ep Panel
Due to NEMP of Different Rise Times, $\tau = 0.1$,
0.02, 0.01, 0.001 μs , $L = 1m$, $d = 8$ Ply

EM PROTECTION OF METALS AND COMPOSITES (TJ)

Transfer Impedance Shielding of Structural Materials and Protective Electromagnetic Coatings

(Valid for Frequencies Below 10⁸ Hz)

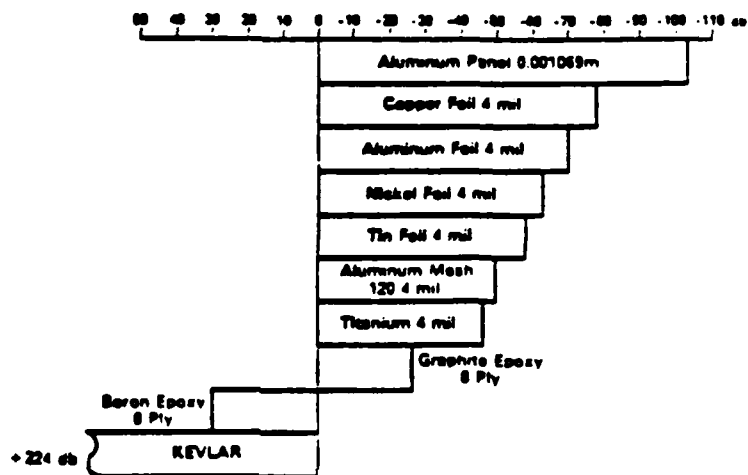


Figure 4-12. Transfer Impedance Shielding of Structural Materials and Protective Electromagnetic Coatings

EM PROTECTION (TJ)

Protective Coatings Improvement Relative to 8-Ply G/E

(Valid for Frequencies Below 10⁸ Hz)

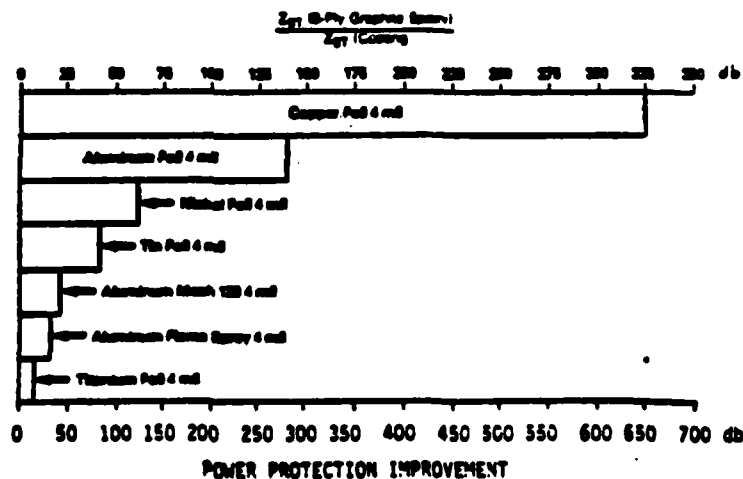


Figure 4-13. Improvement Protective Coatings Provided Relative to 8-Ply Graphite/Epoxy

EM PROTECTION WEIGHT PENALTIES (T_J)

Forward Fuselage AV-8B (Area - 100 Ft²) Weight Penalty
(Pounds) Imposed by Electromagnetic Protective Coatings

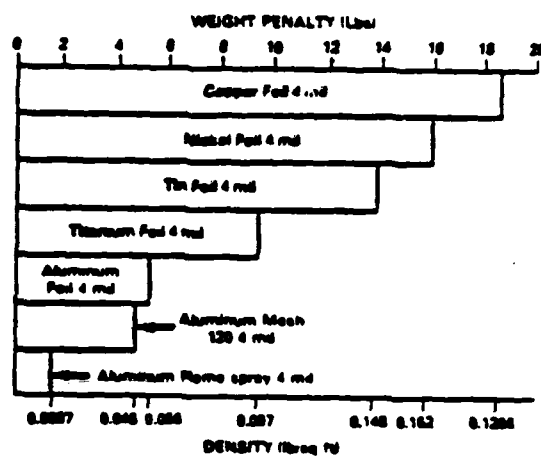


Figure 4-14. Weight Penalty Imposed by Protective Coatings

EM PROTECTION (T_J)

Weight Shielding Figure of Merit

(Protection Beyond 8-Ply G/E Provided by the Weight of 1 Square Foot of Protective Coating)

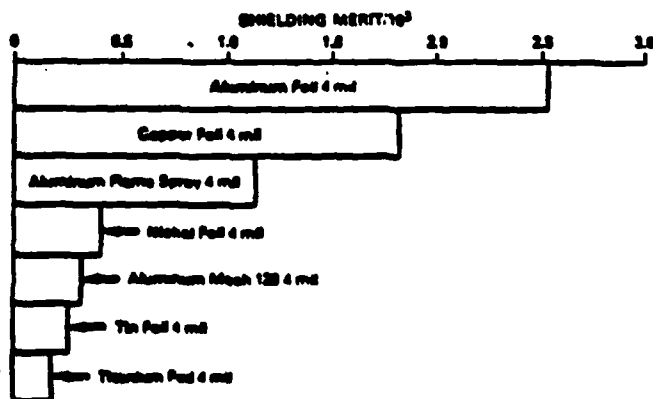


Figure 4-15. Weight/Shielding Figure of Merit of EM Protective Coatings

DATE
FILMED
7-8